

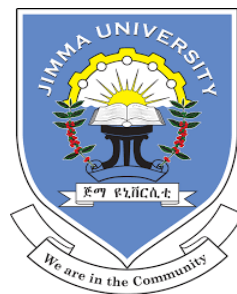
**ALL POLYMER SOLAR CELL MATERIALS:
STRUCTURE-PROPERTY RELATIONSHIP FOR
LOW BANDGAP P(NDI2OD-T2) SOLUTIONS AND BLENDS**

BY
GADA MULETA FANTA

18 SEPTEMBER 2020



JIMMA UNIVERSITY



FACULTY OF MATERIALS SCIENCE AND ENGINEERING
JIMMA INSTITUTE OF TECHNOLOGY
SCHOOL OF GRADUATE STUDIES

**ALL POLYMER SOLAR CELL MATERIALS:
STRUCTURE-PROPERTY RELATIONSHIP FOR
LOW BANDGAP P(NDI2OD-T2) SOLUTIONS AND BLENDS**

A PhD DISSERTATION SUBMITTED TO THE SCHOOL OF GRADUATE
STUDIES OF JIMMA UNIVERSITY IN PARTIAL FULFILLMENT OF THE
REQUIREMENTS FOR THE DEGREE OF DOCTOR OF PHILOSOPHY IN
MATERIALS SCIENCE AND ENGINEERING

BY
GADA MULETA FANTA

ADVISORS: PROF. JUNG YONG KIM (PHD)
PROF. TOMASZ TANSKI (DR.-ING.)

18 SEPTEMBER 2020
JIMMA UNIVERSITY

**EXAMINATION BOARD DISSERTATION APPROVAL FORM
JIMMA UNIVERSITY, SCHOOL OF GRADUATE STUDIES**

Dissertation Title:

All Polymer Solar Cell Materials: Structure–Property Relationship for Low Bandgap P(NDI2OD-T2) Solutions and Blends.

By: Gada Muleta Fanta

Faculty of Materials Science and Engineering, Jimma Institute of Technology, Jimma University.

Approved by the Examining Board:

1. Chair person, examination board (Jury)

Name: Dr. Muluaalem Abebe Mekonnen (PhD) Signature _____ Date _____


2. Promoter (Primary)

Name: Prof. Jung Yong Kim (PhD) Signature _____ Date _____

3. Promoter (Secondary)

Name: Prof. Tomasz Tanski (Dr.-Ing.) Signature  Date _____


4. External Examiner

Name: Prof. Teketel Yohannes Anshebo (PhD) Signature  Date _____

5. External Examiner

Name: Dr. Delele Worku Ayele (PhD) Signature  Date _____

6. Internal Examiner

Name: Dr. Menberu Mengesha Woldemariam (PhD) Signature  Date _____

DEDICATION

This dissertation is dedicated to Almighty God who gave me the strength and perseverance to begin and successfully complete my study.

LIST OF SYMBOLS AND ABBREVIATIONS

AFM	Atomic force microscopy
All-PSCs	All-polymer solar cells
B	Full width at half maximum (FWHM) at the diffraction angle θ
BHJ	Bulk-heterojunction
CB	Chlorobenzene
CF	Chloroform
d	Distance between crystallographic planes (d -spacing)
DCO	1,8-dichlorooctane
DIO	1,8-diiodooctane
DMA	Dynamic mechanical analysis
DSC	Differential scanning calorimetry
FF	Fill Factor
FH	Flory-Huggins
ΔG_M	Gibbs free energy of mixing
ΔH_m	Enthalpy of mixing
HOMO	Highest occupied molecular orbital
J_{SC}	Short current density
κ_B	Boltzmann constant
L-L	Liquid-liquid
LLE	Liquid-liquid phase equilibria
L_D	Diffusion length
L-S	Liquid-solid
LUMO	Lowest unoccupied molecular orbital
MEH-PPV	Poly[2-methoxy-5-(20-ethyl)-hexyloxy-p-phenylenevinylene]
M_n	Number average molecular weight
$M_{n,1 \text{ or } 2}$	Number average molecular weight of component 1 or 2
MW_s	Molecular weight of a solvent
M_w	Weight average molecular weight
n	Total number of segments
n-Type	Acceptor(electron-transport)
N_A	Number of occupied lattice sites by each monomeric unit or molecule
$N_{A/B}$	Degree of polymerization of polymer A/B

NBR	Butadiene/acrylonitrile copolymer
NDI	Naphthalene diimide
NDTI	Naphtho [2,3-b:6,7-b'] dithiophene-4,5,9,10-diimide
NG	Nucleation and growth
ODT	1,8-octanedithiol
OFETs	Organic field effect transistors
OLEDs	Organic light emitting devices
OPV	Organic photovoltaics
OSCs	Organic solar cells
OTFT	Organic thin-film transistor
<i>P</i>	Pressure
P_A	Polymer acceptor
PPO	Polystyrene-poly(2,6-dimethyl-1,4-henylene oxide)
PPV	Poly(p-phenylenevinylene)
PCBM	Fullerene
PC ₆₁ BM	[6,6]-phenyl C ₆₁ butyric acid methyl ester
PC ₇₁ BM	[6,6]-phenyl C ₇₁ butyric acid methyl ester
PCE	Power conversion efficiency
PCPDTBT	Poly(2,6-(4,4-bis(2-ethylhexyl)-4H-cyclopenta(2,1-b;3,4-b')dithiophene)-alt-4,7-(2,1,3-benzothiadiazole)
PBDTTTPD	Poly[4,8-bis(5-(2-ethylhexyl)thiophen-2-yl)benzo[1,2-b:4,5-b0]dithiophene-alt-1,3-bis(thiophen-2-yl)-5-(2-hexyldecyl)-4H-thieno[3,4-c]pyrrole-4,6(5H)-dione]
P_D	Polymer donor
PDI	Polydispersity index
PDI	Perylene diimide
p-Type	Donor(hole-transport)
P(NDI2OD-T2)	Poly{(N,N'-bis(2-octyldecyl)naphthalene-1,4,5,8-bis(dicarboximide)-2,6-diyl)-alt-5,5', -(2,2'-bithiophene)}
P(NDI2HD-T)	Poly[[N,N0-bis(2-hexyldecyl)-naphthalene-1,4,5,8-bis(dicarboximide)-2,6-diyl]-alt-5,5-thiophene]
PFSCs	Polymer-fullerene solar cells
P3HT	Poly(3-hexylthiophene-2,5-diyl)

PTB7	[[4,8-bis[(2-ethylhexyl)oxy]benzo[1,2-b:4,5-b]dithiophene2,6-diyl][3-fluoro-2-[(2-ethylhexyl) carbonyl]thieno[3,4-]thiophenediyl]]
PVC	Poly(vinyl chloride)
$\rho_{1 \text{ or } 2 \text{ or } s}$	Density of component 1 or 2 or solvent
R	Gas constant
Rpm	Revolutions per minute
$r_{1 \text{ or } 2}$	Relative molar volume of component 1 or 2
ΔS_m	Entropy of mixing
SD	Spinodal decomposition
SLE	Solid-liquid phase equilibria
T	Temperature constant
t	Crystallite size
T_c	Crystallization temperature
TEM	Transmission electron microscopy
TGA	Thermogravimetric analysis
TGBC	Top-gate bottom-contact
T_g	Glass transition temperature
T_m	Melting temperature
UCST	Upper critical solution temperature
UV-VIS	Ultraviolet-visible spectrophotometry
V_A and V_B	Molecular volume fractions of the two components ϕ_A and ϕ_B
\hat{V}_s	Molar volume of a solvent
V_s	Lattice site volume for solvent molecules or monomers
V_{OC}	Open-circuit voltage
XRD	X-ray diffraction
XY	P-xylene
χ	Flory-Huggins interaction parameter
χ_{ij}	Flory-Huggins interaction parameter between component i and j
$(\chi_{12})_{crit}$	Flory-Huggins interaction parameter between component 1 and 2 at critical point
$\varphi_{A/B}$	Volume fraction of polymer A/B (with $\varphi_A + \varphi_B = 1$)
ln	Natural logarithm
θ	Contact angle
2θ	Diffraction angle
λ	X-ray wavelength (= 0.154 nm)

μ_h	Hole mobility
μ_n	Electron mobility
δ	Solubility parameter
$\delta_{i \text{ or } j}$	Solubility parameter of component i or j
ϕ_i	Volume fraction of component i
γ_{lv}	Gamma surface energy of liquid-vapour
γ_{sv}	Gamma surface energy of solid-vapour
γ_{sl}	Gamma surface energy of solid-liquid

ACKNOWLEDGEMENTS

First and for most, I would like to express my sincere gratitude to my advisors, Professor Jung Yong Kim (Jimma University) and Professor Tomasz Tanski, (Silesian University of Technology) for their support, guidance, encouragement and patience throughout my PhD study. They contributed a lot to improve my work from the beginning up to the end. I once again thank them for the tremendous effort they made for the success of this study. I would like to thank all examiners for your constructive and valuable comments and questions. Namely, Prof. Teketel Yohannes, Addis Ababa University, Dr. Delele Worku, Bahir Dar University, and Dr. Menberu Mengesha, Jimma University.

I would also like to appreciate my Erasmus plus International Mobility Office and coordinator members, Dr. Abebe Beyene, Jimma University, Joanna Mrowiec-Denkowska, Monika Suchy, Dr. Anna Bzymek, Dr.-Ing. Wojciech Sitek, Silesian University of Technology, Gliwice, Poland, for kindly providing me an opportunity to study and conduct laboratory there. My special thanks go to Dr. Abebe Beyene not only for his giving me an opportunity to study through Erasmus plus scholarship but also for his personal advice. Moreover, I would like to thank Arba Minch University and Jimma University for supporting me financially through Ministry of Science and Higher Education, Addis Ababa, Ethiopia.

I thank all members of the Professor Tomasz Tanski group. I am particularly indebted to Dr.-Ing. Pawel Jarka, who generously helped me adapt to the world of all polymer solar cell materials. Professor Tomasz Tanski group made my laboratory life intellectually stimulating and highly enjoyable. I appreciate Dr.-Ing Marta Musiol, and Dr.-Ing Urszula Szeluga at Centre of Polymer and Carbon Materials-Polish Academy of Sciences, PL41-819 Zabrze for assistance with measuring TGA and DSC, respectively. Mr. Tymoteusz Jung (PhD scholar at SUT) also deserves acknowledgement for measuring XRD of polymer films. I thank the Ministry of Science and Higher Education, Addis Ababa, Ethiopia and Erasmus plus scholarship (Mobility of Students and Staff between EU and Partner Countries) at SUT Poland. I would also like to thank all Polish friends at the Silesian University of Technology, and my best friends in Poland for their constant friendship, valuable advice and warm encouragement.

Finally, I wish to express my heartfelt thanks to my parents, Biritu Dufera Chemedda and Muleta Fanta, as well as my younger brothers and sisters, for their sacrifice, support and prayer throughout my study. My special thanks go to Mr. Dereje Abdeta Bayissa (from Alberta, Canada) and my former colleague at Arba Minch University, Mr. Kebede Abu Aragaw (from Seattle Washington DC, USA) for providing me with humanity support during CoVID-19 pandemic time. Mr. Dereje Abdeta Bayissa allowed me to use his private house for four months without any payment whereas Mr. Kebede Abu Aragaw made my graduation ceremony enjoyable by covering costs for all necessary materials. Most importantly, I deeply thank my lovable son, Ayana Gada Muleta, as well as my beloved wife, Ethiopia Tadesse Tilahun, who patiently supported and cheered me throughout this long time. The completion of this dissertation would not have been possible without my family's support and encouragement.

TABLE OF CONTENTS

DEDICATION.....	ii
LIST OF SYMBOLS AND ABBREVIATIONS	iii
ACKNOWLEDGEMENTS	vii
TABLE OF CONTENTS	ix
LIST OF TABLES	xi
LIST OF FIGURES	xii
LIST OF ANNEXES.....	xv
ABSTRACT.....	xvi
1. INTRODUCTION.....	1
1.1 Background of the Study	1
1.2 Rationale of the Study.....	7
1.3 Significance of the Study	8
1.4 The Scope of the Study.....	9
1.5 Objectives of the Study.....	11
2. LITERATURE REVIEW	12
2.1 Photovoltaic Cell.....	12
2.2 All-Polymer Solar Cells.....	12
2.3 n-Type All-Polymer Solar Cells Application	13
2.4 Organic Solar Cells.....	17
2.4.1 The Bulk-Heterojunction Solar Cell	18
2.4.2 Working Mechanism of Photovoltaic Device.....	18
2.5 Morphological Characterization of Thin-Films Using AFM and XRD Techniques.	20
2.6 Methods for Determining the Solubility Parameter.....	29
2.7 Thermodynamics of Polymer Blends.....	30
2.7.1 Flory-Huggins Theory	31
2.8 Phase Diagrams.....	32
2.8.1 Binary Temperature-Composition Phase Diagram of P3HT: PCBM Blends.	34
2.8.2 Different Phases Formed by Self-Assembly of Coil-Coil Diblock Copolymers in the Bulk as a Function of the Volume Fraction of One of the Blocks.....	35

2.8.3 Phase diagram of the LCST and UCST for Behavior of Polymer Blends.	37
2.8.4 Thermal Properties of Polymers	37
2.8.5 Thermodynamic Phase Transitions (First-and Second-Order).....	39
3. METHODS AND MATERIALS	41
3.1 Experimental Section	41
3.1.1 Materials	41
3.1.2 Contact Angle Measurement.....	44
3.1.3 Solubility Parameter Calculation	44
3.1.4 Thermal Property Characterization.....	45
3.1.5 Film Processing.....	45
3.1.6 Film Characterization.....	46
4. RESULTS AND DISCUSSION	47
4.1 Phase Diagrams of n-Type Low Bandgap Naphthalenediimide-Bithiophene Copolymer Solutions and Blends.....	47
4.1.1 Binary Polymer-Solvent Mixture.....	47
4.1.2 Binary Polymer-Polymer Mixture	57
4.2 Phase Behavior of Amorphous/Semicrystalline Conjugated Polymer Blends	63
4.2.1 Thermal Property of Polymer Materials Analysis	63
4.2.2 Morphology-X-ray Diffraction of Polymer Films Analysis	68
4.2.3 Morphology-Tapping-Mode AFM of Polymer Films Analysis.....	71
5. GENERAL DISCUSSION	73
5.1 The Outputs of Dissertation Research	77
5.2 Strengths and Limitation.....	78
5.3 Conclusions.....	79
5.4 Recommendations.....	81
6. REFERENCES.....	82
7. ANNEXES	102

LIST OF TABLES

Table 2.1 Thin-film XRD data of thermally annealed random copolymers of P(NDI2OD-T2) and NDI-Th-PDIx random copolymers (adapted from (Sharma et al., 2016)).	23
Table 2.2 Grazing-incidence wide-angle X-ray scattering diffraction peak analysis of PCPDTBT(N),PCPDTBT(C5) and PCPDTBT(D5) films (adapted from (Hwang et al., 2017)).	27
Table 4.1 Contact angle, surface energy, and solubility parameter.	49
Table 4.2 Solubility parameter (Belmares et al., 2004), molecular weight, molar volume, density, boiling point, and radius of lattice site volume for each solvent, chlorobenzene, chloroform, and p-xylene.	49
Table 4.3 Relative molar volume and Flory-Huggins χ interaction parameter for binary P(NDI2OD-T2)/solvent and r-reg P3HT/solvent mixtures as a function of solvent (CB, CF, and XY), when P(NDI2OD-T2) has $M_n = 32.1$ kg/mol and $\delta = 7.99$, and r-reg P3HT has $M_n = 29.6$ kg/mol and $\delta = 9.23$.	51
Table 4.4 Crystallite size (t) and d -spacing of P(NDI2OD-T2):PCPDTBT blends with 100:0, 80:20, 50:50, and 0:100 (wt. ratio) at the diffraction angle θ , when X-ray has wavelength (λ) of 0.154 nm. Herein, d -spacing between lattice planes is calculated based on Bragg's law, $\lambda = 2d \sin \theta$.	70

LIST OF FIGURES

Figure 1.1 The types of renewable energy resources listed above: biomass, solar, geothermal, wind, and hydropower (adapted from (Avtar et al., 2019)).	1
Figure 1.2 Steps involved in conversion of sunlight into electricity in a typical solar cell (adapted from (Ushasree and Bora, 2019)).	3
Figure 2.1 Summary of the development of three kinds of rylene diimide polymers for all-PSC application (adapted from (Yang et al., 2017)).	16
Figure 2.2 The chemical structure of the three rylene diimide-based n-type polymers of PPDI-DTT, PNDI-DTT and PNDTI-DTT (adapted from (Yang et al., 2017)).	17
Figure 2.4 Atomic force microscopy images of the surface topography of (a) as-cast, (b) melt-annealed, and (c) zone-cast films. The arrow in (c) indicates the zone-casting direction (adapted from (Schuettfort et al., 2013)).	22
Figure 2.5 (a) and (b) thin-film XRD diffraction patterns of reference P(NDI2ODT2) and random copolymers (adapted from (Sharma et al., 2016)).	24
Figure 2.6 Atomic force microscopy images of the ordering agent-induced polymer surface morphology and height profile. PCPDTBT (a) without OA; (b) with 5 vol % 1-chloronaphthalene; (c) with 10 vol % CN; (d) with 20 vol % CN; (e) with 5 vol % 1,8-diiodooctane; (f) with 10 vol % DIO; and (g) with 20 vol % DIO (adapted from (Hwang et al., 2017)).	25
Figure 2.7 The surface topography of ordering agent-driven PCPDTBT film scanned by an atomic force microscope. $1 \times 1 \mu\text{m}$ (a) PCPDTBT(N), (b) PCPDTBT(C5), (c) PCPDTBT(D5) (adapted from (Hwang et al., 2017)).	26
Figure 2.8 In-plane (IP) and out-of-plane (OOP) line-cuts from GIWAXS images. (a) IP and (c) OOP X-ray scattering profiles of PCPDTBT(C), (b) IP and (d) OOP X-ray scattering profiles of PCPDTBT(D) (adapted from (Hwang et al., 2017)).	28
Figure 2.9 The proposed PCPDTBT film orientation change after OA addition.	28
Figure 2.10 Constructing a tangent to the profile. (a) sessile drop method, (b) adhering air bubble method (adapted from (He, 1989)).	30
Figure 2.11 Phase diagram of P3HT and PF12TBT blend films drawn according to AFM images. Red squares, black circles, and blue triangles represent bicontinuous, droplet, and uniform phase-separated morphologies, respectively. The dashed line and solid line represent the	

boundaries between droplet and bicontinuous morphologies and between droplet and uniform morphologies, respectively (adapted from (Zhou et al., 2015)). 33

Figure 2.12 Binary temperature-composition phase diagram for P3HT:PCBM blends (adapted from (Kim and Frisbie, 2008))...... 34

Figure 2.13 Different phases formed by self-assembly of coil-coil diblock copolymers in the bulk (when the intermolecular interaction is sufficiently large) as a function of the volume fraction of one of the blocks, f_A . Other phases have also been reported for diblocks, and the phase diagrams of BCPs containing more than two blocks are considerably more complex. Switching out one or both coil blocks with a conjugated block that adopts a semi-flexible or rigid rod structure will also qualitatively change this phase diagram (adapted from (Botiz and Darling, 2010))......36

Figure 2.14 Phase diagram showing the LCST and UCST, respectively, behavior of polymer blends. Nonsymmetric phase diagrams are common in binary blends of polymers with large differences in their molecular masses (adapted from (Kalogeris, 2016)). 37

Figure 2.15 Schematic diagram of melting point and glass transition temperature of polymer for (a) crystalline materials (transition from crystalline to melt), (b) amorphous materials (transition from glass to rubbery transition) (adapted from (John Wiley and Sons, 2015)). 38

Figure 2.16 Schematic representation of thermodynamic responses. (a) First-order phase transition: consider, for example, melting of a crystal with defects (—) or of a perfect infinite crystal (--). (b) Second-order transition: transition dominated by intermolecular cooperative phenomena (—), or having only intermolecular cooperative phenomena (--). (c) Glass transition: experimental response (—), and ideal response in an infinitely slow experiment (--). (adapted from (Kalogeris, 2016))...... 40

Figure 3.1 The photographs taken during laboratory experiment (pictured by Gada Muleta)...43

Figure 4.1 (a) Chemical structure of P(NDI2OD-T2) and (c) r-reg P3HT, (b) UV-VIS spectrum of P(NDI2OD-T2)...... 48

Figure 4.2 (a) P(NDI2OD-T2) solution and film, (b) Contact angle measurement for P(NDI2OD-T2) film on glass substrate. 49

Figure 4.3 Phase diagrams of binary P(NDI2OD-T2) solutions: Solvent effect. Theoretical phase diagrams of (a) P(NDI2OD-T2)/CB, (b) P(NDI2OD-T2)/CF, and (c) P(NDI2OD-T2)/XY solutions, based on the Flory-Huggins lattice theory. (d) Schematic explanation of liquid-liquid phase equilibria (LLE) and solid-liquid phase equilibria (SLE) phase transition of P(NDI2OD-T2) molecules in solution. Herein, Path I indicate SLE (i.e., crystallization), whereas Path II denotes LLE (amorphous-amorphous phase separation). Regions correspond to: (A) one-phase liquid state; (B) two-phase liquid state; (C) both L-L and L-S phase separation; and (D) L-S phase separation (i.e., polymer crystallization), respectively54

Figure 4.4 (a) Theoretical phase diagrams of binary r-reg P3HT solutions: r-reg P3HT/CB (green solid line), r-reg P3HT/CF (red), and r-reg P3HT/XY (blue). Inset: Chemical structure of r-reg P3HT. (b) Schematic explanation of SLE (L-S phase transition) of r-reg P3HT molecules in solution.....	57
Figure 4.5 Differential scanning calorimetry thermograms at a scan rate of 10 °C/min: (a) P(NDI2OD-T2), (b) r-reg P3HT, (c) r-reg P3HT:P(NDI2OD-T2) = 50:50 wt.%, and (d) r-reg P3HT:P(NDI2OD-T2) = 80:20 and 20:80 wt.%.....	58
Figure 4.6 Thermogravimetric analysis of P(NDI2OD-T2) and r-reg P3HT.	59
Figure 4.7 Temperature-composition phase diagram for the binary r-reg P3HT/P(NDI2OD-T2) system, in which L and S stand for liquid and solid, respectively. (a) Experimental results obtained from DSC thermograms in Figure 4.5 and (b) Comparison of experimental data (from the second heating curve) with the Flory-Huggins lattice model (Equations 4.1.7) and 4.1.9) with $= 116.8/T - 0.185$	60
Figure 4.8 Theoretical description of melting points for the binary r-reg P3HT/P(NDI2OD-T2) system by using the theory of melting point depression combined with Flory-Huggins model incorporating the polymer-polymer interaction parameters of $116.8 \text{ K/T} + 0.340$, 116.8 K/T , and $116.8 \text{ K/T} - 0.185$, respectively.	62
Figure 4.9 Chemical structures of (a) P(NDI2OD-T2) and (b) PCPDTBT, respectively.....	64
Figure 4.10 TGA curves for P(NDI2OD-T2), P(NDI2OD-T2)/PCPDTBT blend, and PCPDTBT.....	66
Figure 4.11 DSC curves. (a) Heating-cooling-heating curves for P(NDI2OD-T2). (b) 1st heating, (c) 1st cooling, and (d) 2nd heating curves for P(NDI2OD-T2):PCPDTBT = 100:0, 80:20, 50:50 and 0:100 (wt. ratio), respectively.	67
Figure 4.12 Melting and crystallization point depression of P(NDI2OD-T2)/PCPDTBT blends.....	68
Figure 4.13 XRD patterns of P(NDI2OD-T2):PCPDTBT blends with 100:0, 80:20, 50:50 and 0:100 (wt. ratio).	69
Figure 4.14 Schematic explanation of when semicrystalline P(NDI2OD-T2) and amorphous PCPDTBT polymers are mixed together through solution processing. Here, the regular π - π stacking could be destroyed by adding PCPDTBT into a crystalline P(NDI2OD-T2) lamellae.....	71
Figure 4.15 Tapping-mode AFM images of (a) pristine P(NDI2OD-T2), (b) annealed P(NDI2OD-T2), (c) pristine P(NDI2OD-T2):PCPDTBT = 1:1 blend, (d) annealed P(NDI2OD-T2):PCPDTBT = 1:1 blend, (e) pristine PCPDTBT, and (f) annealed PCPDTBT films, respectively.	72

LIST OF ANNEXES

7.1 Annex I - Curriculum Vitae of PhD Candidate	103
7.2 Annex II - Declaration Form (PhD Dissertation Work)	108

ABSTRACT

Nowadays, energy crisis and environment pollution are two big challenges that restrict the development of society. Energy is a very important driving force to improve the standard of living and develop a country. The most versatile material class used in the field of organic photovoltaics is called π -conjugated polymers. Solar energy is a sustainable, environmentally friendly, unlimited energy from the sun and renewable energy source. The morphology of the active film is important for the efficiency of the solar cells. The most important branches in materials science is called polymer blend which has gained considerable attention to meet multifunctional need. Blends of two different polymers are likely to form a large phase separated structure; this is an inherent characteristic of polymers with a long main chain. Phase diagrams display specific information in terms of when the phase separation occurs and which phase-separated structure can be formed and therefore can be a suitable guidance to the phase separation of polymer blend. In this study, the phase diagrams of n-type low bandgap P(NDI2OD-T2) solutions and blends were constructed. To this end, we employed the Flory-Huggins lattice theory for qualitatively understanding the phase behavior of P(NDI2OD-T2) solutions as a function of solvents (chlorobenzene, chloroform, and p-xylene). Herein, the polymer-solvent interaction parameter was obtained from a water contact angle measurement, leading to the solubility parameter. The phase behavior of these P(NDI2OD-T2) solutions showed both liquid-liquid and liquid-solid phase transitions. However, depending on the solvent, the relative position of the liquid-liquid phase equilibria and solid-liquid phase equilibria (i.e., two-phase co-existence curves) could be changed drastically, i.e., $LLE > SLE$, $LLE \approx SLE$, and $SLE > LLE$. Finally, we studied the phase behavior of the polymer-polymer mixture composed of P(NDI2OD-T2) and r-reg P3HT, in which the melting transition curve was compared with the theory of melting point depression combined with the FH model. The FH theory describes excellently the melting temperature of the r-reg P3HT/P(NDI2OD-T2) mixture when the entropic contribution to the polymer-polymer interaction parameter ($\chi = 116.8 \text{ K/T} - 0.185$, dimensionless) was properly accounted for indicating an increase of entropy by forming a new contact between two different polymer segments. Understanding the phase behavior of the polymer solutions and blends affecting morphologies plays an integral role towards developing polymer optoelectronic devices. We report the phase behavior of amorphous/semicrystalline conjugated polymer blends

composed of low bandgap PCPDTBT and P(NDI2OD-T2). As usual in polymer blends, these two polymers are immiscible because $\Delta S_m \approx 0$ and $\Delta H_m > 0$, leading to $\Delta G_m > 0$, in which ΔS_m , ΔH_m , and ΔG_m are the entropy, enthalpy, and Gibbs free energy of mixing, respectively. Specifically, the FH interaction parameter for the PCPDTBT/P(NDI2OD-T2) blend was estimated to be 1.26 at 298.15K, indicating that the blend was immiscible. When thermally analyzed, the melting and crystallization point depression was observed with increasing PCPDTBT amounts in the blends. In the same vein, the X-ray diffraction patterns showed that the π - π interactions in P(NDI2OD-T2) lamellae were diminished if PCPDTBT was incorporated in the blends. Finally, the correlation of the solid-liquid phase transition and structural information for the blend system may provide insight for understanding other amorphous/semicrystalline conjugated polymers used as active layers in all-polymer solar cells, although the specific morphology of a film is largely affected by nonequilibrium kinetics. The thesis is organized into six chapters. Chapter 1 gives a brief general introduction. Chapter 2 focuses on a literature review on the topic of the study. The third chapter focuses on the experimental methods and materials adopted for the present work. The fourth chapter deals with the phase diagrams of n-type low bandgap naphthalenediimide-bithiophene copolymer solutions and blends. Chapter 5 focuses on the phase behavior of amorphous/semicrystalline conjugated polymer blends for which PCPDTBT and P(NDI2OD-T2) was chosen as a model system. Last chapter 6 includes the general discussion of the investigations, overall messages, strengths and limitations, conclusions drawn from the works, and recommendations relates to the outlook for future work. In each case, the goal is to understand the phase behavior of the polymer solutions and blends affecting morphologies that plays an integral role in developing polymer optoelectronic devices.

Keywords: phase diagram, Flory-Huggins theory, n-type polymer, p-type polymer, low bandgap polymer, polymer solution, phase behavior, conjugated polymer, polymer blend, all-polymer solar cell materials, melting point depression, amorphous, semicrystalline, polymer thermodynamics, solar energy

1. INTRODUCTION

1.1 Background of the Study

Nowadays, energy crisis and environment pollution are two big challenges that restrict the development of society (Sthel et al., 2013; Kamanzi and Kahn, 2017). According to the international energy agency as of Avtar et al., 2019 reported that, the energy demand of our globe is expected to increase by twofold in the year 2050, Figure 1.1. As a result, the development of clean and environmentally friendly renewable energy sources is required to meet the growing energy demand caused by rapid economic development and increasing population, by minimizing pollution, global warming and fossil-fuel depletion. Among the renewable energy sources (i.e., fossil fuels, wind energy, hydropower and nuclear energy), solar energy is one that can replace fossil fuels (Kumar, 2020, Martins et al., 2019, Asif and Muneer, 2007).

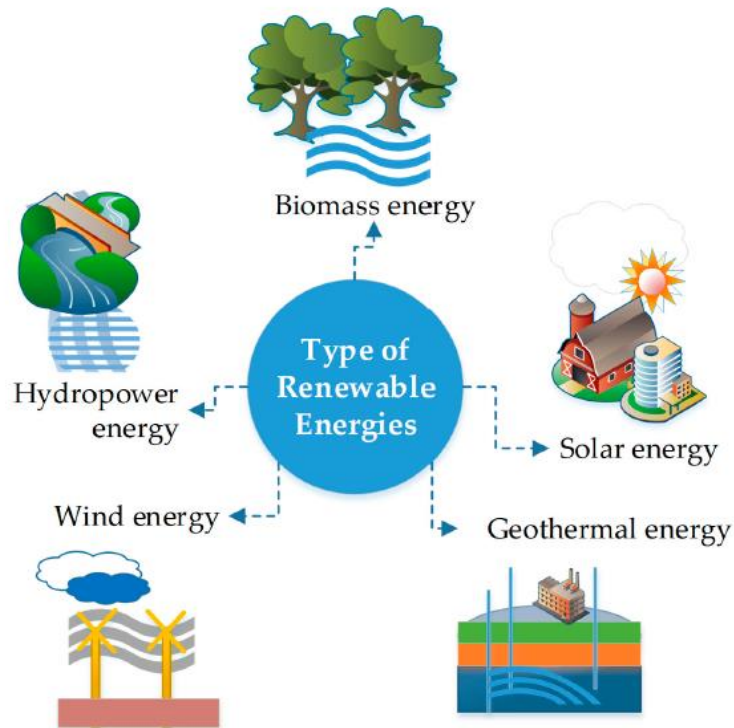


Figure 1.1 The types of renewable energy resources listed above: biomass, solar, geothermal, wind, and hydropower (adapted from (Avtar et al., 2019)).

The silicon solar cell currently dominating the market has been suffered from the various major challenges, such as high production cost which is the main drawback for large-scale energy applications and commercialization (Haitz and Tsao, 2011, Reineke, 2013). Thus, to compete and replace the use of fossil fuels in large scale energy demands, there has been an intensive effort to uncover a cheaper and more efficient solar cell materials alternative to silicon solar cells (Tuller, 2017, Battersby, 2019).

All-polymer solar cells are expected as one of the next generation photovoltaics and also believed to be promising devices that can be substitute silicon solar cells. The worldwide energy consumption continues to rise; leading to an increased exploitation of available energy sources. There has been a surge in global energy demand with the advancement in technology, economic growth, and increasing growth in population. Due to the fact that solar energy is well known as one of the clean and available energy sources, harvesting such solar energy is very important to meet the world's energy demand. Solar energy received by the earth in one hour from the sun is more than the total energy consumption across the planet in one year (Facchetti, 2011, Zhan and Zhu, 2010, Cheng et al., 2009, Boudreault et al., 2011). Figure 1.2, below indicates that one of the mechanisms used to harvest solar energy directly from sun light and convert this light into electricity is called solar cells (Ushasree and Bora, 2019). Solar cells can be categorized into two types depending on the active material used to harvest light (i.e., inorganic and organic solar cells). Today, silicon-based inorganic solar cells are dominating the solar cell market (Venkataraman et al., 2010). In lab-scale devices, the efficiency of multijunction inorganic solar cells is over 43 % and commercially available silicon-based solar cell is above 40 % (Venkataraman et al., 2010, Chen and Cao, 2009). Compared to inorganic solar cells, organic solar cells have many features such as low-cost, flexible, solution-processible, large-scale device fabrication and economically fairness. Besides, to meet the desired needs of solar cells, both the physical and chemical properties of organic polymeric materials can be modified (Zhou et al., 2011, Price et al., 2011, Helgesen et al., 2009, Kim et al., 2007, Lin et al., 2012, Anthony, 2011). Even if organic solar cells have a lot of interesting features, still the efficiency is lagged behind inorganic solar cells. To overcome this problem, a lot of researches have been conducted to enhance the efficiency of organic solar cells by synthesizing new active materials and developing new active layer fabrication methods (Zhou et al., 2011, Helgesen et al., 2009, Lin et al., 2012,

Anthony, 2011, Zhao and Zhan, 2011). In organic solar cells, the active material comprises the hole-electron transporters to generate and move the charges. Currently, 18.22 % power conversion efficiencies have been achieved in the state-of-the-art organic solar cells (Liu et al., 2020).

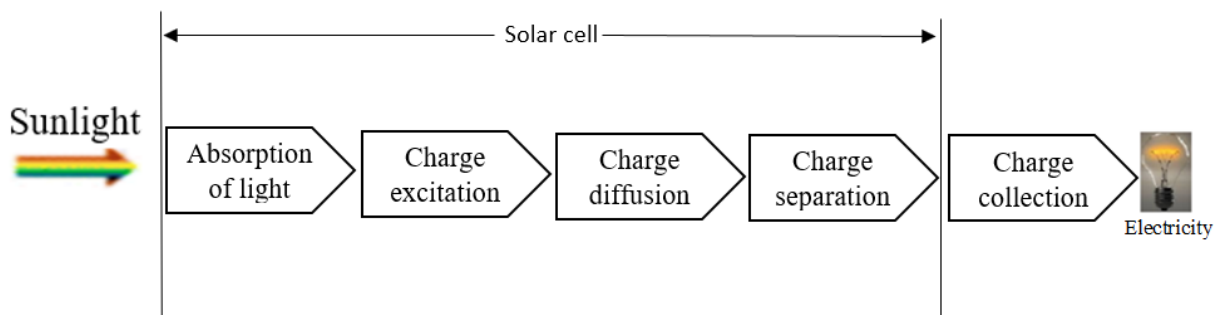


Figure 1.2 Steps involved in conversion of sunlight into electricity in a typical solar cell (adapted from (Ushasree and Bora, 2019)).

Recently, all-polymer solar cells with active layers composed of P_D and P_A have been competitive technologies as an alternative to polymer-fullerene solar cells (Wang et al., 2019, Fan et al., 2017, Li et al., 2017, Li et al., 2018, Kolhe et al., 2018). Increasing the efficiency of photovoltaic devices based on the use of organic materials, especially in the form of nanostructure elements, is the object of the research of scientists from around the world (Tański et al., 2016, Matysiak et al., 2017, Tański et al., 2019, Liu et al., 2019, Liu et al., 2016, Liu et al., 2018, Wen et al., 2018, Liu et al., 2018). Conjugated polymer blends composed of polymer donor and polymer acceptor have been used as an active material for all-polymer solar cells, leading to a high power conversion efficiency of ~10–14.4 % (Jia et al., 2020, Zhao et al., 2020, Zhu et al., 2019, Yao et al., 2019, Wu et al., 2019, Liu et al., 2019, Genene et al., 2019, Li et al., 2019), which still lags behind PFSCs, demonstrating a PCE of over 16 % (Yao et al., 2019, Fan et al., 2019). But all-small-molecule organic solar cells has highest power conversion efficiency reported over ~ 14 % (Qin et al., 2020, Jia et al., 2020). However, all-PSCs have clear advantages compared to PFSCs in that they have electronic tunability, leading to high open-circuit voltage and light absorption, thermodynamic stability in morphologies, mechanical

stability of devices, lower cost of synthesis, large-scale processability in manufacturing, and others.

In 2009, Facchetti et al. reported that P(NDI2OD-T2) has a high electron mobility of ~ 0.85 cm^2/V_s (Yan et al., 2009). Since then, P(NDI2OD-T2) has been mostly used as a benchmark P_A in all-PSCs, based on its properties, including high electronic charge mobility, a small bandgap 1.45 eV leading to effective light absorption, high electron affinity in its lowest unoccupied molecular orbital = -4.0 eV, density = 1.1 g/cm^3 , glass transition temperature ≈ -70 °C, aggregation in common solvents, and controllable face-on or edge-on molecular orientation depending on the molecular weight and its distribution (Moore et al., 2011, Fabiano et al., 2011, Schuettfort et al., 2011, Steyrlleuthner et al., 2012, Schubert et al., 2012, Yan et al., 2012, Mori et al., 2014, Zhou et al., 2015, Zerson et al., 2016, Zhang et al., 2016). However, in spite of the aforementioned strong characteristics, all-PSCs based on r-reg P3HT/P(NDI2OD-T2) showed a very low PCE (~ 0.2 %) initially, because of the geminate recombination of charge pairs originating from its coarse phase separation with a large domain size of $\sim 0.2\text{--}1$ μm (Moore et al., 2011). Note that organic semiconductors, π -conjugated polymers, and small molecules have low dielectric constants and van der Waals bonding (Pope and Swenberg, 1999, Gregg and Hanna, 2003). Hence, for separating small radius (< 5 Å) Frenkel excitons, a phase-separation scale around the exciton diffusion length (~ 10 nm) must be controlled, leading to a sufficient interfacial area (Pope and Swenberg, 1999). Hence, for effectively controlling morphologies, we need to understand the phase-separation mechanism in detail.

Here, when P_D and P_A are mixed together, the goal of this mixing is not to make a miscible blend unlike the versatile commercial blends, e.g., poly(vinyl chloride)-butadiene/acrylonitrile copolymer and polystyrene-poly(2,6-dimethyl-1,4-phenylene oxide) blends (Olabisi, 1979), but an immiscible (or partially miscible) blend for the separation of Frenkel excitons at the P_D/P_A heterojunction (Pope, 1999, Gregg, 2003). In general, the ideal size of phase-separated domains is $\sim 10\text{--}20$ nm because the exciton has a limited diffusion length ($L_D = \sim 10$ nm) due to low dielectric constants of organic macromolecules (Gregg and Hanna, 2003, Mikhnenko et al., 2015, Tamai et al., 2015). However, if two homopolymers are mixed, the polymer blends may undergo macrophase separation because of the increased Gibbs free energy of mixing (Bates,

1991). Figure 1.3, showed that on the other hand, when P_D and P_A are linearly linked by covalent bonds, these block copolymers may undergo microphase separation into ordered structures such as cubic sphere, hexagonal cylinder, bicontinuous gyroid, and lamellae (Leibler, 1980, Bates and Fredrickson, 1990, Dolan et al., 2015). Hence, considering the necessity of nanoscale phase separation (much smaller than micro-/macro-scale domains) for organic photovoltaics, we need to understand the polymer-polymer thermodynamic behavior in the P_D/P_A blend films.

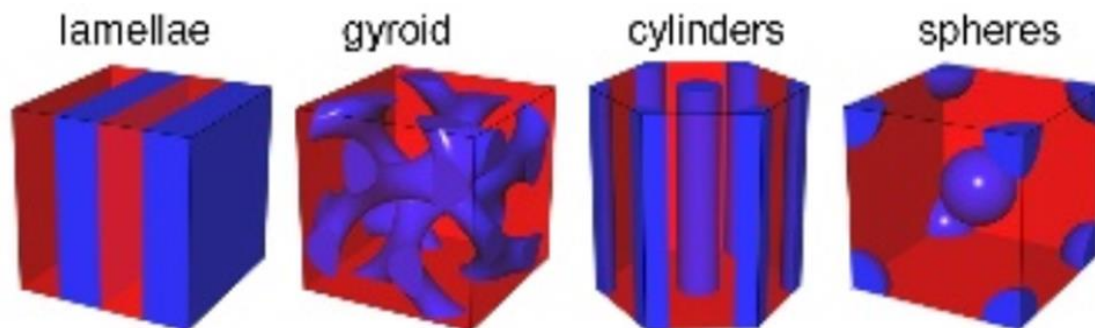


Figure 1.3 Block copolymers and self-assembled equilibrium morphologies of lamellae, bicontinuous gyroid, hexagonal cylinder, and cubic sphere (adapted from (Dolan et al., 2015)).

If P_D and P_A are amorphous, there are two type of phase separation in liquid-liquid phase transition: nucleation and growth, and spinodal decomposition (Cahn, 1965, McNeill and Greenham, 2009). Here, NG proceeds in the metastable region, whereas SD takes place in the unstable region without any energy barrier. However, if P_D and/or P_A are semicrystalline, the liquid-solid phase transition (crystallization) also takes place with L-L phase transition (Kim, 2018, Kim, 2019, Fanta et al., 2019). Indeed, in many P_A/P_D blend systems, they contain a stereoregular (or regioregular) polymer, leading to both L-L and L-S phase transition, directly affecting the morphologies of P_D/P_A blend films. Importantly, the pre-formed aggregation through L-S phase transition in OPV blend solutions may play a significant role in generating nanoscale phase domains instead of macrophase separation (Kim, 2018).

Previous studies (Kim, 2018) showed that the r-reg P3HT solution exhibits L-S phase transition related to order-disorder phase equilibria between single-coiled polymer in solution and polymer in nanocrystalline aggregate. The phase diagrams of low bandgap copolymer,

PCPDTBT solutions as a function of solvent, chain length, polymer species, fullerene size, etc., are constructed theoretically (Kim, 2019). Then, with this understanding of solution phase behavior for crystalline-amorphous, amorphous-amorphous, and crystalline-crystalline mixtures, the phase diagrams of binary PCPDTBT:PC₆₁BM and PCPDTBT:PC₇₁BM blends are constructed based on the thermal and optical properties of the materials (Kim, 2019).

In this study, I report that how n-type low bandgap P(NDI2OD-T2) solution undergoes L-L and L-S phase transition depends on the solvent in comparison with the phase behavior of the r-reg P3HT solutions. These phase behaviors are qualitatively described by the Flory-Huggins lattice theory (Flory, 1953, Flory, 1942, Huggins, 1942), for which the χ interaction parameter is estimated from contact angle measurements, leading to a solubility parameter (Kim, 2018, Kim, 2019). Then, the phase behavior of all semicrystalline polymers, the r-reg P3HT/P(NDI2OD-T2) system, is studied based on both experimental and theoretical analyses. Importantly, for analyzing the melting points of r-reg P3HT/P(NDI2OD-T2), I employ the theory of melting point depression combined with the FH model (Flory, 1953, Flory, 1942, Huggins, 1942), and observe excellent agreement between the theoretical and experimental results when I employ a χ parameter with both enthalpic and entropic contributions. Note that, when a polymer contains impurities (e.g., solvents or copolymerized units or other polymers), the melting point is shifted by re-establishing the condition of equilibrium between liquid and crystalline polymer, which could be described by combining the melting point depression theory with the FH model (Flory, 1953). Also, I further extended my works to an amorphous/semicrystalline conjugated polymer blend for which PCPDTBT and P(NDI2OD-T2) were chosen as a model system. Here, PCPDTBT is a p-type polymer acting as P_D (Mühlbacher et al., 2006, Morana et al., 2008, Gu et al., 2012, Fischer et al., 2015). Interestingly, if PCPDTBT with bulky branched alkyl side chains (ethyl hexyl groups) has a relatively low number average molecular weight, $M_n \approx 3.2$ kg/mol, it shows amorphous or marginally crystallizable behavior, indicating that the chain ends (just like impurities) may disturb polymer crystallization process (Kim, 2019). However, PCPDTBT with high $M_n \approx 35$ kg/mol could be highly crystallized when this polymer was processed with exposure to chlorobenzene vapors and/or with some solvent additives such as 1,8-diiodooctane, 1,8-octanedithiol, and 1,8-dichlorooctane (Mühlbacher et al., 2006, Morana et al., 2008, Gu et al., 2012, Fischer et al., 2015). Note that in such a case, I may not rule out the effect of substrate

on polymer's crystallization. On the other hand, P(NDI2OD-T2) is a highly crystallizable n-type polymer acting as P_A in all-PSCs or n-channels exhibiting very high electron mobility ($\mu_n \approx 0.85 \text{cm}^2 / \text{Vs}$) in the top-gate bottom-contact organic thin-film transistor (Yan et al., 2009, Rivnay et al., 2010, Brinkmann et al., 2012, Takacs et al., 2013, Zhou et al., 2014, Zhou et al., 2015, Zhang et al., 2016). Here, it is notable that P(NDI2OD-T2)'s glass transition temperature was reported to be - 70 and - 40 °C based on dynamic mechanical analysis and differential scanning calorimetry, respectively (Schuettfort et al., 2011, Gu et al., 2016). Hence, inspired by the important properties of these two polymers (Kim, 2019, Mühlbacher et al., 2006, Morana et al., 2008, Gu et al., 2012, Fischer et al., 2015, Yan et al., 2009, Rivnay et al., 2010, Brinkmann et al., 2012, Takacs et al., 2013, Zhou et al., 2014, Zhou et al., 2015, Zhang et al., 2016, Schuettfort et al., 2011, Gu et al., 2016), I further studied the thermodynamic behavior of PCPDTBT/P(NDI2OD-T2) blends based on the thermal and structural analyses. Specifically, the melting phenomena of crystalline P(NDI2OD-T2) with added amorphous PCPDTBT material was investigated using DSC and confirmed by X-ray diffraction, in which π -stacking was observed to be dependent on the amount of amorphous PCPDTBT in the blend film. Finally, the morphologies of the pure polymer and 1:1 blend film were investigated using the tapping-mode atomic force microscopy.

1.2 Rationale of the Study

The main motives of our research are solution-processable conjugated polymers have attracted enormous attention because of their potential application in the generation of cheaper to fabricate, flexible, lightweight, disposable, have fewer adverse environmental impacts and printed electronics (Beaujuge and Frechet, 2011, Li et al., 2010, Wu et al., 2015). The phase behavior of conjugated polymer-solvent and polymer-polymer mixtures has been an interesting topic of research in which there are two important phase-separation mechanisms, i.e., liquid-liquid and liquid-solid phase transitions (Flory, 1953, Kim, 2018, Kim, 2019). Herein, the L-L phase transition is similarly divided into two: spinodal decomposition, and nucleation and growth (Cahn, 1965, Bates, 1991, McNeill, 2009). The former proceeds in an unstable region through spontaneous phase separation without energy barriers, leading to a high interconnectivity of two phases, whereas the latter exists in a metastable region (Cahn, 1965, Binder, 1983, Favvas

and Mitropoulos, 2008). Specifically, in the field of polymer optoelectronics, L-L or amorphous–amorphous phase transition through SD has been emphasized because the bicontinuous phase morphologies of polymer/fullerene or polymer/polymer resemble those generated through SD demixing (McNeill, 2009, Vaynzof et al., 2011). However, many well-known conjugated polymers, including regioregular r-reg P3HT and P(NDI2OD-T2), are semicrystalline, not pure amorphous, indicating that they may exhibit not only liquid-liquid phase equilibria but also solid-liquid phase equilibria, i.e., self-assembly for crystallization (Whitesides and Grzybowski, 2002, Whitesides and Boncheva, 2002) in the thin-film process from solution (Kim, 2018, Kim, 2019). Hence, in the case of stereoregular polymer-based solutions, it becomes very important to elucidate both SLE and LLE mechanisms and their sequences SLE to LLE or LLE to SLE for understating morphology-formation mechanisms. Figure 1.4 showed that the Wikipedia of the free encyclopedia on website of (https://en.wikipedia.org/wiki/Materials_science), the four components (i.e., processing, structure, properties and performance) of the discipline of materials science engineering and their interrelationship were showed which was commonly named as materials tetrahedron, from this materials paradigm represented below my research work was mainly focused on structure-property relationship.

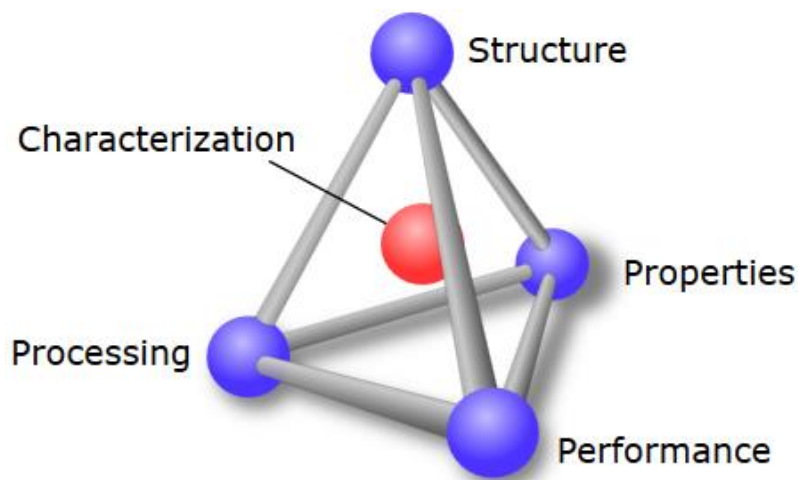


Figure 1.4 The materials paradigm represented in the form of a tetrahedron (adapted from (https://en.wikipedia.org/wiki/Materials_science)).

1.3 Significance of the Study

The importance of this dissertation research is conjugated polymers or copolymers have different applications today as of polymeric materials such as organic solar cells, organic field effect transistors, organic light emitting devices or thermoelectric generators. The main reason why conjugated polymers are used in such applications was because of their electronic structure. The P3HT is the next generation material with thiophene based backbone where as both PCPDTBT and P(NDI2OD-T2) are the state-of-the-art copolymers materials. Despite the lower power conversion efficiencies, all-polymer solar cell still has some advantages over polymer-fullerene systems. One of such advantages is the possibility to improve absorption by tuning the polymers to absorb in different parts of the solar spectrum, whereas fullerenes generally absorb poorly solar spectrum (Bavel et al., 2010). Solution processability may also be easier with all-polymer systems because of the possibilities to easily change the solution viscosity (Facchetti, 2013). One of the problems that all-polymer solar cells face is low electron mobilities due to, for example, large portions of amorphous materials. By using polymers and conditions such that crystalline structures may be formed in the film mobility may be increased, but the mobility may also get anisotropic, that is why the orientation of crystalline regions may become important. All-polymer solar cell is an emerging technology as a new subject of active research because polymer-polymer blend technique can avoid the aforementioned drawbacks of polymer-fullerene systems (Ding et al., 2015). Therefore, the conjugated polymer has much significance specially in polymer solar cells. The combination of p-type and n-type polymeric materials is important for polymer-polymer photovoltaics and complementary logic circuit applications (Rivnay et al., 2011).

1.4 The Scope of the Study

The major objective of the study is on the morphology and phase behavior of polymer/solvent solution and polymer/polymer blends; this research work contributes to the development of organic solar energy for devices that make use of polymer/solvent and polymer/polymer blend systems. Therefore, my dissertation research work was focused on three low bandgap polymeric materials (i.e., r-reg P3HT, PCPDTBT and P(NDI2OD-T2)); and includes common solvents of CB, CF and p-xylene for studies on the morphology and phase behavior of polymer/solvent solution and polymer/polymer blends. Both the r-reg P3HT and

P(NDI2OD-T2) are semicrystalline not pure amorphous, but the PCPDTBT is amorphous conjugated polymer. F-H lattice theory was used to study the thermodynamics (statistical thermodynamics) of the polymer solution and blends; and the effect of the interaction that exists in polymer/solvent solution and polymer/polymer blends were examined using the interaction parameter obtained from the Flory Huggins lattice theory. The solubility parameters were determined with the help of contact angle measurement. The phase diagram was plotted and analyses using experimental and theoretical studies. The thermal behavior was also studied using differential scanning calorimeter and thermogravimetric analysis. The morphology and structural behavior of the blends were studied with the help of the X-ray diffraction spectroscopy and Atomic force microscopy. Our research suggests an alternative to achieve well-defined morphology in polymer/solvent solution and polymer/polymer blends; and also provides a better understanding of the background knowledge of the thermodynamics and phase separation mechanism in polymer blends.

1.5 Objectives of the Study

- To construct the phase diagrams of n-type low bandgap P(NDI2OD-T2) solutions and blends.
- To investigate the phase behavior of the polymer-polymer mixture composed of P(NDI2OD-T2) and r-reg P3HT, in which the melting transition curve was compared with the theory of melting point depression combined with the FH model.
- To apply the FH lattice theory to qualitatively understand the phase behavior of P(NDI2OD-T2) solutions as a function of solvents (CB, CF, and XY).
- To apply the FH lattice theory for which the polymer-solvent interaction parameter (χ) is estimated from contact angle measurements, leading to a solubility parameter.
- To report the phase behavior of amorphous/semicrystalline conjugated polymer blends composed of low bandgap PCPDTBT and P(NDI2OD-T2).
- To study the correlation of the solid-liquid phase transition and structural information for the blend system may provide insight for understanding other amorphous/semicrystalline conjugated polymers.
- To investigate the morphologies of the pure polymer and 1:1 blend films were compared using the tapping-mode AFM.

2. LITERATURE REVIEW

2.1 Photovoltaic Cell

Energy is a very important driving force to improve the standard of living and develop a country. Solar energy is a sustainable, environmentally friendly, unlimited energy from the sun and renewable energy source, from a global perspective (Ali et al., 2016, Li et al., 2014). Since solar energy is clean (Late et al., 2015), there is large interest in developing efficient photovoltaic device for the conversion of solar energy to electrical energy (Li et al., 2014). At present, the photovoltaic market is dominated by silicon solar cells. However, the high production cost of crystalline silicon and long payback times, decreases its economic feasibility of widespread application. So, there has been a strenuous endeavor to find a cheaper alternative to silicon solar cells (Noel et al., 2013). The performance and efficiency of new technologies for solar energy conversion strongly depends on the materials (Liu et al., 2012).

2.2 All-Polymer Solar Cells

All-polymer solar cells (i.e., polymer-polymer blends), are composed from both conjugated polymer donor and conjugated polymer acceptor, and they have advantages such as tunable chemical and electronic properties, morphological stability and enhanced mechanical properties (Lei et al., 2016). In 1995, Halls et al. reported that the pioneering work on all-polymer blend solar cells and the materials they used as of photoactive layer to produce a polymer blend film are two soluble poly(p-phenylenevinylene) derivatives, poly[2-methoxy-5-(20-ethyl)-hexyloxy-p-phenylenevinylene] and cyano-PPV (Halls et al., 1995). All-PSCs have been proved as of alternative to the polymer-fullerene blend (Lei et al., 2016). Currently, state-of-the-art single-junction all-PSCs show power conversion efficiency over ~10–14.4 %, which still lag behind of polymer-fullerene system (i.e., due to not well-defined blend morphology and limited charge transport) (Lei et al., 2016b, Yao et al., 2019, Fan et al., 2019). Polymer-fullerene blends-based bulk-heterojunction polymer solar cells have gained good attention over the past decade and the power conversation efficiencies have reached over ~16 % (Fan et al., 2019). Moreover, it is still difficult to extend the absorption of fullerene derivatives into the near-infrared regions of the solar spectrum (Lei et al., 2016).

In recent years, many efforts have focused on developing optimal polymer donor and polymer-acceptor combinations with well-controlled bulk-heterojunction morphologies. Among the non-fullerene acceptors, naphthalene diimide-based copolymers have been the most successful polymer acceptors with high electron affinities and high electron mobilities, which are a result of their highly extended π -conjugated structure and strong π - π intermolecular interaction. The power-conversion efficiencies of all-PSCs have improved greatly to ~ 10 – 14.4 %, and there is still great potential for further enhancement, provided that simultaneous adjustment of polymer-donor and polymer-acceptor energy levels can improve their light harvesting and increase the open-circuit voltage. Compared with conventional polymer-fullerene solar cells, all-PSCs can potentially exhibit much better mechanical strength and stability, because polymer acceptors are not only intrinsically more ductile than fullerenes but also are entangled with other polymers within the acceptor domain and at the interface. In consideration of the application of PSCs in flexible devices, the mechanical properties of the all-PSCs should be investigated. All-PSCs are better candidates than fullerene-based solar cells for applications in flexible and portable electronics. The better performance of the all-PSCs was attributed to the high open circuit potential of 1.06 V. The optimized BHJ active layers of polymer donor and acceptor with favorable interfacial interactions. Kim et al. also studied the mechanical properties of the all-PSCs and found that, compared with fullerene-based blend films, all-polymer blend films offer superior flexibility, stretching and bending properties.

2.3 n-Type All-Polymer Solar Cells Application

In 1995, the history of the polymer acceptors was started as early as the fullerenes, but their progress lags far behind. Primarily n-type polymers such as cyanated polyphenylenevinylenes (Kietzke et al., 2005), benzothiadiazole (Arias et al., 2001, McNeill et al., 2007) and rylene diimide-based polymers (Guo et al., 2015). The polymers based on rylene diimide such as perylene diimide, naphthalene diimide, and naphtho [2,3-b:6,7-b'] dithiophene-4,5,9,10-diimide are among the most efficient acceptors for all-PSCs.

In 2007, Zhan et al. synthesized the first perylene diimide-based polymer, PDI-co-dithienothiophene, and investigated the photovoltaic performance. After modulation of the chemical structures of PDI-based polymer and utilization of promising p-type polymers, the

photovoltaic performance improved gradually. In 2011 and 2014, PCEs of 2.2 % (Zhou et al., 2011) and 4.1 % (Zhou et al., 2014) were realized by utilizing PDI-co-carbazole and PDI-co-thiophene copolymers, respectively. In 2016, Yan *et al.* adopted a vinylene-bridged PDI-based polymer and achieved a high PCE of 7.57 %, which is also the highest value for PDI-based polymers (Guo et al., 2016). Perylene diimide has the most effective acceptor in the polymer solar cells field because of its properties of solubility, environmental stability and thermal stability, low cost, broad and strong absorption (Ganesamoorthy et al., 2017).

NDI-based copolymers have been the most successful polymer acceptors among the non-fullerene acceptors by having both high electron affinities and electron mobilities, which are a result of their highly extended π -conjugated structure and strong π - π intermolecular interaction. For instance, PBDTTTPD as the electron donor, P(NDI2HD-T) as the electron acceptor. Therefore, based on the above materials, the BHJ all-PSCs of PBDTTTPD-P(NDI2HD-T) showed a PCE of 6.64 %, which is higher than that of PBDTTTPD-PCBM BHJ PSCs PCE of 6.12 % (Kim et al., 2015). Studies on NDI-based acceptor polymers (Yan et al., 2009), for organic photovoltaic began with the work of Loi and co-workers in 2011 (Fabiano et al., 2011). They studied the photovoltaic properties of the classic NDI-co-bithiophene copolymer (N2200) in the blend with the P3HT and achieved a high fill factor of nearly 70 %, suggesting high charge separation efficiency and balanced electron and hole mobility. In 2013, Zhou et al. synthesized a n-type polymer of NDI-co-carbazole and achieved a PCE of 3.6 % (Zhou et al., 2013) and almost at the same time, Jenekhe et al. also realized a PCE of 3.3 % by using a polymer of NDI-co-selenophene (Earmme et al., 2013). In 2014 and 2015, all-PSCs based on NDI-based polymers realized high PCE of 5.7 % (Mori et al., 2014) and 7.7 % (Hwang et al., 2015) by both the material designs and the device optimizations. In 2016, Li *et al.* utilized medium bandgap benzodithiophene-alt-benzotriazole copolymers as the donor and N2200 as the acceptor to achieve the highest PCE of 8.27 % with a high FF of 70.24 % (Gao et al., 2016). Up to now, NDI-based polymers were the most efficient polymer acceptors in all-PSCs (Schubert et al., 2014, Geng et al., 2015, Wang et al., 2015, Xiao et al., 2015). All-PSCs is an effective approach to further promote the state-of-the-art all-PSC technique at this early stage. NDI-based copolymers, (Mori et al., 2013, Zhou et al., 2014, Earmme et al., 2014, Mori et al., 2014, Zhou et al., 2013) especially P(NDI2OD-T2), also known as Activink N2200, (Yan et al., 2009) have

been demonstrated the most effective acceptors in all-PSCs as their superior properties in thermal stability, electron affinity, mobility and absorption coefficient in the visible and near-infrared wavelength region. The blending of polymeric materials of P(NDI2OD-T2) as an acceptor and P3HT as a donor were investigated as of photovoltaic properties of solar cells. In 2011, Sirringhaus et al. reported that the PCEs 0.21 % and 0.17 % were the initial P3HT:P(NDI2OD-T2) blends solar cell (Moore et al., 2011) and Fréchet et al. (Holcombe et al., 2011), respectively. Again, in this year for the first time Loi et al. obtained a high FF of 0.67% for P3HT/P(NDI2OD-T2) blends solar cells which is comparable to the polymer: fullerene blends efficient values reported (Fabiano et al., 2011). However, the PCE of these devices was 0.16 %, because of their limited J_{sc} value of 0.48 mA cm^{-2} . The entropy of mixing has an effect for the formation of large domains in these two polymers, which is driven by preferential segregation and crystallization, is the dominating factor behind the relatively poor J_{sc} , which limits the overall device performance (Yan et al., 2012). In 2012, the poor J_{sc} was improved by the addition of chloronaphthalene suppressed the pre-aggregation of P(NDI2OD-T2) in solution (Schubert et al., 2012, Steyrlleuthner et al., 2012). For P3HT:P(NDI2OD-T2) blends which were prepared from a mixture of p-xylene and cyanonaphthalene as spin-coating solvent a PCE of 1.4 % with a J_{sc} of 3.77 mA cm^{-2} and an FF of 0.65 results were achieved (Schubert et al., 2012).

Compared with above-mentioned two rylene dimides, Naphthodithiophene Diimide is a relatively new class of building block (Fukutomi et al., 2013) with an extended π -plane of thiophenes. It was first used in all-PSCs by Zhou and co-workers in 2014 (Zhou et al., 2014). A polymer acceptor based on NDTI and bithiophene exhibited an extended absorption in NIR region up to 900 nm and achieved a PCE of 2.59 % in all-PSCs with PTB7 as the donor. In 2016, a comprehensive study was carried out on NDTI-based copolymers with thiophene, thienothiophene, and dithienothiophene units (Nakano et al., 2016). Interestingly, PNDTI-T and PNDTI-DTT showed a face-on orientation, but PNDTI-TT gave an edge-on orientation to the substrate due to the difference of the linearity for the polymer main chain. A highest PCE of 3.6 % and J_{sc} of 10.7 mA / cm^2 were achieved in PSC with PNDTI-DTT as the electron acceptor and PTB7 as the electron donor. Because of the strong absorption spectra in the near-infrared region for NDTI-based polymers, higher J_{sc} could be obtained after choosing suitable large band

gap p-type polymers. As shown in Figure 2.1, PDI- and NDI-based photovoltaic materials have achieved a rapid growth in recent years with PCEs exceeding 7.5 % and 8.2 %, respectively. Although NDTI-based polymers still show lower PCE than PDI- and NDI-based polymers, considering the limited number of the PNDTI-based materials and only preliminary investigations on the photovoltaic applications, there is much room for improvement (Yang et al., 2017). Figure 2.2, shown the chemical structures of the three rylene diimide-based n-type polymers of PPDI-DTT, PNDI-DTT and PNDTI-DTT (Yang et al., 2017).

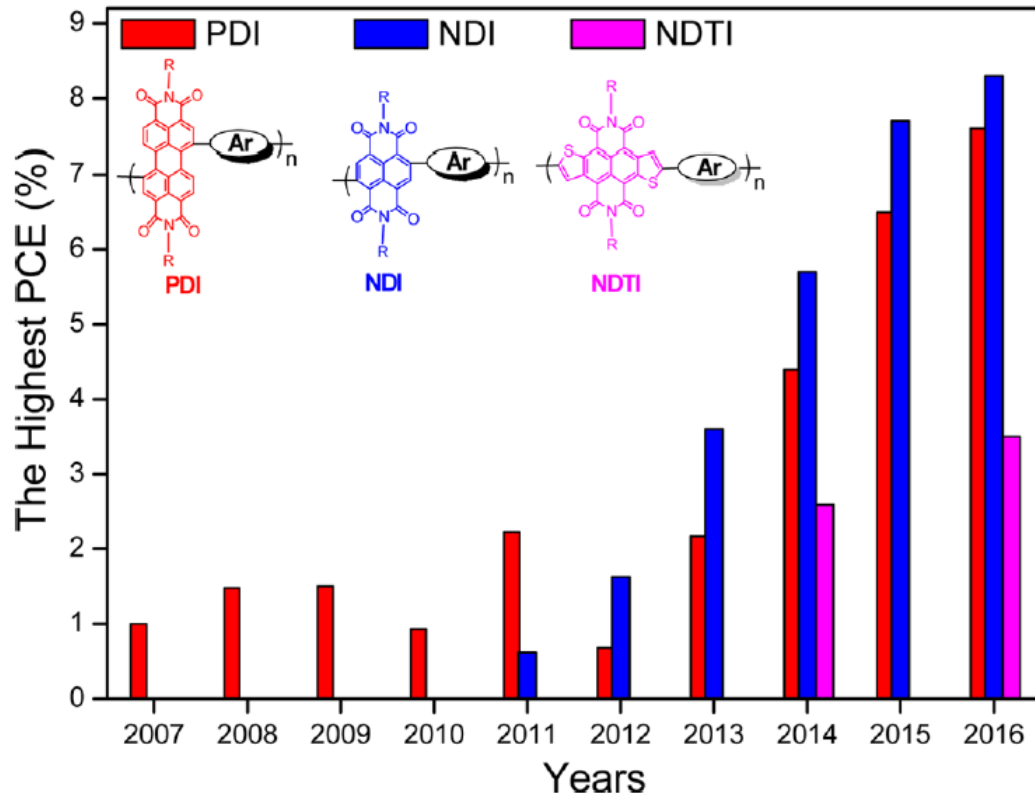


Figure 2.1 Summary of the development of three kinds of rylene diimide polymers for all-PSC application (adapted from (Yang et al., 2017)).

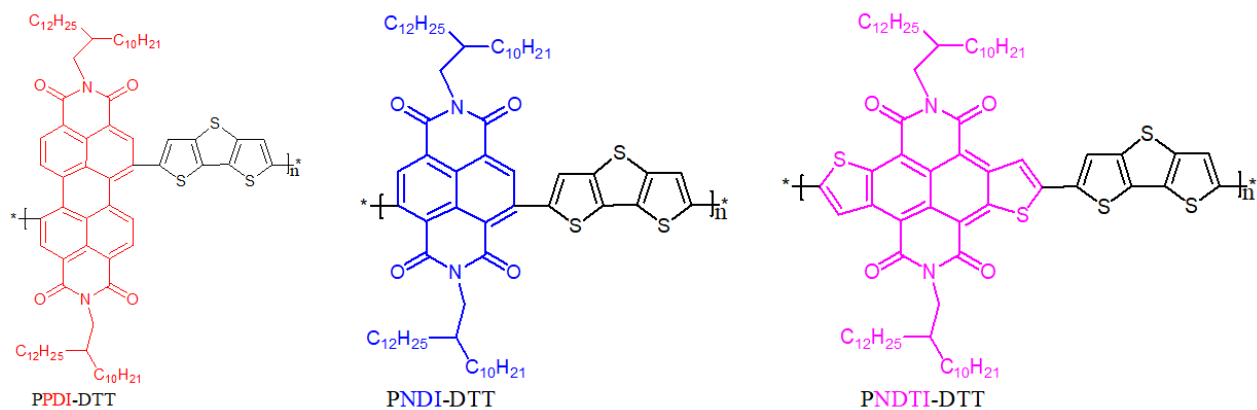


Figure 2.2 The chemical structure of the three rylene diimide-based n-type polymers of PPDI-DTT, PNDI-DTT and PNDTI-DTT (adapted from (Yang et al., 2017)).

2.4 Organic Solar Cells

Organic solar cells have a photoactive layer of organic semiconductors, also known as the active layer or active film of the device, which is used for harvesting solar energy. The three most common types of organic (or semi-organic) solar cells are all-polymer solar cells, polymer-fullerene solar cells and polymer-nanoparticles solar cells. Organic solar cells are currently viewed as promising power generation technologies that can be integrated into these devices because they are lightweight, semitransparent and flexible (Thompson and Frechet, 2008, shrotriya, 2009). To date, most highly efficient OSCs have been based on polymer-fullerene blends, in which fullerenes such as phenyl- C_{61} -butyric acid methyl ester act as the electron acceptor. However, fullerenes are not ideal acceptor materials due to many intrinsic issues, such as weak light absorption and un-optimized energy levels, limiting the design adaptability of the electron donor pair. Moreover, fullerene-based OSCs have low flexibility and stretch ability due to the brittle crystalline features of the fullerenes (Lipomi et al., 2012, Savagatrup et al., 2015). To resolve these drawbacks, a number of non-fullerene acceptors, including small molecules, nanoparticles and polymers, have been developed to replace fullerenes (Moore et al., 2011, Zhou et al., 2011, Anthony, 2011).

One of the reasons for using organic materials is to reduce environmental problems, which is the major concern nowadays. At the same time, using organic materials should reduce

production costs, provide a large surface area for light absorption (Zhu et al., 2007), and consume less energy. Organic solar cell is divided into two types-polymer solar cell and small molecule solar cell. These two types of organic electronics materials are essential for light absorption and charge flow. General differences between these solar cells are the materials used in accordance with their constituent molecules, either small or large (polymers), as well as their preparation technique. Spin coating or ink-jet printing is the common technique to fabricate polymer solar cell, whereas small molecule solar cells are processed by thin film deposition techniques in vacuum condition (Mühlbacher et al., 2006).

2.4.1 The Bulk-Heterojunction Solar Cell

Solution-processed polymer-polymer BHJ solar cells, consisting of a conjugated polymer donor and a conjugated polymer acceptor, have advantages including tunable chemical and electronic properties, morphological stability and enhanced mechanical properties (Lei et al., 2016). The concept of bulk-heterojunction solar cell was to improve the performance of organic bilayer solar cells. This is because, in the organic bilayer structure, only a small number of excitons are collected at the interface of donor and acceptor materials (Kim, 2009). In contrast to bilayer structure, the active layer in the bulk-heterojunction structure is extended. This is a result of mixing an electron donor and an electron acceptor together. This is to increase light absorption and improve efficiency of the optical thickness of the film while maintaining the current flows (Mühlbacher et al., 2006, Peet et al., 2007, Zhou et al., 2012). In other words, the separation of charge in the bulk-heterojunction structure occurs in the whole surface of active layer compared to the bilayer structure that only occurs in the interlayer. Thus, the tendency of excitons dissociation is higher in the bulk-heterojunction type. The major issue for OPV is to find suitable materials of the active layer to improve the interface, charge separation, excitation, and efficiency.

2.4.2 Working Mechanism of Photovoltaic Device

Figure 2.3 is a schematic illustration of the working mechanism of polymer/polymer blend solar cells. Photovoltaic conversion processes can be divided into several sequential processes: (a) absorption of an incident photon by the constituent polymers, leading to the

formation of polymer singlet excitons; (b) diffusion of the excitons to a donor/acceptor domain interface (heterojunction); (c) charge transfer at the interface driven by either the LUMO-LUMO or HOMO-HOMO energy offsets of the donor and acceptor polymers, along with dissociation of the interfacial charge transfer state into free charge carriers; and (d) transport of the free charge carriers to the anode and cathode through bicontinuous networks of donor (hole-transporting) and acceptor (electron-transporting) polymers (McNeill and Greenham, 2009, Clarke and Durrant, 2010, Ohkita and Ito, 2011, Ohkita and Ito, 2013, Ohkita et al., 2016). As a result, the incident photon energy can be converted into electricity and a direct current is supplied to an external circuit. Among these conversion processes, exciton diffusion to the domain interface is particularly important, because the diffusion length of a polymer singlet exciton (L_D) is typically as short as only 10nm (Mikhnenko et al., 2012, Mikhnenko et al., 2015, Wang et al., 2014, Tamai et al., 2014, Tamai et al., 2015).

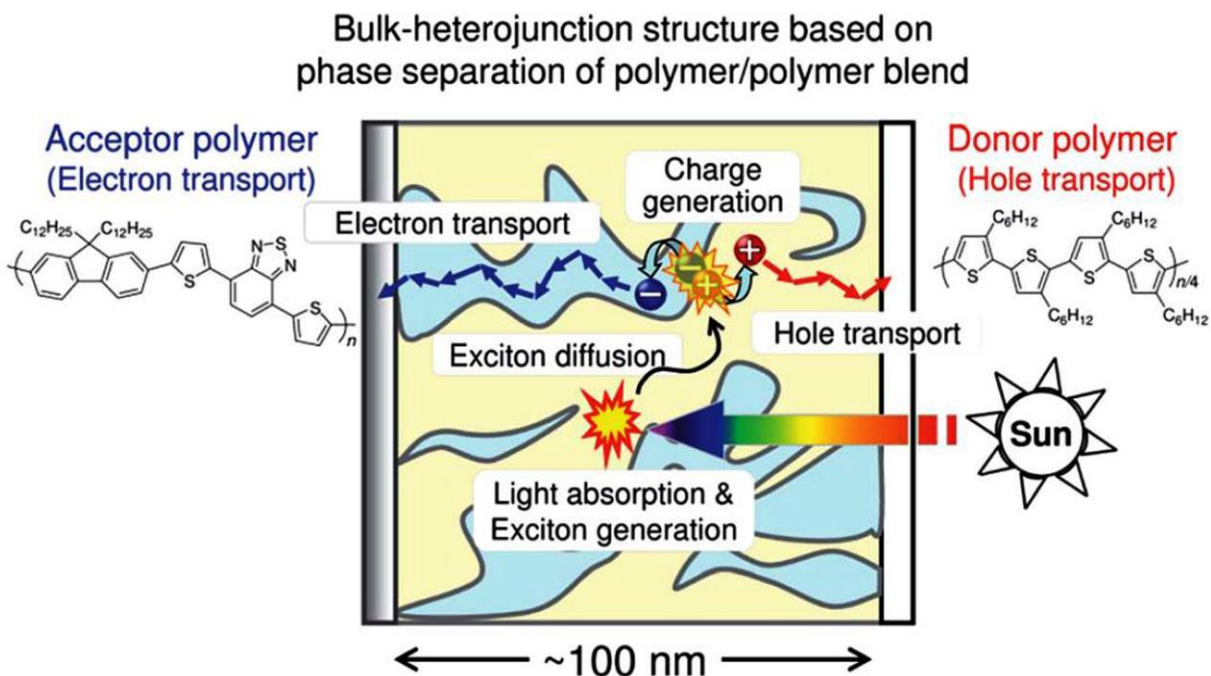


Figure 2.3 Photovoltaic conversion processes in polymer/polymer blend solar cells: (a) exciton generation via photon absorption; (b) exciton diffusion at a donor/acceptor interface; (c) charge transfer at the interface and charge dissociation into free charge carriers; and (d) charge transport to each electrode (adapted from (Ohkita et al., 2016)).

The overall photovoltaic performance is, thus, significantly affected by the morphological characteristics of the blends, such as the domain size, domain composition (purity), and domain connectivity. The ideal BHJ structure for efficient charge generation and transport is considered to be a nanostructure blend based on bicontinuous interpenetrating networks of pure donor and acceptor domains with a characteristic spacing length of ~ 10 nm, which is comparable to L_D . Therefore, excitons generated at a distance of more than 10nm from the donor/acceptor domain interface cannot contribute to the photocurrent generation. In addition, even if charge carriers are converted from the excitons, the charges generated in isolated polymer domains cannot be transported by the electrodes.

2.5 Morphological Characterization of Thin-Films Using AFM and XRD Techniques.

The morphology of the active film is important for the efficiency of the solar cells. A common way to achieve a favorable morphology is to use a bulk heterojunction, which contains random domains of the two polymers throughout the whole structure. Several parameters affect the microstructure of an organic film, such as (Moons, 2002): chemical structure of the donor-acceptor, solvent used for processing materials, concentration of the materials used in solution during processing, the donor-acceptor ratio and the choice of post-production treatments, such as thermal annealing at different conditions and exposing the resulting film to different solvents. Long polymer chains do not normally gain enough entropy by mixing for a homogeneously mixed phase to be energetically favorable (Moons, 2002). Therefore, the thermodynamically stable situation should involve a phase separation. The kinetics of film manufacturing may, however, not allow for thermodynamic equilibrium to be reached. If the solvents evaporate fast enough, the polymer chains may be frozen in a morphology that does not correspond to thermodynamic equilibrium (McNeill, 2012). Annealing may then give the film opportunity to approach a more thermodynamically favorable morphology (Bavel et al., 2010). Thermal annealing is also good for mimicking conditions under which the device may have to operate (Bavel et al., 2010). It is believed that an ordered structure of the film is favorable. An ordered structure is assumed to give better charge transport and larger delocalization of charge carriers (Schubert et al., 2014). There have been indications that the relative direction of the crystallites in donor and acceptor is important for the efficiency. In a system of the two polymers P3HT as

donor and N2200 as acceptor, is also known as P(NDI2OD-T2). The charge dissociation would have been more efficient if the polymer chains in the crystal grains on adjacent sides had been parallel at the interface between donor and acceptor (Schubert et al., 2014).

The P(NDI2OD-T2) has the property of strong tendency of chain aggregation in solution which leading to form a more “face-on” crystallites orientation of the conjugated backbone is showed in the bulk of the film which indicates the lamellae confirmed by GIWAXS, from the technique of as-cast films, Figure 2.4a. The photophysical evidence was reported for this chain aggregation. A high aggregate content of ~45 % was obtained from solution via the coiling of individual polymer chains with film formation due its chain collapse. During spin-coating and drying techniques the flattening of the globuli will cause the formation of face-on lamellae. The most important thing in polymer property is polymer with shorter chain is less likely to aggregate and will be more soluble than longer molecular weight chains. Information about the surface morphology of the as-cast, melt-annealed, and zone-cast films which were all show different surface morphologies can be obtained from AFM images, as shown in Figure 2.4a-c, as of Scherrer investigated of the width of the (100) peak) the films regardless of showing similar surface slant angles and bulk crystal grain size, $\alpha \approx 33^\circ \pm 3^\circ$ and 20 ± 2 nm, respectively. As we see on Figure 2.4c, by zone-casting technique the highly aligned P(NDI2OD-T2) film was produced. This information will give us to understand the film drying conditions can affect the upper part of the film surface morphology. All films adopt a similar edge-on surface orientation. This “edge-on” orientation is also observed at the surface of the film with surface-sensitive NEXAFS spectroscopy, but P(NDI2OD-T2) films formation is independent of both substrate and solution processing. The reason is because of the high-performance top-gate transistors fabricated on different substrates by a range of deposition techniques (spin-coating, gravure, flexographic, and inkjet printing) (Schuettfort et al., 2011, Schuettfort et al., 2013, Zerson et al., 2016).

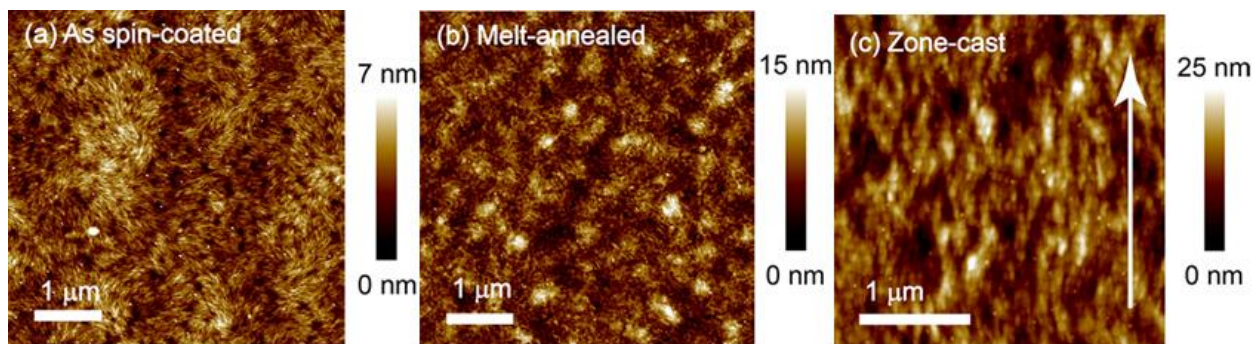
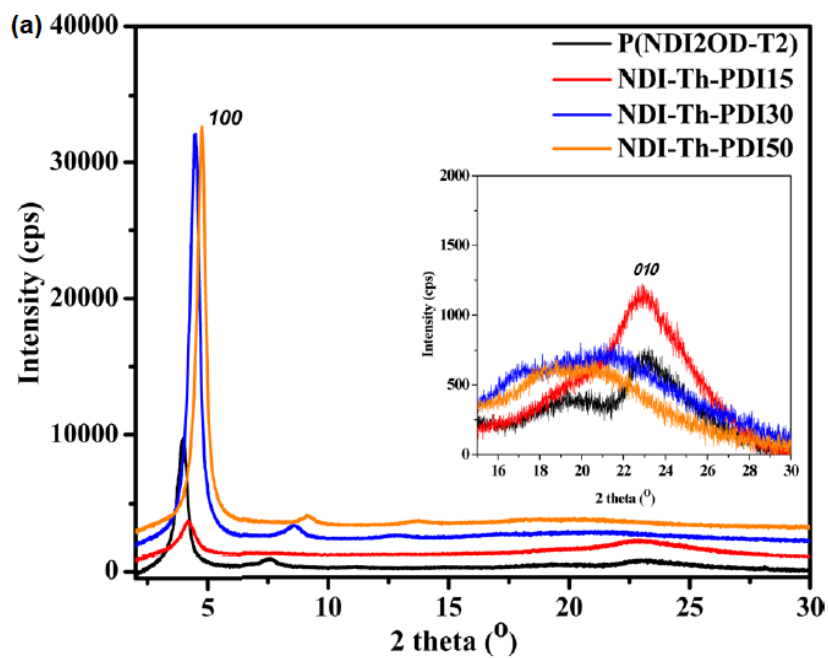


Figure 2.4 Atomic force microscopy images of the surface topography of (a) as-cast, (b) melt-annealed, and (c) zone-cast films. The arrow in (c) indicates the zone-casting direction (adapted from (Schuettfort et al., 2013)).

The reference polymer P(NDI2OD-T2) and new n-type random copolymers were analyzed using wide-angle X-ray diffraction measurement for their studies on bulk crystalline and molecular packing nature. The X-ray diffraction patterns for thin films of copolymer which were spin-coated on glass substrate and also thermally annealed at 160 °C for 10 min shown in Figure 2.5a and b. And also, in Table 2.1, the relevant data obtained from X-ray diffraction patterns are given. At angle $2\theta = 4.06^\circ$ with corresponds to the peak (100) we can observe lamellar crystalline from X-ray diffraction pattern for the reference polymer P(NDI2OD-T2) and also at $2\theta = 23.10^\circ$ the π - π stacking peak (010) observed, which corresponded to lamellar packing distance of 21.72 Å and π - π stacking distance of 3.84 Å. At $2\theta = 4.21^\circ$, 4.58° , and 4.80° with d-spacing 20.96, 19.27, and 18.38 Å for NDI-Th-PDI15, NDITh-PDI30, and NDI-Th-PDI50, respectively, the lamellar peak (100) for random copolymers was observed. With increasing incorporation of PDI moiety in the random copolymer chain the lamellar packing distance was diminished gradually, but in contrast the π - π stacking distance increased linearly (Figure 2.5a, inset). In reference polymer P(NDI2OD-T2) is started to increase from 3.84 Å to whereas in NDI-Th-PDI15, NDI-Th-PDI30, and NDI-Th-PDI50, 3.85, 3.93, and 4.00 Å, respectively. In general, in Figure 2.5b, sharp and intense peaks with the lamellar ordering are observed up to third order in X-ray diffraction patterns for all the random copolymers of NDI-Th-PDI_x, this indicating that due to their highly crystalline nature (Sharma et al., 2016).

Table 2.1 Thin-film XRD data of thermally annealed random copolymers of P(NDI2OD-T2) and NDI-Th-PDI_x random copolymers (adapted from (Sharma et al., 2016)).

2θ (deg.)		d -spacing (Å)	
(100)	(010)	d_{100}	d_{010}
4.06	23.10	21.72	3.84
4.21	23.03	20.96	3.85
4.58	22.59	19.27	3.93
4.80	21.92	18.38	4.00



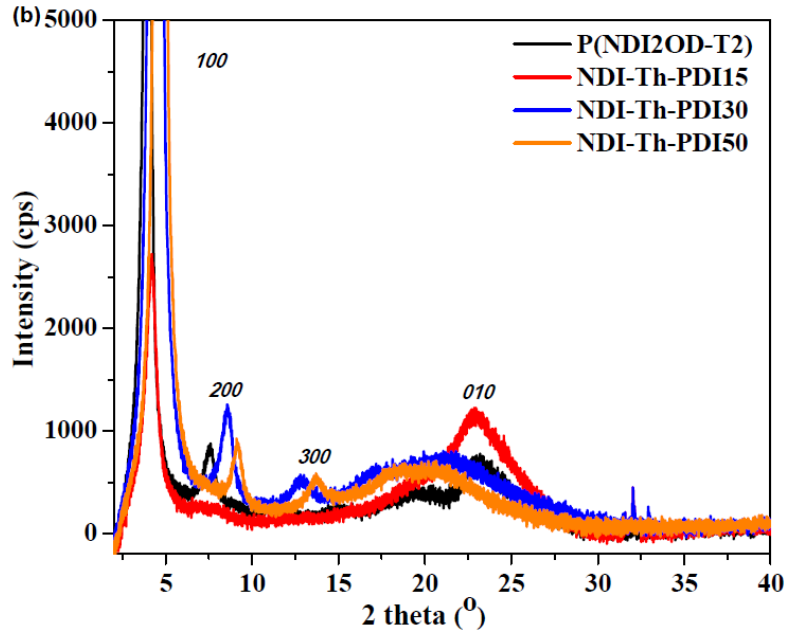


Figure 2.5 (a) and (b) thin-film XRD diffraction patterns of reference P(NDI2ODT2) and random copolymers (adapted from (Sharma et al., 2016)).

The polymer topography and height profile which scanned by AFM were shown in Figure 2.6. The root-mean-square roughness value for PCPDTBT(C5) and PCPDTBT (D5) from 1.16 nm - 4.33 nm to 10.8 nm, respectively, which resulted in increased surface area were due to the addition of ordering agent (OA) roughened the polymer surface. The importance of introducing OA in to films has an effect which produced both roughened the polymer surface and unique nano-morphology. Both PCPDTBT(C) and PCPDTBT(D) films have nano-fibril-like morphology and rough morphology, respectively. In Figure 2.7, the CN-driven morphology has shown that a high-resolution image in which this information tells as a fibril is composed of several circular polymer domains in a row. For domain formation there is no any known exact mechanism, but Liu et al. proposed that while spin coating, a polymer can be aggregate in solution and form fibril-like aggregates by using high boiling point additives. Having the above information, it can be suggested that the major cause of having different nano structures on the polymer surface is due to the OAs has different chemical structure.

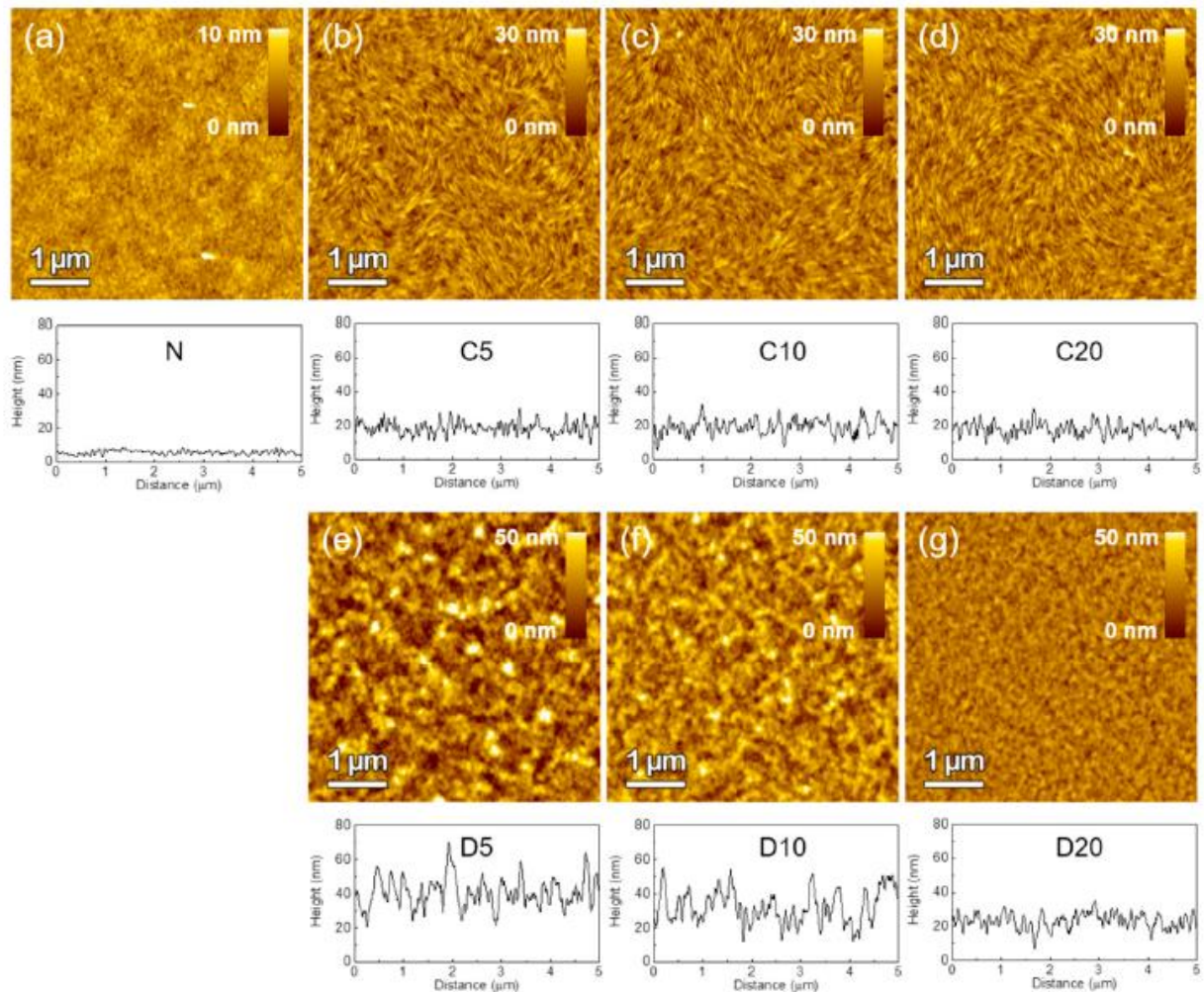


Figure 2.6 Atomic force microscopy images of the ordering agent-induced polymer surface morphology and height profile. PCPDTBT (a) without OA; (b) with 5 vol % 1-chloronaphthalene; (c) with 10 vol % CN; (d) with 20 vol % CN; (e) with 5 vol % 1,8-diiodooctane; (f) with 10 vol % DIO; and (g) with 20 vol % DIO (adapted from (Hwang et al., 2017)).

Both CN and chlorobenzene solvents have a similar benzene ring-based structure and polymer main chain, while DIO has no conjugated rings. Accordingly, there is stronger π - π interactions in between CN-containing solvent with the polymer main chain than the DIO-containing solvent. This evidence gives distinct fibril array morphology formation (Hwang et al., 2017).

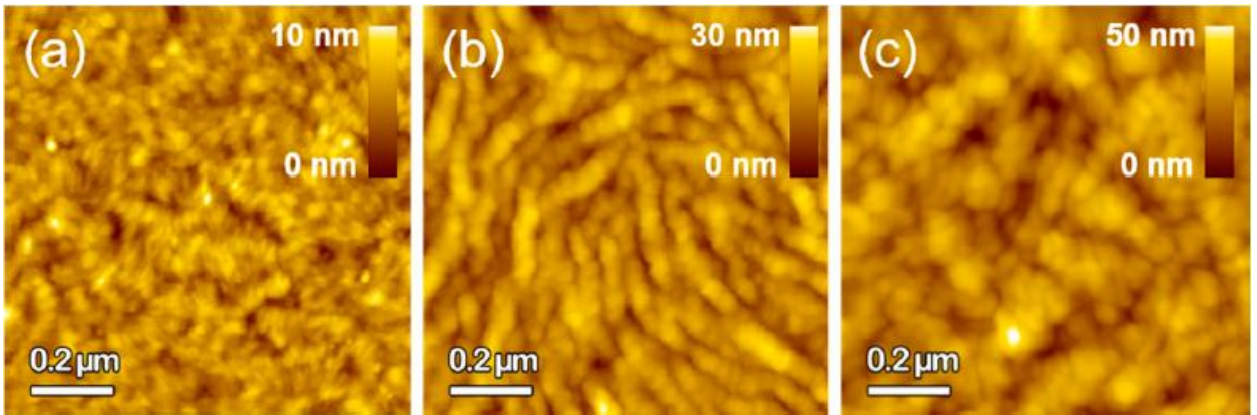


Figure 2.7 The surface topography of ordering agent-driven PCPDTBT film scanned by an atomic force microscope. $1 \times 1 \mu\text{m}$ (a) PCPDTBT(N), (b) PCPDTBT(C5), (c) PCPDTBT(D5) (adapted from (Hwang et al., 2017)).

An instrument grazing-incidence wide-angle X-ray scattering (GIWAXS) was used on study of PCPDTBT films in which a silicon wafer spin-coated on PEDOT:PSS to investigate the crystalline structure of the nanostructured polymer films. Figures 2.8a-d shows in-plane (IP) and out-of-plane (OOP) line-cuts profiles of PCPDTBT(N), PCPDTBT(C5) and PCPDTBT(D5), PCPDTBT(C) and PCPDTBT(D) diffraction patterns and profiles of the other PCPDTBT films with different OA volumes. For each film the results of diffraction peak analysis were summarized in Table 2.2. As other studies reported that the both the peak position values (q) and full-width at half-maximum values (Δq) are showed similar consistent (Guilbert et al., 2014, Liu et al., 2012). The PCPDTBT(N) film shows a peak at $q_z \approx 1.57 \text{ \AA}^{-1}$ in the OOP X-ray profiles, which corresponds to the π - π stacking reflection of (010). The peak (010) intensity indicates much weak in both PCPDTBT(C) and PCPDTBT(D) films, which confirms no π - π stacking occurs along the direction normal to the substrate. The Δq value for the peak (100) is reduced in the OOP profiles, due to this peak indicates that the inter-chain separation within lamellae. The increases of both domain size and crystallinity in polymer associated with the reduction of full-width at half-maximum values. Besides to this the coherence length (ξ) increased for both C5 and D5 from 28.0 nm - 51.0 nm to 61.3 nm, respectively which reveals a larger size of the ordered domains.

Table 2.2 Grazing-incidence wide-angle X-ray scattering (GIWAXS) diffraction peak analysis of PCPDTBT(N),PCPDTBT(C5) and PCPDTBT(D5) films (adapted from (Hwang et al., 2017)).

OA	Index	q^a (\AA^{-1})	d^b (\AA)	Δq^c (\AA^{-1})	ξ^d (\AA)
N	OOP (100)	0.555	11.3	0.202	28.1
	OOP (010)	1.58	3.98	0.294	19.2
	IP (001)	0.489	12.9	0.199	28.4
	IP (010)	1.44	4.36	0.455	12.4
C5	OOP (100)	0.548	11.5	0.111	51.0
	IP (001)	0.538	11.7	0.0856	66.1
	IP (010)	1.62	3.89	0.184	30.8
D5	OOP (100)	0.549	11.4	0.0922	61.3
	IP (001)	0.532	11.8	0.0945	59.9
	IP (010)	1.62	3.89	0.140	40.3

^aPeak position; ^bspacing distance; ^cfull-width at half-maximum; ^dcoherence length, calculated using the Scherrer equation ($\xi = 2\pi/\Delta q$).

After OA addition, in the IP line-cut profile the intensity of the (010) plane became stronger and which leads to the coherence length increased in the IP direction. For both PCPDTBT(C5) and PCPDTBT(D5), the peak positions slightly shifted to higher values ($q_{xy} \approx 1.62 \text{ \AA}^{-1}$) means that a decrease in the π - π stacking spacing to $\sim 3.89 \text{ \AA}$ was observed. The spacing distances along the polymer backbone direction is due to the (001) reflection in the IP profile and also for (010) shows similar changes. To conclude that from GIWAXS profile the incorporation of both CN and DIO solvents into the PCPDTBT solution would bring significantly enhanced the polymer ordering in the edge-on direction after spin coating, while both the mixed face-on and edge-on orientations belongs to the PCPDTBT(N) film in Figure 2.9 (Hwang et al., 2017, Guilbert et al., 2014).

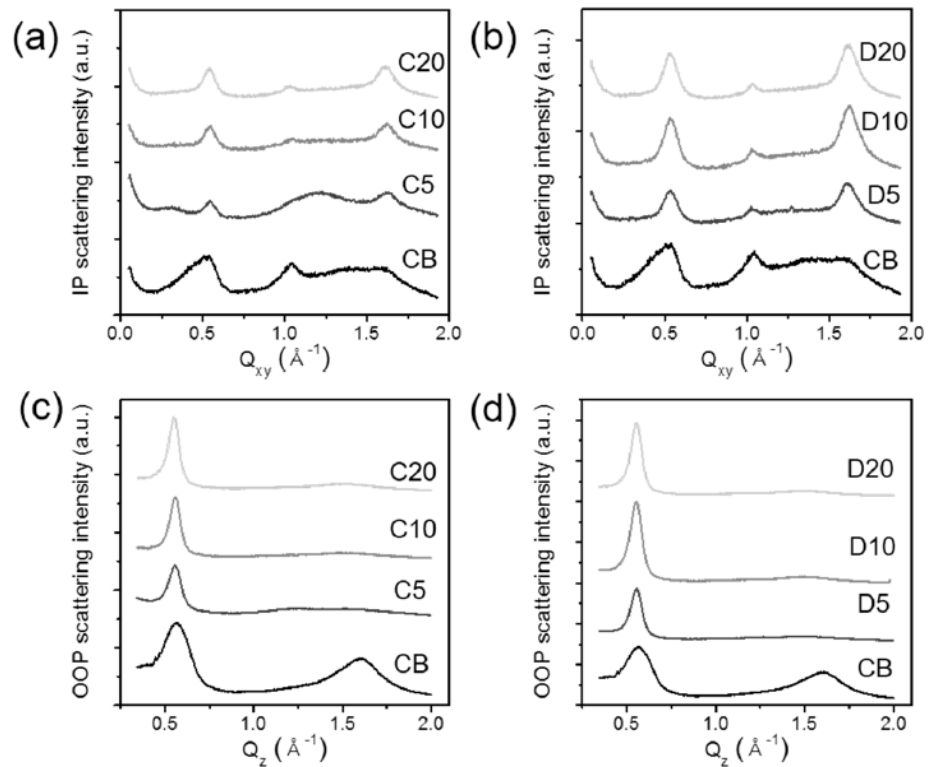


Figure 2.8 In-plane (IP) and out-of-plane (OOP) line-cuts from GIWAXS images. (a) IP and (c) OOP X-ray scattering profiles of PCPDTBT(C), (b) IP and (d) OOP X-ray scattering profiles of PCPDTBT(D) (adapted from (Hwang et al., 2017)).

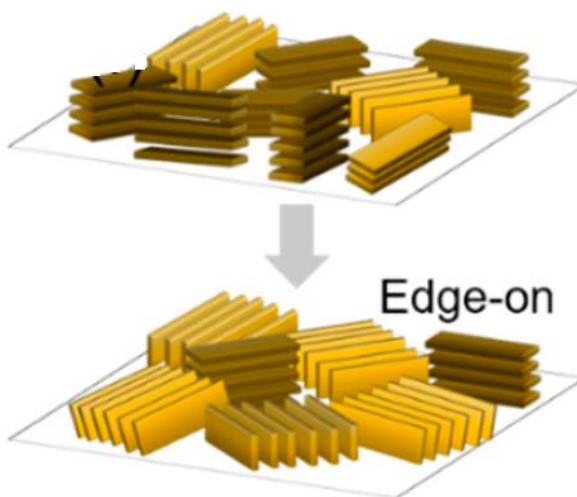


Figure 2.9 The proposed PCPDTBT film orientation change after OA addition.

2.6 Methods for Determining the Solubility Parameter

Solvent selection is approximated by the solubility parameter for coating materials. Even to predict the compatibility of polymers and others materials solubility parameters have been used. During polymer synthesis to avoid phase separation the solvent selection is crucial so as to develop stable situations which meet environmental friendship, safety and quality standards. The basic principle of “like dissolves like” applied to polymers. A polymer will dissolve in solvents when it’s solubility parameters matching with the solvent. May be there are a number of techniques used to determine the solubility parameters, from such techniques let me discusses the three widely applicable to measures polymer solution are the Hildebrand, Hansen and contact angle solubility parameters. The Hildebrand δ used a single parameter, defined as the square root of the cohesive energy density ($\delta = (E/V)^{1/2}$), to determine whether a substance is a good solvent or nonsolvent for a polymer. Whereas V is the molar volume of the pure solvent, and E is its (measurable) energy of vaporization. The Hansen model utilizes three parameters, δ_D , δ_p , and δ_H , to quantify polymer solution. These three parameters represent the dispersion, polar, and hydrogen bonding components, respectively, of the Hildebrand parameter δ , such that, $\delta^2 = \delta_D^2 + \delta_p^2 + \delta_H^2$. If visualized as a three-dimensional plot, the axes being $2\delta_D$, δ_p , and δ_H (Venkatram et al., 2019, Hansen, 2007). In general, there are two types of techniques that used for contact angle measurements; which means direct (i.e., the angle value is directly obtained) and indirect (i.e., the value of the contact angle is calculated) contact angle measurements. The most commonly employed techniques of direct measurement on the profile is called sessile and liquid drop, and the adhesion air bubble methods. In order to determine the contact angle, directly creating a tangent line to the profile at the point of contact of three phases, Figure 2.10. Using telescope integereated with a goniometer eyepiece, on imaged of the drop profile the angle can be directly measured. Among the direct contact angle measurement methods, the technique of using sessile drop has more advantages compered to adhering air bubble methods because of some complications of solubility and swelling can be dealt wth more easily with the sessile drop method. The adhering air bubble method has minimizing contamination from airborne substances. Among the different methods of determing the solubility parameter above, why I prefer to apply ramé-hart model 290-F1 standard goniometer cntacte

angle measurement to measure solubility parameter value because of the technique is popular model with scholars due to wide spectrum of demanding tasks it can perform and very simple and as well as time saving to apply it (Li and Neumann, 1990, Li and Neumann, 1992, He, 1989).

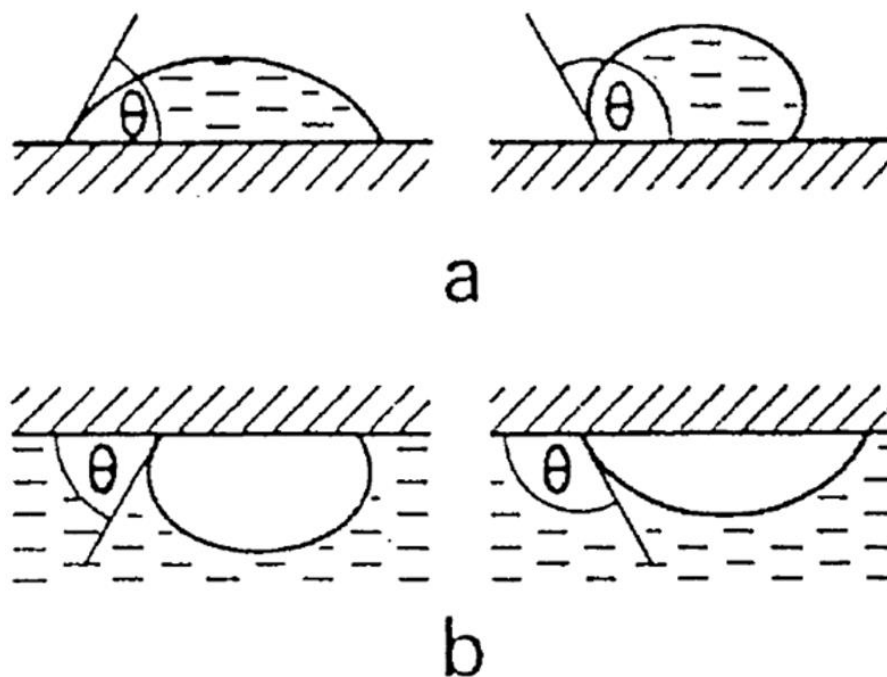


Figure 2.10 Constructing a tangent to the profile. (a) sessile drop method, (b) adhering air bubble method (adapted from (He, 1989)).

2.7 Thermodynamics of Polymer Blends

The most important branches in materials science is called polymer blend which has gained considerable attention to meet their multifunctional need (Paul and Newman, 1978, Paul and Barlow, 1980, McNeill, 2012). Due to the negligible mixing entropy, a vast majority of polymer blends are thermodynamically immiscible, leading to the occurrence of phase separation (Bates, 1991). In the process of phase separation, either bicontinuous or droplet morphology will be constructed by a spinodal decomposition mechanism and nucleation and growth mechanism, respectively. For conjugated polymer blends, the phase separation process is always coupled with crystallization, in which blend ratio and quenching temperature will function dramatically (Tanaka and Nishi, 1985).

Therefore, control of phase separation in conjugated polymer blends becomes more complicated and necessary.

From thermodynamics of blends and solutions point of view, mixtures are systems consisting of two or more different components. Blends or mixtures can be categorized according to the miscibility of their phases in homogeneous, one-phase mixtures or heterogeneous, multi-phase systems. One phase mixture consists of completely miscible components, forming homogeneous, uniform and well intermixed systems. Heterogeneous systems consist of different phases, with partly or not miscible components. Miscibility is usually defined by thermo-dynamical dimensions. The two decisive parameters are the entropy and the energetic interactions between components. Entropy always favors mixing whereas it is the energy that influence as entropy is always favored. The free energy is therefore varying mainly because of energy not entropy. For real solution energy term has effect (Machui, 2014).

2.7.1 Flory-Huggins Theory

Blends of two different polymers are likely to form a large phase separated structure; this is an inherent characteristic of polymers with a long main chain. According to the Flory-Huggins theory (Strobl, 2007; Flory, 1953), the change in the Gibbs free energy when two polymers are mixed ΔG_{mix} can be derived as follows:

$$\frac{\Delta G_{mix}}{n\kappa_B T} = \frac{\varphi_A}{N_A} \ln(\varphi_A) + \frac{\varphi_B}{N_B} \ln(\varphi_B) + \chi\varphi_A\varphi_B \quad (2.1.1)$$

where $\varphi_{A/B}$ is the volume fraction of polymer A/B (with $\varphi_A + \varphi_B = 1$), $N_{A/B}$ is the degree of polymerization of polymer A/B, n is the total number of segments, κ_B is the Boltzmann constant, T is the temperature, and χ is the Flory-Huggins interaction parameter. The first two terms on the right-hand side of equation (2.7.1) represent the entropy component, whereas the final term represents the enthalpy contribution. For polymer/polymer blends, the entropy gain is reduced by a factor of $N_{A/B}$. That is, when long polymer chains are mixed, they do not gain sufficient entropy to yield a negative ΔG_{mix} . In addition, in the enthalpy component, χ is an

interaction parameter between two polymers, where a small value of χ is required in order to obtain a well-mixed structure. The entropy terms are negative but small, and the enthalpy of mixing is likely to be positive. Consequently, polymer-polymer blends tend to phase-separate on a micrometer scale, which is undesirable with regard to the photocurrent generation, because the majority of the excitons cannot reach the donor-acceptor heterojunction for charge generation (Mikhnenko et al., 2012, Mikhnenko et al., 2015, Wang et al., 2014, Tamai et al., 2014, Tamai et al., 2015). For polymer-polymer blends, it is, therefore, critically important to suppress phase separation.

2.8 Phase Diagrams

Phase diagrams display specific information in terms of when the phase separation occurs and which phase-separated structure can be formed and therefore can be a suitable guidance to the phase separation of polymer blend (Bates, 1991). The phase diagrams of some polymer/small molecule systems have been depicted by collection of the differential scanning calorimetry data about the phase transition of each component and have been applied to study the thermal stability, crystalline behaviors, and their effect on the device performance (Li et al., 2011, Zhao et al., 2009, Miller et al., 2011). However, phase diagrams based on DSC data merely represent the bulk properties of the polymer/small-molecule system and lack the information about blend solutions from which the photovoltaic devices are prepared. Recently, the ternary phase diagrams, which comprise two solutes and one process solvent, have been drawn based on the theoretical calculation (Kouijzer et al., 2013; Nilsson et al., 2007). From the ternary phase diagrams, the phase-separated process, which is sensitive to the solvent property, components interaction, and blend ratio can be expressed with the evaporation of solvent, while the information about the phase-separated morphology is seldom involved. Meanwhile, for polymer blend systems, the effect of blend ratio and drying time on morphological evolution is rarely systematically investigated.

2.8.1 Phase Diagram of P3HT and PF12TBT Blend Films Drawn According to AFM Images.

In 2015, Zhou, et al. reported that by using both the images of AFM and TEM, a corresponding and approximate phase diagram of the polymer-polymer blends (i.e., P3HT-PF12TBT blend system) based on the morphological evolution with varying blend ratios and drying time can be drawn and is shown in Figure 2.11.

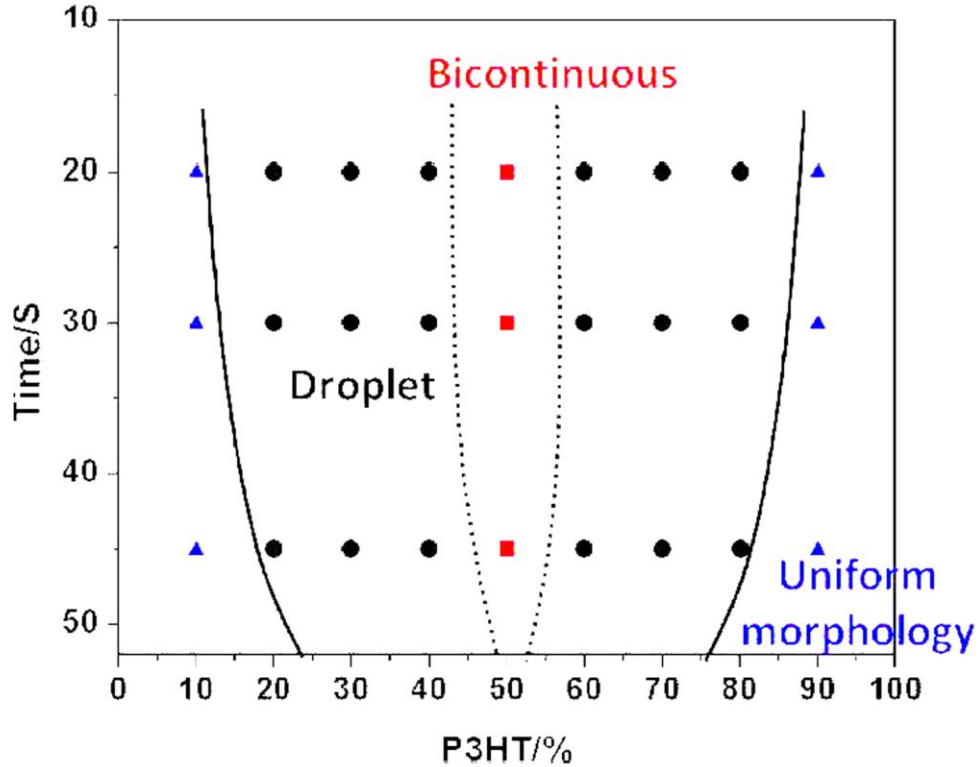


Figure 2.11 Phase diagram of P3HT and PF12TBT blend films drawn according to AFM images. Red squares, black circles, and blue triangles represent bicontinuous, droplet, and uniform phase-separated morphologies, respectively. The dashed line and solid line represent the boundaries between droplet and bicontinuous morphologies and between droplet and uniform morphologies, respectively (adapted from (Zhou et al., 2015)).

When the P3HT weight fraction is 50 %, the thin films display typical bicontinuous morphologies (red squares in phase diagram). When the P3HT weight fraction ranges from 20 % to 40 % and from 60 % to 80 %, the thin films show apparent droplet morphologies (black circles in phase diagram), and an increased domain size can be observed with extended drying

time. The boundary between droplet and bicontinuous morphologies must be located at the middle of 40 % and 50 % or 50 % and 60 % which are marked as the dashed line. When the P3HT weight fraction is greater than 80 % or less than 20 %, there will be no apparent phase separation (blue triangles in the phase diagram) because one of the polymer blends will be dominated (Zhou et al., 2015).

2.8.2 Binary Temperature-Composition Phase Diagram of P3HT: PCBM Blends.

The morphologies of a variety of polymer/fullerene blends useful for solar cells have been studied extensively as a function of blending compositions, casting solvents, annealing conditions, chemical structures, solution concentrations, additives and poling electric fields. Much less attention has been paid to complete characterization of the temperature-composition phase diagram for polymer/fullerene systems. An exception is the recent calculation of the ternary phase diagram of polyfluorene-PCBM-solvent mixtures using the Flory-Huggins model.

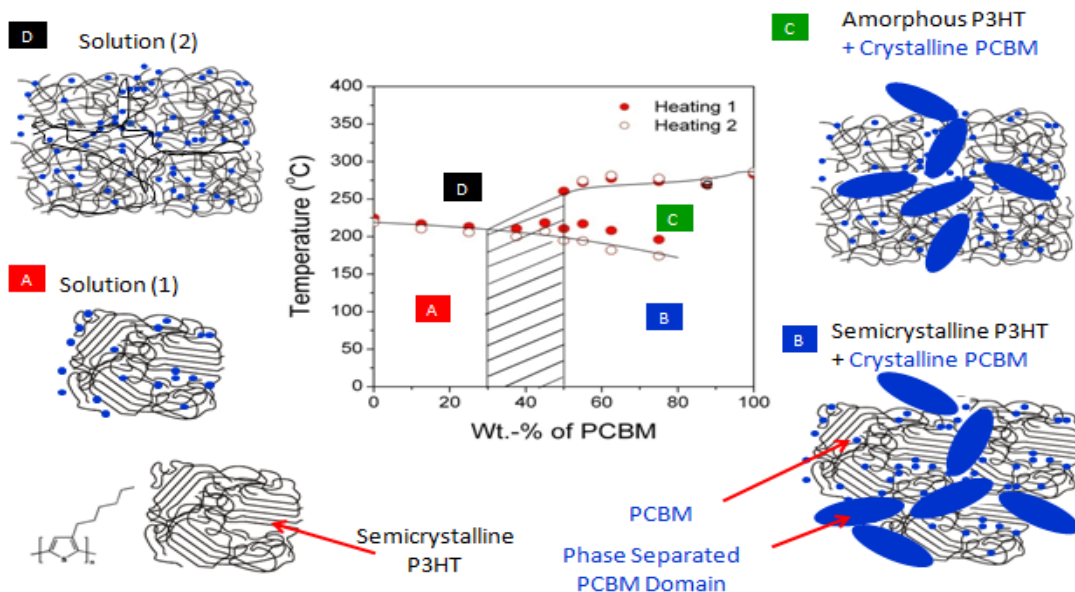


Figure 2.12 Binary temperature-composition phase diagram for P3HT:PCBM blends (adapted from (Kim and Frisbie, 2008)).

A binary temperature-composition phase diagram for P3HT: PCBM blends were also recently reported using thermal analysis and shown in Figure 2.12. Given the central importance

of phase behavior to the performance of BHJ-based polymer solar cells, it seems reasonable to develop a full understanding of the phase behavior of conjugated polymer: PCBM mixtures. In particular, the solubility limit (phase separation points at a given temperature) is an important thermodynamic parameter to control phase separation and nanomorphology in a blend film. Furthermore, the correlation of the phase behavior with electrical transport facilitates better understanding of structure-property relationship in polymer/fullerene blends and may allow the development of rational strategies for improving polymer solar cell performance (Kim and Frisbie, 2008).

2.8.3 Different Phases Formed by Self-Assembly of Coil-Coil Diblock Copolymers in the Bulk as a Function of the Volume Fraction of One of the Blocks.

Recently, from block copolymers (BCPs) properties point of view there were plenty of significant interest generated information to the scientific community these is because of having highly tunable nanoscale self-assembly. BCPs are defined as macromolecules and connected to each other by a covalent bond, which are made up of from two or more blocks of different polymerized monomers. Usually, there are an interaction in between the blocks of BCPs that will bring render them as of incompatible. A microphase separation process will be driven due to this incompatibility situation, as of the presence of covalent bonds are prohibited the bulk phase separation. Therefore, taking in to considerations of the ratio of block lengths, strength of interaction, and as well as a number of blocks will define the polymer chains self-assemble into nanoscopic ordered domains with a morphology. There are possibilities to design BCP macromolecules by modern synthetic chemistry which provides an information with specific length scales and geometries. The main target of such macromolecules showing properties of self-assemble in a hierarchical way on multiple length-scales (i.e., ranging from nanometers to macroscopic sizes), leading to a vast variety of (idealized) nanostructures, in addition to fundamental studies of this macromolecules, which have also a wide spectrum of an applications (i.e., ranging from nanolithography to controlled drug delivery to organic photovoltaics to organic light emitting diodes).

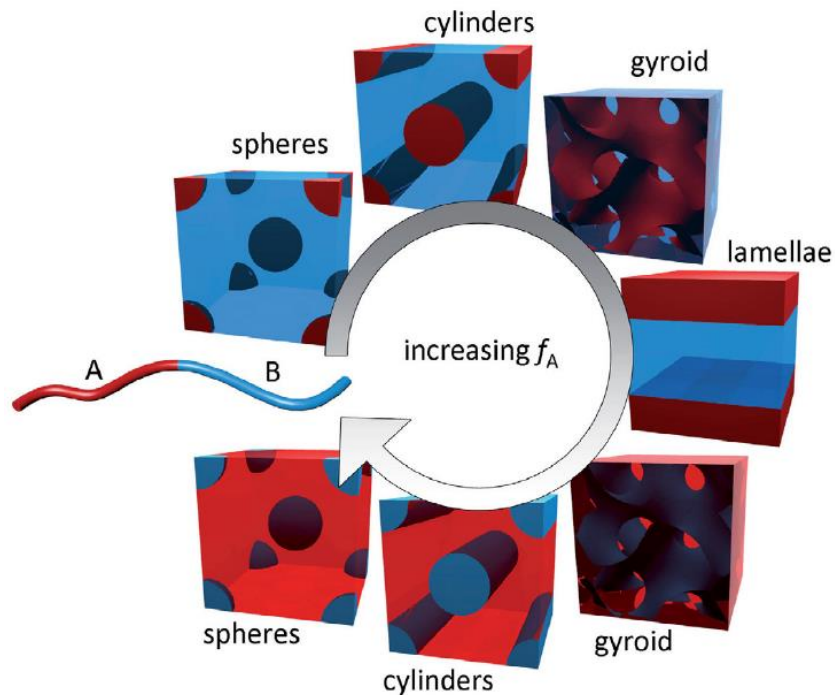


Figure 2.13 Different phases formed by self-assembly of coil-coil diblock copolymers in the bulk (when the intermolecular interaction is sufficiently large) as a function of the volume fraction of one of the blocks, f_A . Other phases have also been reported for diblocks, and the phase diagrams of BCPs containing more than two blocks are considerably more complex. Switching out one or both coil blocks with a conjugated block that adopts a semi-flexible or rigid rod structure will also qualitatively change this phase diagram (adapted from (Botiz and Darling, 2010)).

Figure 2.13, showed that phase separation at microscopic level with various morphologies of body-centered cubic spheres, hexagonally packed cylinders, and lamellae that are observed in coil-coil diblock copolymers (BCPs comprised of two incompatible and flexible blocks, A and B). The volume fraction of block A is indicated by f_A . In most of conjugated polymers, when a coil blocks are replaced by blocks that are semi-flexible or rigid rods, will change this phase diagram. Furthermore, a competition takes place between crystallization and microphase separation due to introducing the crystallizable blocks, this can affect the morphology substantially (Botiz and Darling, 2010).

2.8.4 Phase diagram of the LCST and UCST for Behavior of Polymer Blends.

The binary behavior of polymer blends (diagram of T versus volume fraction) for both a lower critical solution temperature, LCST and an upper critical solution temperature, UCST are shown in Figure 2.14. It has the following different important regions which includes spinodal, binodal, stable, unstable, metastable, one phase, and two-phase region for binary blends. The spinodal divides that the two-phase region into a metastable region, which is observed between the spinodal and the binodal, and an unstable region (two-phase), above, LCST and below, UCST of the spinodal, whereas the binodal one shows that stable region (one-phase) (Kalogeris, 2016).

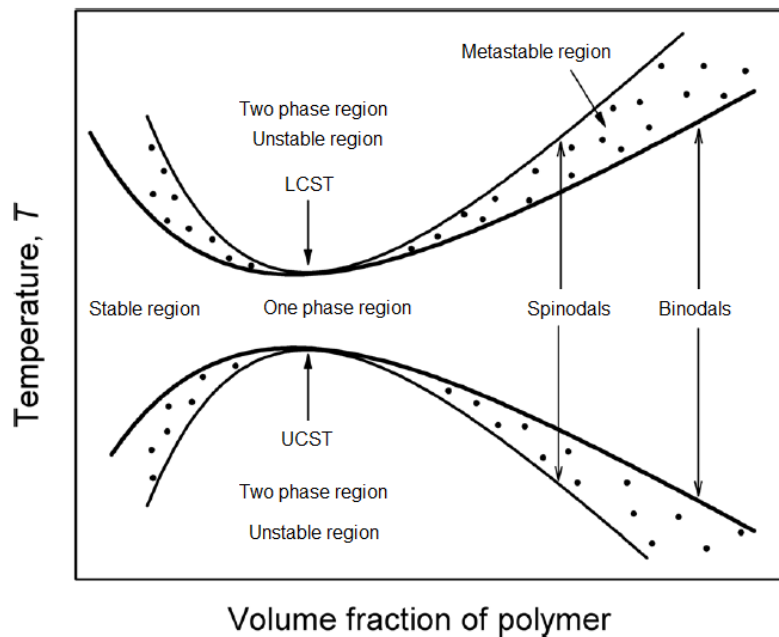


Figure 2.14 Phase diagram showing the LCST and UCST, respectively, behavior of polymer blends. Nonsymmetric phase diagrams are common in binary blends of polymers with large differences in their molecular masses (adapted from (Kalogeris, 2016)).

2.8.5 Thermal Properties of Polymers

Polymers have different chemical and physical properties in their nature. They can be subdivided into amorphous, crystalline and semi-crystalline polymers. In such a way that when the amorphous region of the polymer is exposed to lower temperature, the polymer molecules (frozen state), at this stage the molecules show that they can slightly vibrate but are not able to move

significantly. This state is called glassy state. The polymer can be brittle, hard and rigid which is similar to glass in this state. When the molecular motion is in the frozen state the glassy state is analogous to supercooled liquid. Therefore, the glassy state indicates that hard, rigid, and brittle nature which has similar to crystalline solid with molecular disorder as a liquid. Here, the state is called rubbery state, the polymer is heated then chains can able to wiggle around each other and then after it becomes soft and flexible the same to rubber. The glass transition temperature, T_g is the temperature of amorphous materials that show transition from glassy transition to rubbery state whereas melting temperature, T_m is for crystalline materials show transition from crystalline to melt, and semi-crystalline materials like polymers will have both temperature transitions. During the glass transition in the semi-crystalline polymer, the T_g affect only amorphous region while the crystalline region remains unaffected.

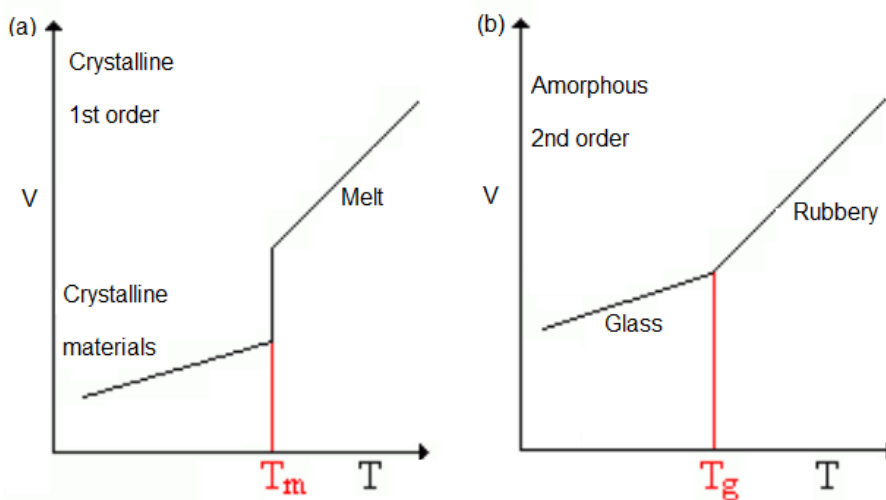


Figure 2.15 Schematic diagram of melting point and glass transition temperature of polymer for (a) crystalline materials (transition from crystalline to melt), (b) amorphous materials (transition from glass to rubbery transition) (adapted from (John Wiley and Sons, 2015)).

In terms of thermodynamics we can describe the glass transition temperature (2nd order transition) and the melting point (1st order transition). There are several factors can affect the value of T_g , such as molecular weight, measurement method, and the rate of heating or cooling. Because of polymer having the double bonds, aromatic groups, bulky or large side groups are

present in their chain, the flexibility of the chain is restricted. The melting point of a polymer decreased due to the existence of branches in chains (Kalogeras, 2016, John Wiley and Sons, 2015).

2.8.6 Thermodynamic Phase Transitions (First-and Second-Order).

The phase transition is basically associated with a thermodynamic system which means that the phase is formed by a change in an intensive variable. For instance, the transformation of one phase or state of matter changed to another. Phase transition is described as a function of state variables (P, V or T, pressure, volume, temperature, respectively) by Paul Ehrenfest using traditional scheme classification based on the behavior of Gibbs free energy. Phase transitions are labeled under this scheme, by the lowest derivative of the Gibbs free energy function (discontinuous at the transition). In the first derivative of the Gibbs free energy (first-order phase transitions indicate discontinuity) with respect to some thermodynamic variable. When heat is applied to materials, a certain amount of heat will be absorbed by that materials during a first-order transition, which undergoes in its constant-pressure heat capacity, C_p is called latent heat of transition. Melting or freezing, boiling, and condensation are the temperature showed at which crystal-liquid-gas phase transitions occur, density, ρ is discontinuously changed and the first derivative of the Gibbs free energy with respect to the chemical potential. The second-order phase transitions are continuous in the first derivative of the Gibbs free energy, but exhibit discontinuity in a second derivative of it. This is occurred in both alloys and ferromagnetic phase transition which indicates an order-disorder transitions. In such transitions no latent heat will be present but the material will undergo a change in its heat capacity. By the thermodynamic Gibbs free energy function the order of phase transition can be described. The second order phase transition (Gibbs free energy changes continuously with T and P and no abrupt change (first derivative). But the second derivative changes have abrupt change (discontinuous across the phase boundary) for instance, isobaric heat capacity, thermal compressibility, κ_T and thermal expansion coefficient, α are discontinuous across the phase boundary as a function of T).

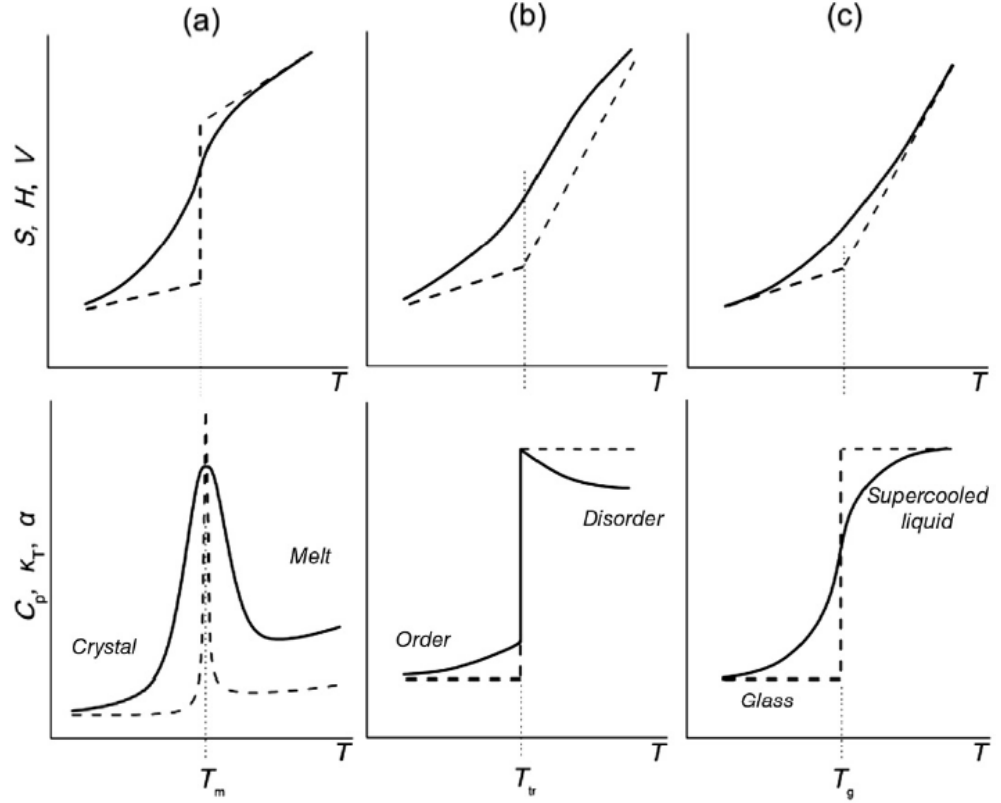


Figure 2.16 Schematic representation of thermodynamic responses. (a) First-order phase transition: consider, for example, melting of a crystal with defects (—) or of a perfect infinite crystal (--). (b) Second-order transition: transition dominated by intermolecular cooperative phenomena (—), or having only intermolecular cooperative phenomena (--). (c) Glass transition: experimental response (—), and ideal response in an infinitely slow experiment (--). (adapted from (Kalogeris, 2016)).

Both the first- and second-order transitions with the response of the experimental glass transition for comparison of the thermodynamic purpose are shown in Figure 2.16 (Kalogeris, 2016).

$$S = -(\partial G / \partial T)_P, \quad V = (\partial G / \partial P)_T \quad \text{and} \quad H = -(\partial(G/T) / \partial(1/T))_P \quad (2.1.2)$$

$$C_p = -T(\partial^2 G / \partial T^2)_P = T(\partial S / \partial T)_P = (\partial H / \partial T)_P \quad (2.1.3)$$

$$\kappa_T = -1/V(\partial^2 G / \partial P^2)_T = -1/V(\partial V / \partial P)_T \quad (2.1.4)$$

$$\alpha = 1/V(\partial / \partial T(\partial G / \partial P)_T)_P = 1/V(\partial V / \partial T)_P \quad (2.1.5)$$

3. METHODS AND MATERIALS

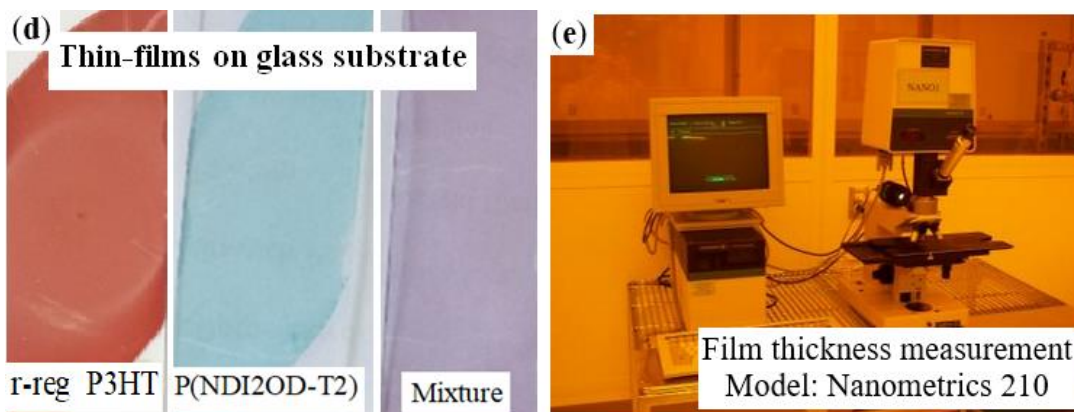
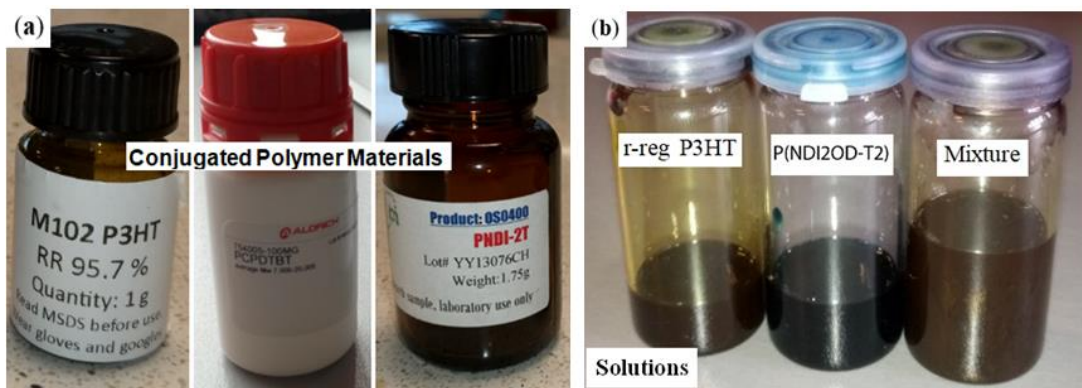
This part includes the relevant experimental methods and techniques used in the experiments presented in this dissertation. The new techniques discussed include the contact angle measurement which comprises determining the wetting ability of surfaces on thin-film samples of conjugated polymers, analysis of contact angles was carried out, the phase behaviors of conjugated polymer blends are described by FH lattice theory for which χ interaction parameter is estimated from contact angle measurement leading to solubility parameter. Finally, the film was processed and characterized. Organic materials and solvents are listed; the methods such as sample preparation, substrate cleaning, thin-film preparation, spin-coating and annealing methods; the experimental techniques thermal and thin-film morphological characterizations were described.

3.1 Experimental Section

3.1.1 Materials

The polymers and solvents used in this work were P(NDI2OD-T2) ($M_n = 32.1$ kg/mol, $M_w = 90.0$ kg/mol, polydispersity index (PDI) = 2.8, and molecular formula = $C_{62}H_{88}N_2O_4S_2$)_n) was purchased from 1-Material Inc. (Dorval, Quebec). R-reg P3HT ($M_n = 29.6$ kg/mol, $M_w = 65.2$ kg/mol, PDI = 2.2, and molecular formula = $(C_{10}H_{14}S)$ _n) was acquired from Sigma-Aldrich Inc. (Taufkirchen, Germany). Inc. PCPDTBT [$M_n = 4.50$ kg/mol, $M_w = 13.5$ kg/mol, PDI = 3.0, PDI = 3.0, and molecular formula = $(C_{31}H_{38}N_2S_3)$ _n], chlorobenzene, and chloroform were provided from Sigma-Aldrich, Inc. All these materials were used as received without further purification. Figure 3.1 below showed that photographs taken during the laboratory works at the Silesian University of Technology, Gliwice, Poland. From this photographs what we observed are includes polymeric materials (a) already used for this dissertation, polymer solution (b) preparation for the purpose of making thin-films using spin-coater on glass substrate (c and d), after producing this thin-films and then after that the thin-films characterized by using Nanometrics 210 Film thickness measurement (e), X-ray diffraction measurements (f), atomic force microscopy (g) and ramé-hart model 290-F1 contact angle goniometer (h). And the other photographs indicate that from these polymeric materials I was prepared the samples as of mass

ratio in the form of powdered for different thermal properties test according to the machine. These machines include thermogravimetric analysis (i) and differential scanning calorimetry (j).



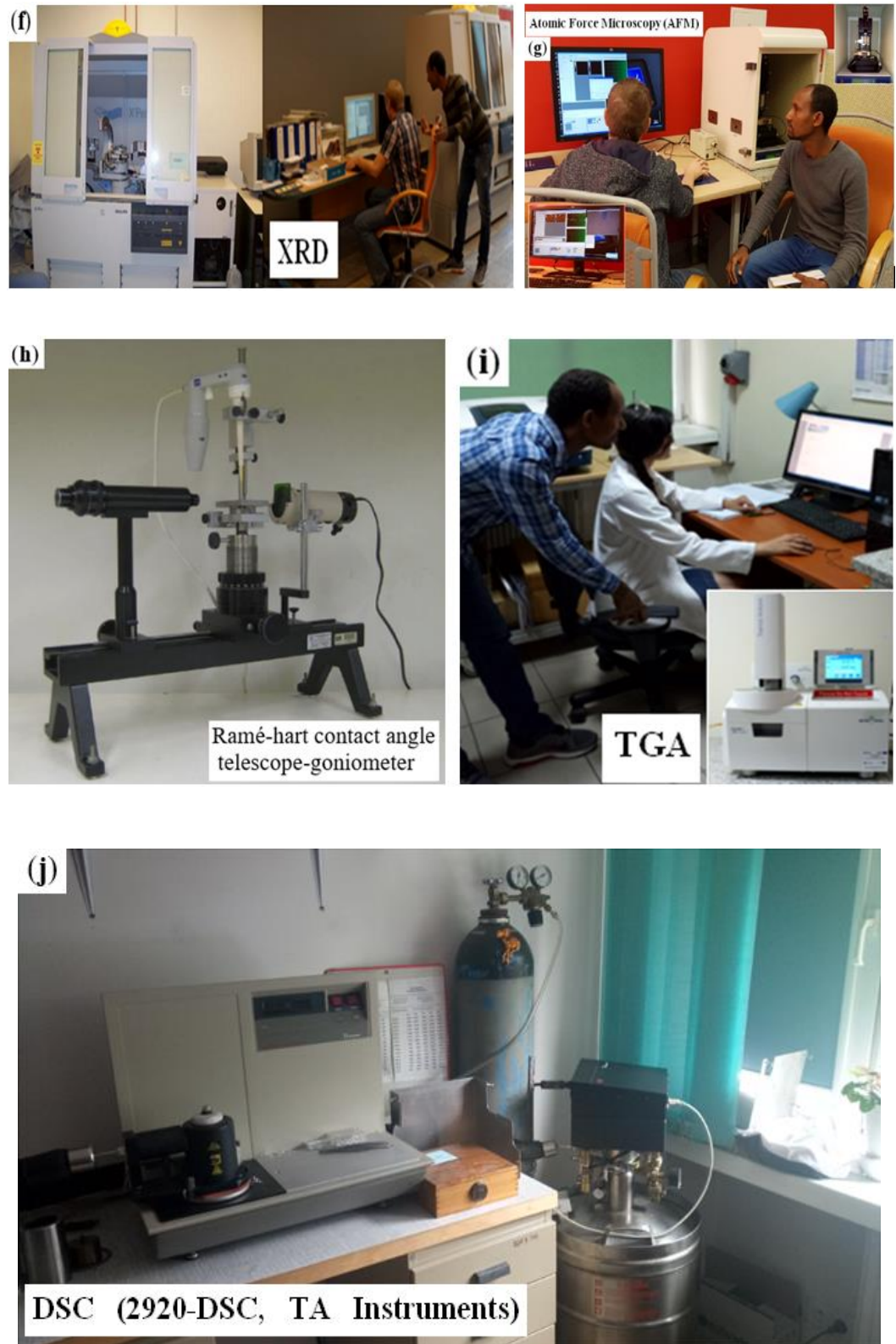


Figure 3.1 The photographs taken during laboratory experiment (pictured by Gada Muleta).

3.1.2 Contact Angle Measurement

The goniometer (its accuracy about ± 3 degrees) is a powerful tool for measuring contact angle, which has different parts of horizontal stage, micrometer pipette, illumination source and telescope with a protractor eyepiece. This telescope-goniometer is not only limited to measure contact angle but also measures surface energy, surface tension, interfacial tension, and surface dilatational elasticity and viscosity. The techniques of measurements were obtained positioning the tangent of the sessile (i.e., permanently attached to a substrate) drop profile at the contact point with the surface and directly reading the protractor (i.e., used to draw angles) through the eyepiece. The drop profile pictures taken by the camera which was attached to the equipment to measure the contact angle at leisure. In order to determine the wetting ability (i.e., interaction between fluid and solid phases) of surface energy on thin-film samples of P(NDI2OD-T2) and r-reg P3HT, were carried out using ramé-hart model 290-F1 contact angle goniometer and analyzed using surface energy (one liquid) tool implemented in DROP image 2.4.05 software. A 10 mg/ml chloroform solutions of sample films were prepared. Measurements of the contact angle were made using distilled water. The measurement of a drop of liquid applied to the surfaces of the samples (i.e., a spin-coated film on glass substrate) was made on the OEG SURFTENS UNIVERSAL test bench. Five drops of distilled water, each with a volume of $1\mu\text{L}$, were applied to the surface of each sample. The measurement was taken 15 s from the moment the drop was applied. Then the contact angles were observed and the mean values with standard deviation were calculated (Li and Neumann, 1992).

3.1.3 Solubility Parameter Calculation

According to Li and Neumann (Li and Neumann, 1990, Li and Neumann, 1992), the contact angle (θ) can be expressed as follows:

$$\cos \theta = -1 + 2 \sqrt{\frac{\gamma_{sv}}{\gamma_{lv}}} e^{-\beta(\gamma_{lv} - \gamma_{sv})^2} \quad (3.1.1)$$

where γ_{lv} , γ_{sv} , and γ_{sl} are surface energies for surface energy of liquid-vapour, surface energy of solid-vapour and surface energy of solid-liquid, respectively, and the constant β is 0.000115

$(\text{m}^2/\text{mJ})^2$. The value of γ_{sv} is unknown; whereas both γ_{lv} and θ are measurable quantities. As already stated above in the contact angle measurement case, the contact angle already measured by a telescope-goniometer technique. Therefore, the output values of surface energy, contact angle, drop volume, surface area and radius of the phase can be obtained from the telescope-goniometer. For data analysis I used a FORTRAN computer program, which provides the correct answer for input of the measurable quantities (i.e., surface energy of liquid-vapour (γ_{lv}) and contact angle (θ)). Finally, the solubility parameter is calculated from surface energy and then we find δ based on this equation, $\delta \propto \sqrt{\gamma_{sv}}$ can be calculated with the assistance of data analysis computer software (Kim, 2019).

3.1.4 Thermal Property Characterization

Differential scanning calorimetry (2920-DSC, TA Instruments, Champaign, IL, USA) was performed to characterize the transition temperature of materials at a scan rate of 10 °C/min from 20 to 350 °C under N₂ according to the instrumental set-up conditions. Thermogravimetric analysis was carried out using a METTLER TOLEDO Thermal Analysis (STARe System) (Warsaw, Poland), in which samples were heated from 50 to 600 °C using a conventional heating ramp with a scan rate of 10 °C/min under N₂.

3.1.5 Film Processing

Two conjugated polymers, PCPDTBT and P(NDI2OD-T2), were dissolved in the mixed solvents, CB:CF = 1:1wt. ratio according to literature reports (Yang et al., 2015, Van Franeker et al., 2015, Kadem et al., 2014). The total concentration of the blend system was 10 mg/mL. After the solvent dissolved completely, the samples were spin-coated on a glass substrate with the dimensions of 1.5 x 1.5 cm² for thin film deposition. Prior to spin-coating, the glass substrate was sequentially cleaned in deionized water, chloroform, and isopropanol for 5 min, respectively, and then dried under a nitrogen atmosphere. The condition of spin-coating was 2000 rpm for 15 s in the air, leading to the film thickness of about 140 nm using Nanometrics 210 Film thickness measurement. The annealing condition for a film was 180 °C for 15 min. Film thickness measurement equipment (Model: Nanometrics 210) was used to measure the film

thickness. Film thickness measurements up to 50 nm. The Nanometrics 210 is a computerized film thickness measurement system that employs the principle of optical interferometry. It includes a spectrophotometer head which can measure in the wavelength range of 370 to 800 nm using a computer-controlled grating monochromator, photomultiplier tube detector, and amplifier. The amplifier output is converted to a digital signal by the computer, which then calculates film thickness with one of several algorithms based on interference patterns.

3.1.6 Film Characterization

X-ray diffraction measurements (PANalytical Inc., Malvern, United Kingdom; PX 3040 PR; Cu K α radiation; $\lambda = 1.5418 \text{ \AA}$) were performed to examine the structure and ordering of a film on glass substrate at room temperature. According to the XRD's instrumental set-up condition, the diffraction angle (2θ) ranged from 10° to 100° . An AFM imaging technique typically requires a method by which the tip can track the topography of the sample. A relatively simple method of doing this is to monitor the cantilever deflection. The morphologies of the polymer films were characterized by the tapping-mode AFM (XE-100 Park Systems, Mannheim, Germany). Here, the data were analyzed using the software Park Systems XEI. UV-VIS absorption spectra were obtained on a Perkin- Elmer Lambda 950 spectrophotometer.

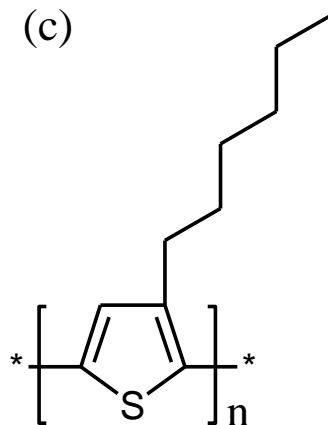
4. RESULTS AND DISCUSSION

This section describes about the phase diagrams of P(NDI2OD-T2) solutions and blends, the Flory-Huggins lattice theory, the polymer-solvent interaction parameter, the phase behavior of P(NDI2OD-T2) solutions, the phase behavior of the polymer-polymer mixture composed of P(NDI2OD-T2) and r-reg P3HT, the melting transition curve, the theory of melting point depression combined with the FH model, the entropic contribution to the polymer-polymer interaction parameter, the phase behavior of the polymer solutions and blends affecting morphologies. The phase behavior of amorphous/semicrystalline conjugated polymer blends, i.e., PCPDTBT/P(NDI2OD-T2); the Flory-Huggins interaction parameter for the PCPDTBT/P(NDI2OD-T2) blend; thermally analyzed; melting and crystallization point depression of P(NDI2OD-T2)/PCPDTBT blends; the regular π - π stacking could be destroyed by adding PCPDTBT into a crystalline P(NDI2OD-T2) lamellae, which was confirmed through XRD and AFM data; and finally, tapping-mode AFM images.

4.1 Phase Diagrams of n-Type Low Bandgap Naphthalenediimide-Bithiophene Copolymer Solutions and Blends

4.1.1 Binary Polymer-Solvent Mixture

Figure 4.1a and b shows the chemical structure of n-type low bandgap P(NDI2OD-T2) and its UV-VIS absorption spectra, harvesting light near infrared regions, about 855 nm.



r-reg P3HT

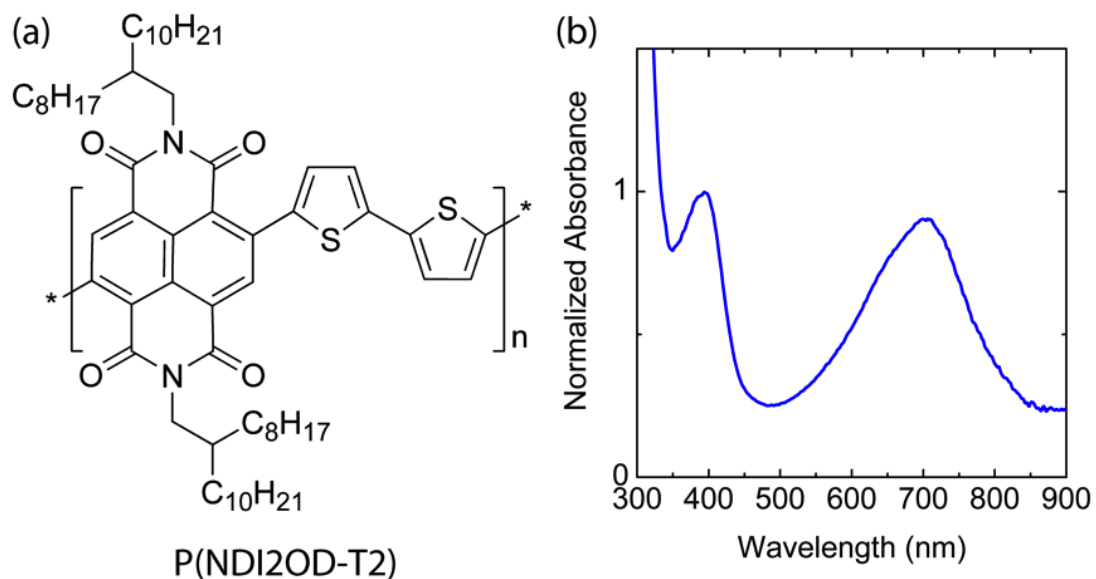


Figure 4.1 (a) Chemical structure of P(NDI2OD-T2) and (c) r-reg P3HT, (b) UV-VIS spectrum of P(NDI2OD-T2).

When P(NDI2OD-T2) is dissolved in a common solvent such as chlorobenzene, the solution color is almost black, but its film is bluish, as shown in Figure 4.2a. For estimating the solubility parameter, we measured the contact angle, as shown in Figure 4.2b.

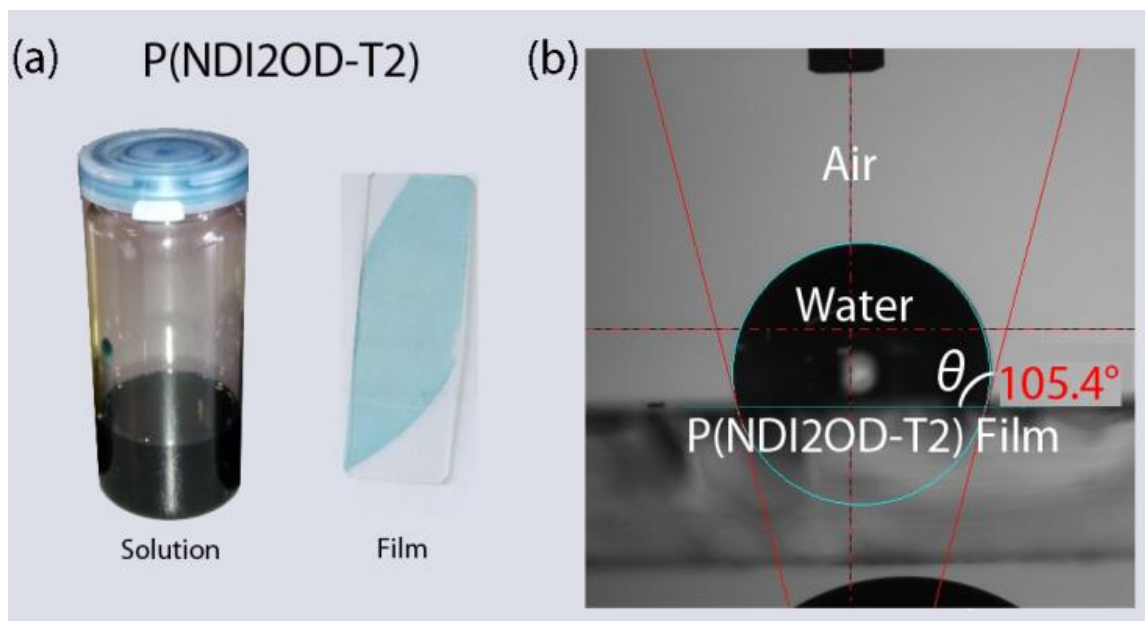


Figure 4.2 (a) P(NDI2OD-T2) solution and film, (b) Contact angle measurement for P(NDI2OD-T2) film on glass substrate.

The calculated solubility parameter and surface energy are summarized in Table 4.1. As shown in Table 4.1, P(NDI2OD-T2) has $\delta = 7.99 \text{ (cal/cm}^3)^{1/2}$ [= 16,386.31(J/m³)^{1/2}], whereas r-reg P3HT ($M_n = 29.6 \text{ kg/mol}$, PDI = 2.2) has $\delta = 9.23 \text{ (cal/cm}^3)^{1/2}$ [= 18,908.58 (J/m³)^{1/2}], indicating P(NDI2OD-T2) is much more hydrophobic compared to r-reg P3HT. Note that in previous studies (Kim, 2018), when estimating the δ of r-reg P3HT ($M_n = 22.0 \text{ kg/mol}$, PDI = 2.1) from the contact angle measurement, a value of 8.72 was obtained. Hence, the average δ of r-reg P3HTs with $M_n = \sim 22.0\text{--}29.6 \text{ kg/mol}$ could be 8.98 ± 0.36 .

Table 4.1 Contact angle, surface energy, and solubility parameter.

Materials	Contact Angle (°)	Surface Energy (mJ/m ²)	Solubility Parameter (cal/cm ³) ^{1/2}
P(NDI2OD-T2)	105.40	19.07	7.99
r-reg P3HT	94.90	25.48	9.23

Table 4.2 shows some properties, including the δ for common solvents [chlorobenzene, chloroform, and p-xylene] (Belmares et al., 2004), which are used for studying the phase behavior of n-type P(NDI2OD-T2) solutions in comparison with p-type r-reg P3HT ones.

Table 4.2 Solubility parameter (Belmares et al., 2004), molecular weight, molar volume, density, boiling point, and radius of lattice site volume for each solvent, chlorobenzene, chloroform, and p-xylene.

Solvent	Solubility Parameter (cal/cm³)^{1/2}	Molecular Weight (g/mol)	Molar Volume (cm³/mol)	Density (g/cm³)	Boiling Point (°C)	Radius of Lattice Site Volume (nm)
CB	9.5	112.56	101.41	1.11	132	0.34
CF	9.2	119.38	80.12	1.49	61	0.31
XY	8.8	106.16	123.44	0.86	138	0.36

According to the FH theory, the molar Gibbs energy of mixing is given by:

$$\frac{\Delta G_M}{RT} = \frac{\phi_1}{r_1} \ln \phi_1 + \frac{\phi_2}{r_2} \ln \phi_2 + \chi \phi_1 \phi_2 \quad (4.1.1)$$

where ϕ_1 , ϕ_2 , r_1 ($= 1$ for solvent in polymer-solvent mixture; $\neq 1$ for polymer in polymer-polymer blends), r_2 , R , and T are the volume fraction, relative molar volumes of component 1 and 2, the gas constant, and temperature, respectively. Note that a single lattice site is decided by the molecular volume of the solvents (e.g., CB, CF, and XY) or the polymer's structural unit for the polymer-polymer blend (e.g., r-reg P3HT's repeat unit). Herein, χ applies to lattice site volume with a radius of 0.34 nm for CB, 0.31nm for CF, and 0.36 nm for XY, respectively, Table 4.2. The FH interaction parameter can be divided into enthalpic and entropic contributions (Flory, 1953, Patterson, 1969).

$$\chi = \chi_H + \chi_S = \frac{z\Delta w_H}{kT} - \frac{z\Delta w_S}{k} \quad (4.1.2)$$

$$\Delta w_G = \Delta w_H - T\Delta w_S \quad (4.1.3)$$

where, Δw_G is the interchange free energy of a segment pair with enthalpic (Δw_H) and entropic (Δw_S) contributions, z is the coordination number (e.g., z is in the range of 6 to 12 (Flory, 1953). Herein, we used $z = 6$ for theoretical calculation, and k is the Boltzmann constant. Here,

we assign $(\chi_s) = 0.34$ for the polymer-solvent system. Then, (χ_H) (dimensionless) can be re expressed in terms of δ as follows:

$$\chi_H = \frac{\hat{V}_1}{RT} (\delta_i - \delta_j)^2 \quad (4.1.4)$$

where $\hat{V} =$ lattice site volume and $\delta_{i \text{ or } j}$ are the molar volume of component 1 (solvent) [$\hat{V}_1 = (112.56 \text{ g/mol}) / (1.11 \text{ g/cm}^3) = 101.41 \text{ cm}^3 / \text{mol}$ for CB] and the solubility parameter (subscript i or $j = 1, 2$; solvent = 1 and polymer = 2 for the polymer-solvent mixture), respectively. Based on Tables 4.1 and 4.2, the estimated r_2 and χ_H values are listed in Table 4.3. Note that in some experimental observations (Koningsveld and Staverman, 1968, Riedl and Prud'Homme, 1988), χ is a function of not only a temperature-dependent interaction parameter, $D(T)$, but also a composition-dependent parameter $B(\phi_2)$. Hence, in an extended FH theory, Qian et al., 1991 suggested $\chi = D(T) B(\phi_2) = (d_0 + d_1/T + d_2 \ln T)(1 + b_1\phi_2 + b_2\phi_2^2)$, where d_0, d_1, d_2, b_1 , and b_2 are adjustable parameters. When χ is independent of concentration, i.e., $B(\phi_2) = 1$, χ is recovered to $\chi = D(T)$. In this work, when $B(\phi_2) = 1$, we used $\chi = D(T) = \chi_H + \chi_s = d_0 + d_1/T + d_2 \ln T$, where $d_0 = 0.34 = \chi_s$, $d_1 = (\hat{V}/R) (\delta_i - \delta_j)^2 = \chi_H \cdot T$, and $d_2 = 0$ for the polymer-solvent system according to Equations 4.1.3 and 4.1.5.

Table 4.3 Relative molar volume and Flory-Huggins χ interaction parameter for binary P(NDI2OD-T2)/solvent and r-reg P3HT/solvent mixtures as a function of solvent (CB, CF, and XY), when P(NDI2OD-T2) has $M_n = 32.1 \text{ kg/mol}$ and $\delta = 7.99$, and r-reg P3HT has $M_n = 29.6 \text{ kg/mol}$ and $\delta = 9.23$.

Solvent	P(NDI2OD-T2)/Solvent Mixture		R-reg P3HT/Solvent Mixture	
	r_2	χ	r_2	χ
CB	288	116.4 K/T + 0.34	265	3.72 K/T + 0.34
CF	364	59.0 K/T + 0.34	336	0.04 K/T + 0.34
XY	236	40.8 K/T + 0.34	218	11.49 K/T + 0.34

Figure 4.3 shows the phase diagram of binary P(NDI2OD-T2)/CB, P(NDI2OD-T2)/CF and P(NDI2OD-T2)/XY solutions, for which Equations 4.1.6 and 4.1.7 are solved simultaneously:

$$\Delta\mu_1^\alpha = \Delta\mu_1^\beta \quad (4.1.5)$$

$$\Delta\mu_2^\alpha = \Delta\mu_2^\beta \quad (4.1.6)$$

where $\Delta\mu_1 = \partial\Delta G_M / \partial n_1$ and $\Delta\mu_2 = \partial\Delta G_M / \partial n_2$ are the chemical potentials of component 1 and 2, respectively, and; α and β indicate two different phases at equilibrium. Then, for describing the melting point depression (i.e., the melting point of a material decreases with the reduction of its size) of the polymer-solvent system, the below equations were used (Flory, 1953, Kim, 2018, Kim, 2019):

$$\frac{1}{T_{m,2}} - \frac{1}{T_{m,2}^0} = - \frac{R}{\Delta H_{u,2}} \frac{V_u}{r_2 \hat{V}_1} [\ln \phi_2 + (1 - \frac{r_2}{r_1})\phi_1 + r_2 \chi \phi_1^2] \quad (4.1.7)$$

$$\frac{1}{T_{m,2}} - \frac{1}{T_{m,2}^0} \approx \frac{R}{\Delta H_{u,2}} \frac{V_{u,2}}{\hat{V}_1} (\phi_1 - \chi \phi_1^2) (r_2 \gg r_1 \approx 1) \quad (4.1.8)$$

where $T_{m,2}$ and $T_{m,2}^0 = 587.95$ K are the melting temperature of P(NDI2OD-T2) with solvent and the melting temperature of pure P(NDI2OD-T2) without solvent, respectively. Note that in Equation 4.1.7, $V_u / r_2 \hat{V}_1$ is introduced for calculating per structural unit of polymer. $\Delta H_{u,2}$ and $V_{u,2} [= (989 \text{ g/mol}) / (1.1 \text{ g/cm}^3) = 899.09 \text{ cm}^3 / \text{mol}]$ are the unit enthalpy and the unit volume of P(NDI2OD-T2), respectively. Herein, the density of P(NDI2OD-T2) is ca. 1.1 g/cm^3 . However, P(NDI2OD-T2)'s $\Delta H_{u,2}$ with crystallinity $x_c \approx 100 \%$ is still unknown, even though (Takacs et al., 2013) reported remarkable order, “face-on lamella”, in a P(NDI2OD-T2) film. Importantly, (Clark et al., 2009) estimated the crystallinity, $x_c \approx 39 \pm 10 \%$ of r-reg P3HT (Plextronics and Merck) based on spectroscopic methods. Hence, when we examined r-reg P3HT's x_c based on the previous studies, $\Delta H_{u,r-reg P3HT} \approx 47.5 \text{ J/g}$ (Kim, 2018), $x_c \approx 17.80/47.50 \times 100 = 37.5 \%$, which falls in Clark et al.'s spectroscopic results. In the same vein, Neher et al. (Steyrleuthner et

al., 2012) estimated that non-amorphous aggregation in P(NDI2OD-T2) ($M_n = 36.2$ kg/mol, PDI = 5.0) is about 45 % based on their spectroscopic results, following Clark et al.'s approach. Considering our P(NDI2OD-T2)'s M_n and PDI were 32.1 kg/mol and 2.8, respectively, our P(NDI2OD-T2) was roughly similar to Neher et al.'s polymer. Hence, if we consider that our P(NDI2OD-T2) has an enthalpy of 14.46 J/g with the assumption of $x_c \approx 45 \pm 10$ %, the $\Delta H_{u,2}$ of P(NDI2OD-T2) with $x_c \approx 100$ % is estimated to be $\sim 32.13 \pm 7.58$ J/g. In Figure 4.3, LLE is calculated based on Equations 4.1.6 and 4.1.7, and SLE is based on Equation 4.1.8 with $\Delta H_{u,2} \approx 32.13$ J/g. Figure 4.3a–c shows three representative cases of phase transition in semicrystalline polymer solutions. Note that, if we consider ± 10 % error in x_c , the estimated deviation in the SLE curve is about ± 23 K in average from the SLE curve with for the P(NDI2OD-T2)/CB system see Figure 4.4. Based on the data shown in Figure 4.3, three representative cases can be discussed, keeping in mind that the FH lattice theory provides qualitative descriptions.

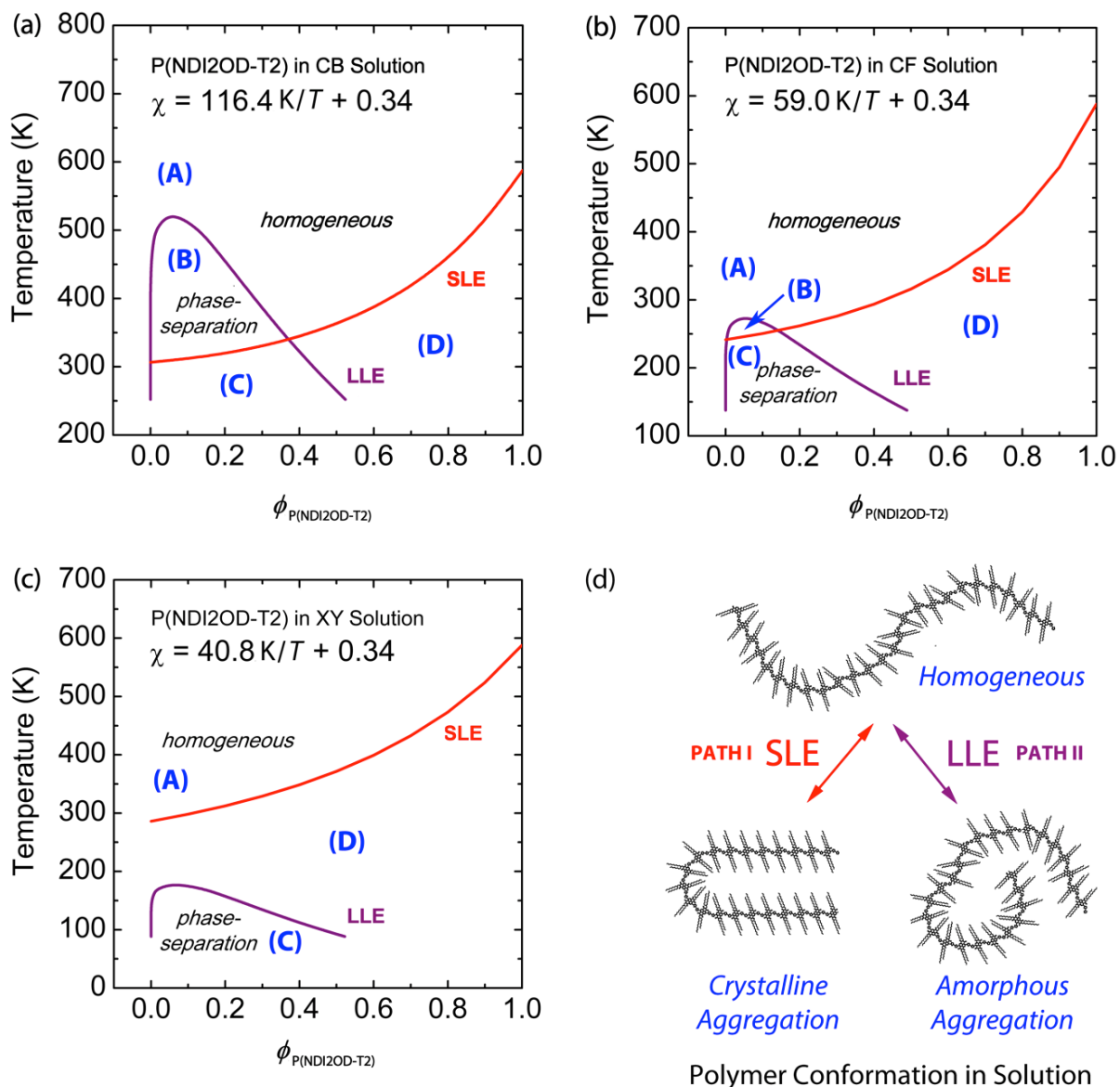


Figure 4.3 Phase diagrams of binary P(NDI2OD-T2) solutions: Solvent effect. Theoretical phase diagrams of (a) P(NDI2OD-T2)/CB, (b) P(NDI2OD-T2)/CF, and (c) P(NDI2OD-T2)/XY solutions, based on the Flory-Huggins lattice theory. (d) Schematic explanation of liquid-liquid phase equilibria (LLE) and solid-liquid phase equilibria (SLE) phase transition of P(NDI2OD-T2) molecules in solution. Herein, Path I indicate SLE (i.e., crystallization), whereas Path II denotes LLE (amorphous-amorphous phase separation). Regions correspond to: (A) one-phase liquid state; (B) two-phase liquid state; (C) both L-L and L-S phase separation; and (D) L-S phase separation (i.e., polymer crystallization), respectively.

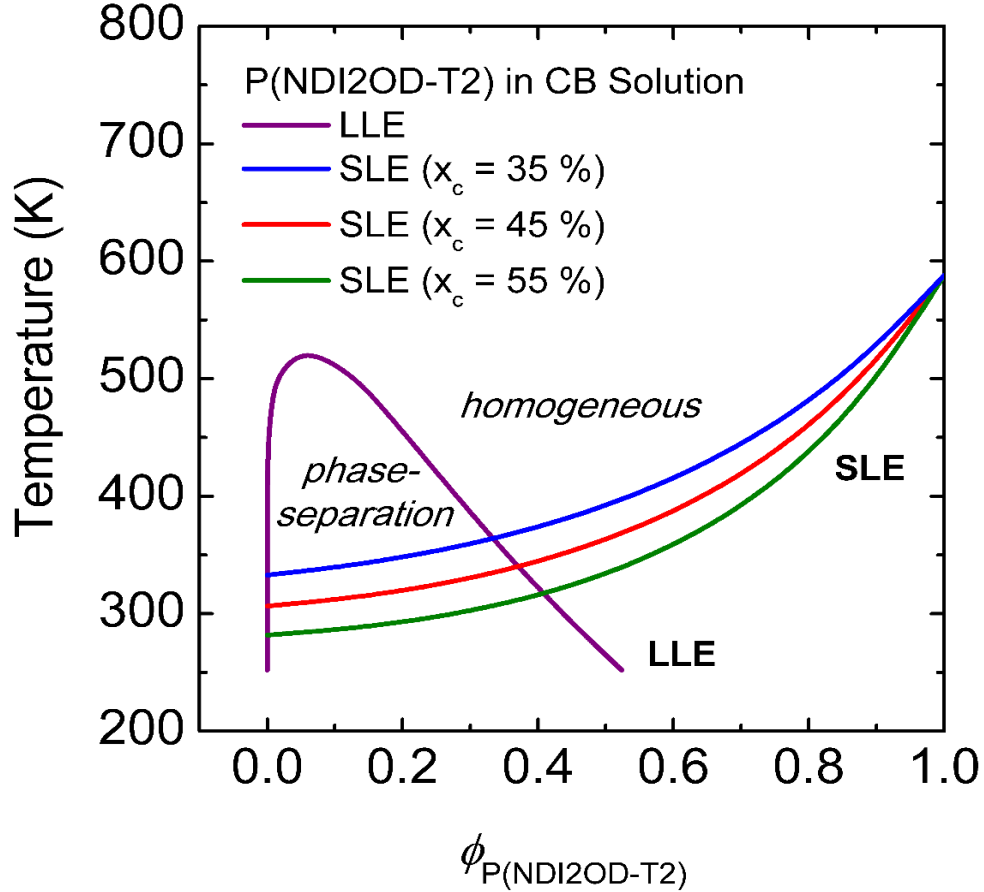


Figure 4.4 Theoretical phase diagrams of binary polymer solutions: P(NDI2OD-T2)-CB. Melting point depression curves are calculated for three hypothetical crystallinities of P(NDI2OD-T2), i.e., $x_c = 35\%$ (blue line), 45% (red), and 55% (green).

Case 1: LLE > SLE.

Figure 4.3a shows the phase behavior of the P(NDI2OD-T2)/CB system, which displays both L-L and L-S phase transition, $LLE > SLE$ when $\phi_{P(NDI2OD-T2)} < 0.37$. This kind of phase behavior ($LLE > SLE$) was also observed in polyethylene/nitrobenzene, PE/amyl acetate and poly (*N,N'*-sebacoylpiperazine)/diphenyl ether systems (Richards, 1946, Flory et al., 1951). However, note that r-reg P3HT, PC₆₁BM, and PC₇₁BM show $SLE > LLE$ in CB (Kim, 2018). This difference between $LLE > SLE$ and $SLE > LLE$ should make polymer solutions undergo

different pathways for morphology formation, in which the former undergoes SD or NG, but the latter crystallization. If we use chloronaphthalene, $\delta = 10.3$ (Dereje et al., 2017) or 1,2-dichlorobenzene, $\delta = 10.0$ (Belmares et al., 2004) or 1,2,4-trichlorobenzene, $\delta = 10.2$ (Dereje et al., 2017) as a solvent for P(NDI2OD-T2), the phase behavior is included in Case 1, because their solubility parameters are larger than CB's $\delta = 9.5$, inducing more L-L demixing in solution. The regions in Figure 4.3a correspond to: (A) one-phase liquid state; (B) two-phase liquid state; (C) both L-L and L-S phase separation; and (D) L-S phase separation (i.e., polymer crystallization), respectively.

Case 2: LLE \approx SLE.

Figure 4.3b shows the phase behavior of the P(NDI2OD-T2)/CF system, in which the upper critical solution temperature, i.e., the binodal coexistence line, is around the melting point depression curve, indicating L-L phase transition may compete with L-S phase transition, i.e., self-assembly for crystallization at $\phi_{P(NDI2OD-T2)} < 0.15$. Note that, in Figure 4.3b, the regions (A), (B), (C), and (D) correspond to each state in Figure 4.3a except for the minimized (B) region, indicating both L-L and L-S phase transition may occur around the region (B).

Case 3: SLE $>$ LLE.

Figure 4.3c shows the phase behavior of the P(NDI2OD-T2)/XY system, in which SLE $>$ LLE is displayed. This kind of phase behavior (SLE $>$ LLE) is observed also for r-reg P3HT/CB, PC₆₁BM/CB, and PC₇₁BM/CB, in which the system undergoes phase separation in solution over crystallization, followed by L-L phase transition. Note that, in Figure 4.3c, the region (B) completely disappears but the other ones, (A), (C), and (D), exist, only.

Figure 4.3d summarizes the phase transition in the P(NDI2OD-T2)/solvent mixtures. Path I generate crystalline aggregation, in which there is equilibrium between a polymeric chain in liquid and self-assembled crystals in aggregation. On the other hand, Path II induces two liquid phases: a polymer-rich phase and a solvent-rich phase. Lastly, as explained in Case 2, it is possible that Paths I and II may compete each other, i.e., simultaneously, the L-L and L-S transitions occur together.

Finally, for the purpose of clear comparison, when we calculated the phase diagrams of r-reg P3HT solution for the same solvent, CB, CF and XY, we can observe only Case 3 (i.e., SLE > LLE) as shown in Figure 4.4. Hence, we can say that the r-reg P3HT solution may undergo phase separation primarily through crystallization, whereas P(NDI2OD-T2) solution may phase separately via SD or NG; crystallization or any combination of SD/NG and crystallization, depending on the solvent, CB or CF or XY.

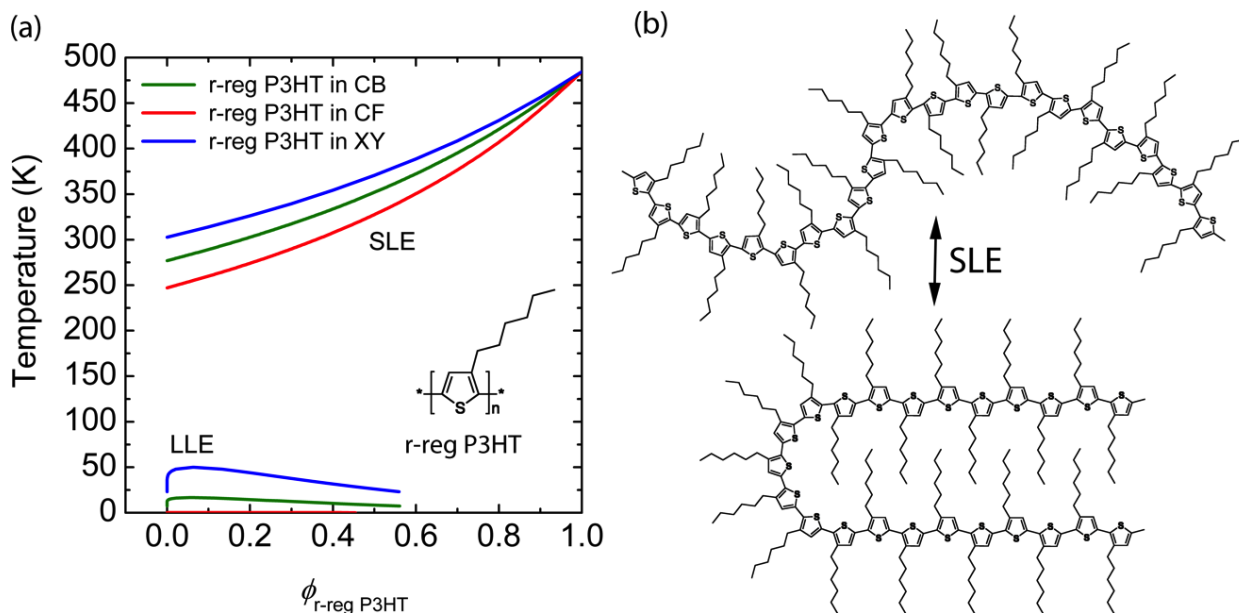


Figure 4.4 (a) Theoretical phase diagrams of binary r-reg P3HT solutions: r-reg P3HT/CB (green solid line), r-reg P3HT/CF (red), and r-reg P3HT/XY (blue). Inset: Chemical structure of r-reg P3HT. (b) Schematic explanation of SLE (L-S phase transition) of r-reg P3HT molecules in solution.

4.1.2 Binary Polymer-Polymer Mixture

In the previous section, we noticed that, when CB was used as a solvent, P(NDI2OD-T2) showed LLE > SLE, whereas r-reg P3HT displayed SLE > LLE. In this section, we mixed these two different semicrystalline polymers, r-reg P3HT and P(NDI2OD-T2), in solvents to observe phase behavior. To this end, DSC thermal analysis was employed for some model compositions such as 0, 20, 50, 80, and 100 wt.% P(NDI2OD-T2). Note that two different polymer-polymer systems may be immiscible if there is no specific interaction, because

$\Delta G_M = \Delta H_M - T\Delta S_M > 0$ ($\Delta S_M \approx 0$ and $\Delta H_M > 0$), where ΔH_M and ΔS_M are the enthalpy and entropy of mixing, respectively.

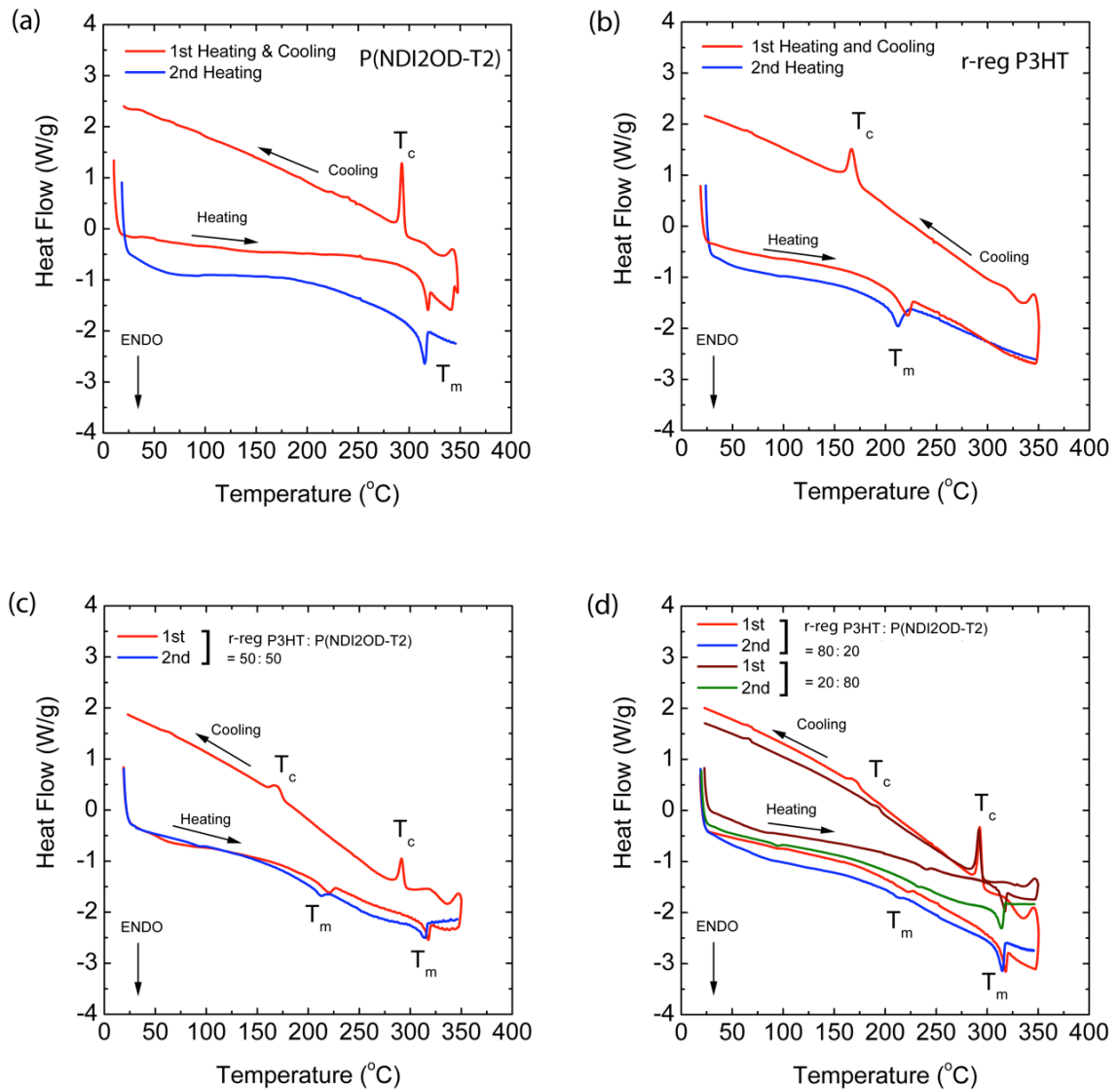


Figure 4.5 Differential scanning calorimetry thermograms at a scan rate of 10 °C/min: (a) P(NDI2OD-T2), (b) r-reg P3HT, (c) r-reg P3HT:P(NDI2OD-T2) = 50:50 wt.%, and (d) r-reg P3HT:P(NDI2OD-T2) = 80:20 and 20:80 wt.%.

In Figure 4.5, the red solid lines are the first heating and cooling curves, and the blue line represents the second heating. Through the first heating/cooling cycle, the thermal history of the

samples was erased (Hiemenz and Lodge, 2007) and through the second heating, we may acquire data related to the melting and crystallization temperatures. The pure polymers, P(NDI2OD-T2) and r-reg P3HT show T_m at 314.80 °C (with an enthalpy of 14.46 J/g) and at 211.37 °C (that of 17.80 J/g) in Figure 4.5a and b, respectively. These two polymers were mixed together and compositions of 20, 50, and 80 wt.% P(NDI2OD-T2) were made, resulting in the T_m and T_c shown in Figure 4.5c and Figure 4.5d, in which all the blend compositions showed each T_m and T_c , originating from pure P(NDI2OD-T2) and r-reg P3HT, indicating that these polymers were immiscible, as expected from two different polymer-polymer systems in the absence of any specific interaction. Note that P(NDI2OD-T2) and r-reg P3HT have a similar thermal stability, showing decomposition in the range of ~ 430–500 °C and then when the maximum temperatures of 600 °C were reached, the residual mass of both conjugated polymers were 31 and 35 % of the initial mass, respectively, see Figure 4.6.

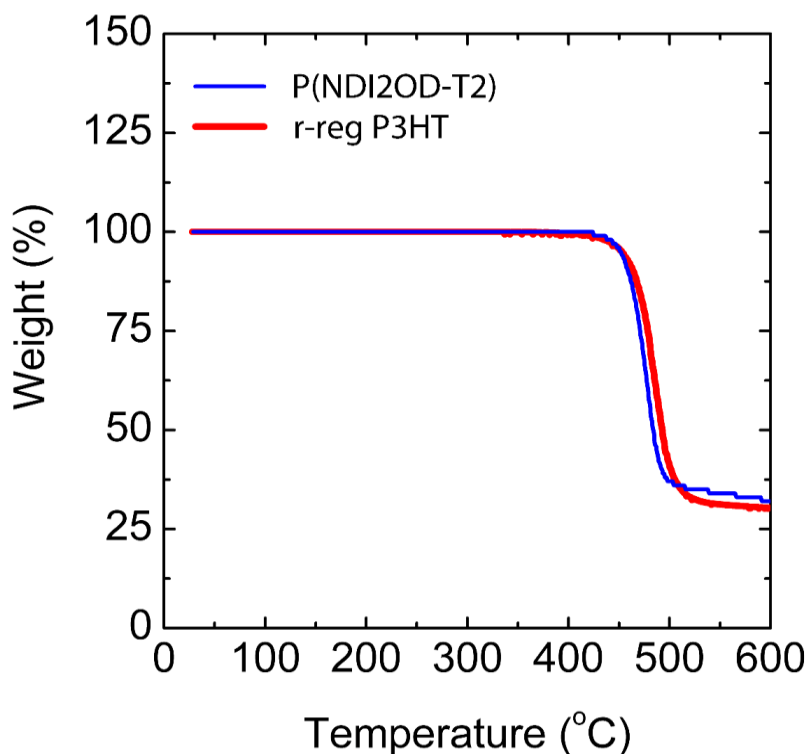


Figure 4.6 Thermogravimetric analysis of P(NDI2OD-T2) and r-reg P3HT.

As a result, based on the information in Figure 4.7, we constructed the temperature-composition phase diagram of the r-reg P3HT/P(NDI2OD-T2) system, see Figure 4.7a, in which the first observation was that T_m and T_c were very similar in blends compared to those of each pure polymer, indicating they were immiscible. Note that in the case of the r-reg P3HT/PC₆₁BM system, there was a significant melting point depression and miscibility (a miscibility limit at ~ 40 wt.% PC₆₁BM) (Kim and Frisbie, 2008). Conversely, as shown in Figure 4.7a, the phase behavior of the r-reg P3HT/P(NDI2OD-T2) system was very simple, in which **L** and **S** stand for liquid and solid state, respectively. When the temperature was lower than T_m of r-reg P3HT, the resultant phase was two solid mixtures, $S_{P(NDI2OD-T2)} + S_{r-reg P3HT}$. However, when the temperature was increased above the T_m of r-reg P3HT but less than the T_m of P(NDI2OD-T2), the phase was $S_{P(NDI2OD-T2)} + L_{r-reg P3HT}$. Finally, when the temperature was increased above the T_m of P(NDI2OD-T2), the phase became a liquid state, **L**.

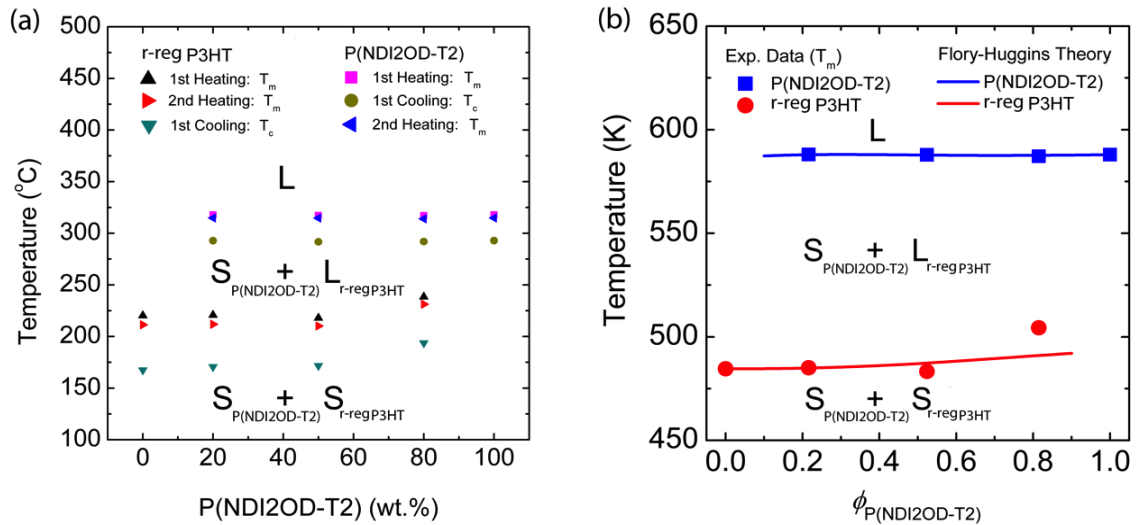


Figure 4.7 Temperature-composition phase diagram for the binary r-reg P3HT/P(NDI2OD-T2) system, in which **L** and **S** stand for liquid and solid, respectively. (a) Experimental results obtained from DSC thermograms in Figure 4.5 and (b) Comparison of experimental data (from the second heating curve) with the Flory-Huggins lattice model (Equations 4.1.7) and 4.1.9) with $\chi = 116.8/T - 0.185$.

Importantly, based on the T_m data from the second heating curves, we compared the experimental results with the FH model's prediction, see Figure 4.7b. For describing the melting points of P(NDI2OD-T2) (i.e., component 2) and r-reg P3HT (i.e., component 1), we used Equation 4.1.7 above and Equation 4.1.9 below, respectively. Note that the χ interaction parameter for the r-reg P3HT/P(NDI2OD-T2) system was shared together for Equations 4.1.7 and 4.1.9.

$$\frac{1}{T_{m,1}} - \frac{1}{T_{m,1}^0} = - \frac{R}{\Delta H_{u,1}} \frac{V_{u,1}}{r_1 \hat{V}_1} [\ln \phi_1 + \phi_2 (1 - \frac{r_2}{r_1}) + r_1 \chi \phi_2^2] \quad (4.1.9)$$

where $r_1 = 178$ and $r_2 = 193$, and we assume $\hat{V}_1 = V_{u,1}$, indicating the segment volume is decided by the size of r-reg P3HT's structural unit with the molar volume of $150.9 \text{ cm}^3/\text{mol}$ ($= 166/1.1$) based on the unit molar weight of 166 g/cm^3 and the density of 1.1 g/cm^3 . Hence, χ applies to lattice site volume with the radius of 0.39 nm for r-reg P3HT. Herein, once again the $V_{u,1}/r_1 \hat{V}_1 (= 1/r_1)$ term is related with calculation per r-reg P3HT's structural unit, because r-reg P3HT is a polymeric chain. And, as in the previous section, when estimating $\chi = \chi_H + \chi_S$ from the solubility parameter, here also we use $\chi_H = \hat{V}_1 / RT(\delta_1 - \delta_2)^2$. Resultantly, we obtain $\chi_H = 150.9 \text{ cm}^3/\text{mol} / (1.987 \text{ cal/mol/KT}) (9.23 - 7.99)^2 \text{ cal/cm}^3 = 116.8 \text{ K/T}$. However, in this study for the r-reg P3HT/P(NDI2OD-T2) system, if we use 0.34 for χ_S , we observe that the theory Equations 4.1.7 and 4.1.9 shows a large deviation from the experimental data, see Figure 4.8. Hence, as a first attempt towards describing the data, we employed Equation 4.1.10 as:

$$\chi = D(T)B(\phi_2) = (\chi_H + \chi_S)B(\phi_2) = (116.8 \text{ K/T} + 0.34)(1 + b_1\phi_2 + b_2\phi_2^2) \quad (4.1.10)$$

depending on both temperature and composition vis-á-vis Qian et al.'s extended FH model (Qian et al., 1991). However, upon attempting to fit the data using Equation 4.1.7 with $\chi = (116.8 \text{ K/T} + 0.34) (1 + b_1\phi_2 + b_2\phi_2^2)$, i.e., in the presence of $\chi_S = 0.34$ and two adjustable parameters (b_1 and b_2), the theory could not fit the data.

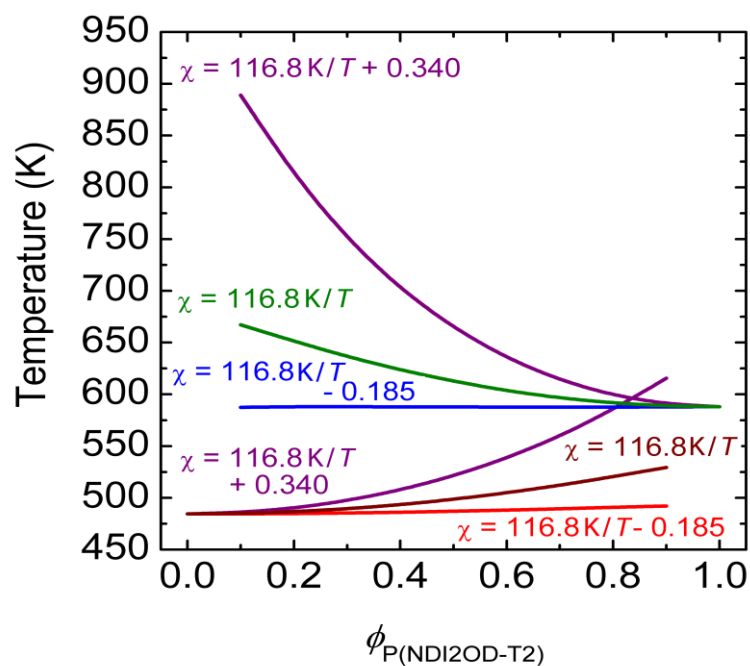


Figure 4.8 Theoretical description of melting points for the binary r-reg P3HT/P(NDI2OD-T2) system by using the theory of melting point depression combined with Flory-Huggins model incorporating the polymer-polymer interaction parameters of $116.8 \text{ K/T} + 0.340$, 116.8 K/T , and $116.8 \text{ K/T} - 0.185$, respectively.

Alternatively, if we use the entropic part χ_s as an adjustable parameter instead of a fixed value of 0.34, we find that the FH model (Equations 4.1.7 and 4.1.9) can describe the experimental data excellently. Resultantly, using Equation 4.1.7, we find that, when χ_s is -0.185, the model accurately describes the T_m of the r-reg P3HT/P(NDI2OD-T2) system. In general, this fitting using an adjustable χ parameter is one of the most common methods in polymer science (Hiemenz and Lodge, 2007). Hence, according to Equations 4.1.2 and 4.1.3 ($\chi = \chi_H + \chi_s = z\Delta w_H / kT - z\Delta w_s / k$; $\Delta w_G = \Delta w_H - T\Delta w_s$), if $\chi_s < 0$ and $\Delta w_s > 0$, this condition indicates an increase of entropy by forming a new contact between the r-reg P3HT and P(NDI2OD-T2) segments (Li and Neumann, 1992), although $\Delta S_M \approx 0$ in a polymer-polymer mixture. Interestingly, Ade et al. reported that PCDTBT: PC₇₁BM mixture has an amorphous–amorphous interaction parameter χ with $\chi_s = -1.63$ or -2.21 (i.e., $\Delta w_s > 0$) (Ye et al., 2018),

although, in a polymer-solvent system, $\chi_s \approx 0.34$ is usually larger than zero (i.e., $\Delta w_s < 0$), because of the dissimilarity of free volume (Li and Neumann, 1992).

To describe in further detail, χ_s is obtained by fitting the T_m data of P(NDI2OD-T2) in Figure 4.7b by using Equation 4.1.7. Then, using the same value of $\chi = 116.8 \text{ K/T} - 0.185$, we described the T_m of r-reg P3HT in Figure 4.7b by using Equation 4.1.9. As shown in Figure 4.7, the FH model adequately explains the experimental data. Note that Ade et al. studied the correlation of amorphous-amorphous phase separation and morphologies through the solid-state bilayer inter-diffusion experiments (Ye et al., 2018), where as we herein investigated π -conjugated polymer solutions and blends by elucidating a phase-separation mechanism in solutions, affecting the eventual morphologies of a film.

4.2 Phase Behavior of Amorphous/Semicrystalline Conjugated Polymer Blends

4.2.1 Thermal Property of Polymer Materials Analysis

Figure 4.9 shows the chemical structures of (a) P(NDI2OD-T2) and (b) PCPDTBT. In the previous works, we reported that the solubility parameter of P(NDI2OD-T2) is 7.99 (Fanta et al., 2019), whereas that of PCPDTBT ($M_n = 3.2 \text{ kg/mol}$ and $\text{PDI} = 2.2$) is 10.70 (Kim, 2019). Note that in this work, PCPDTBT has ($M_n = 4.5 \text{ kg/mol}$ and $\text{PDI} = 3.0$, indicating a very minor difference between the two PCPDTBT samples. Hence, based on the former δ data, the Flory-Huggins interaction parameter (Fanta et al., 2019, Flory, 1953, Hiemenz, 2007) for the PCPDTBT/P(NDI2OD-T2) polymer blends could be estimated using Equation 4.2.1:

$$\chi_{ij} = \frac{\hat{V}_s}{RT} (\delta_i - \delta_j)^2 \quad (4.2.1)$$

where \hat{V}_s (= lattice site volume) and $\delta_{i \text{ or } j}$ were the molar volume of a solvent [$\hat{V}_s = (112.56 \text{ g/mol}) / (1.11 \text{ g/cm}^3) = 101.41 \text{ cm}^3 / \text{mol}$ for CB] and the solubility parameter [subscript i or $j = 1, 2$; PCPDTBT = 1 and P(NDI2OD-T2) = 2]. R and T were the gas constant and temperature. Then χ_{12} was estimated to be 374.82 K/T , indicating that $\chi_{12} = 1.26$ at $T = 298.15 \text{ K}$ and

$\chi_{12} = 0.5$ at $T = 749.64$ K. Hence, considering the critical value of interaction parameter (Lipatov

and Nesterov, 1997), $(\chi_{12})_{crit} = \frac{1}{2} \cdot \left(\frac{1}{\sqrt{r_1}} + \frac{1}{\sqrt{r_2}} \right)^2 \approx 0.022$ and $\chi_{12} > (\chi_{12})_{crit}$, we conclude that

PCPDTBT and P(NDI2OD-T2) were immiscible as usual for many polymer-polymer mixtures.

Here we used $r_1 = \left(\frac{M_{n,1}}{p_s} \right) = \frac{4500}{112.56} \approx 44$ and $r_2 = \left(\frac{M_{n,2}}{p_s} \right) = \frac{32100}{112.56} \approx 288$, in which r_1 and r_2

were the relative molar volumes of component 1 and 2, $M_{n,1}$ and $M_{n,2}$ were the number average molecular weights of component 1 and 2, MW_s was the molecular weight of a solvent (CB), and ρ_1 , ρ_2 , and ρ_s were the densities of component 1, 2, and solvent, respectively. At this moment, keep in mind that the Flory-Huggins theory should be understood qualitatively, not quantitatively.

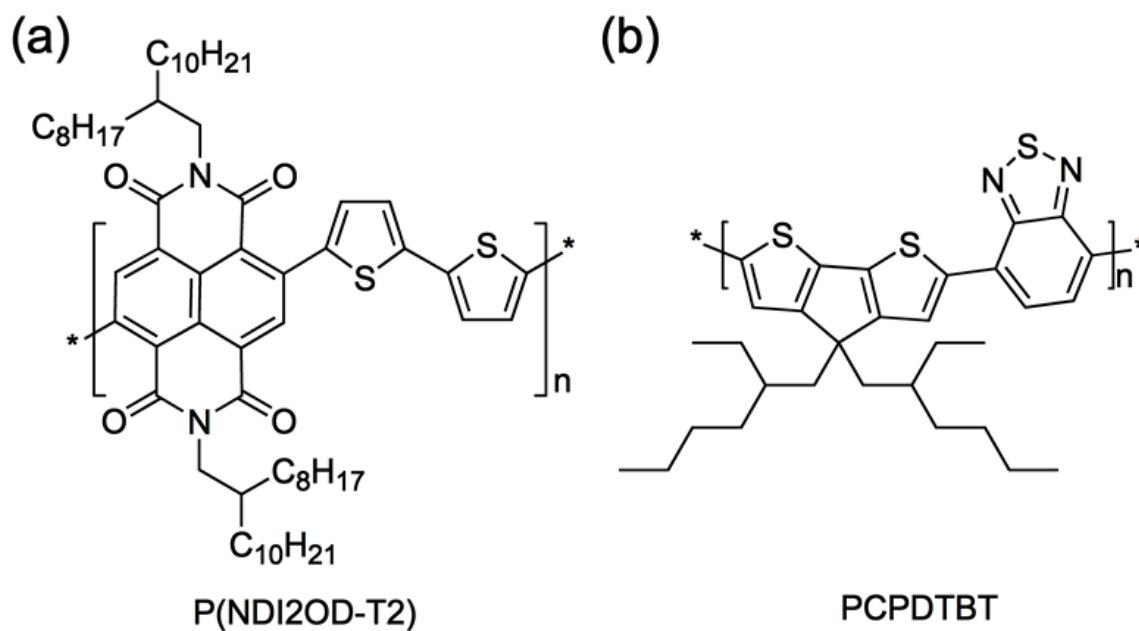


Figure 4.9. Chemical structures of (a) P(NDI2OD-T2) and (b) PCPDTBT, respectively.

As demonstrated in the aforementioned example, the PCPDTBT/P(NDI2OD-T2) mixture was an immiscible blend, which could be understood based on $\Delta G_m = \Delta H_m - T\Delta S_m$ where ΔG_m

was the Gibbs free energy of mixing, ΔH_m was the enthalpy of mixing, and ΔS_m was the entropy of mixing. When mixing long chain macromolecules, $\Delta S_m \approx 0$ and $\Delta H_m > 0$ leading to $\Delta G_m > 0$. Note that the stability condition for a single phase is $\left(\frac{\partial^2 \Delta G_m}{\partial \phi_i^2}\right)_{T,P} > 0$ where ϕ_i is volume fraction of component i and P is pressure. Hence most polymer-polymer blends including PCPDTBT and P(NDI2OD-T2) are immiscible but phase-separated. Usually, the same structural units are more attractive each other than different ones, leading to aggregation and clusters, i.e., the phase separation of blends.

Figure 4.10 exhibits TGA data, indicating that PCPDTBT and P(NDI2OD-T2) decompose at around ~ 400 - 500 °C in organic molecules. Figure 4.11 shows the DSC thermograms for the PCPDTBT/P(NDI2OD-T2) blends. As shown in Figure 4.11a, P(NDI2OD-T2) was a semicrystalline polymer with $T_m = 324$ °C (1st heating) or 318 °C (2nd heating) and $T_c = 294$ °C (1st cooling). On the other hand, PCPDTBT did not show any melting point, indicating it was a typical amorphous polymer (Kim et al., 2012); see Figure 4.11b–d. About the glass transition temperature, P(NDI2OD-T2) showed it at -44 °C in the DSC thermogram, which agreed with Gu et al.'s report $T_g = -40$ °C within experimental uncertainties. Although in the previous work (Kim, 2019), PCPDTBT showed $T_g \approx 112$ °C, in this work we could not observe it clearly. That is because, as shown in Figure 4.11d, some artifacts were observed for all the samples around 100 °C from the DSC instrumental conditions. Note that T_g is a second order transition, but in many conjugated polymer systems, it is hard to determine T_g due to a weak signal in DSC thermal curves.

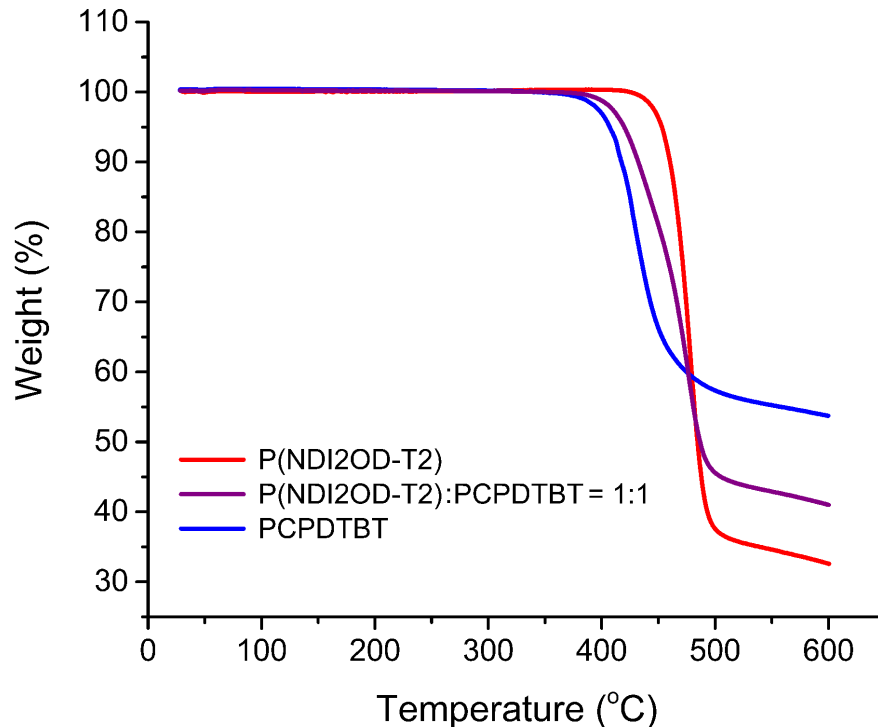


Figure 4.10 TGA curves for P(NDI2OD-T2), P(NDI2OD-T2)/PCPDTBT blend, and PCPDTBT.

It may be from the rigid or semirigid backbone structure of conjugated polymers, leading to relatively small free volume (and heat capacity) changes around the second-order transition when compared to flexible coil polymers.

Note that, in this work, our research interest lies primarily in the S-L phase equilibria (the 1st order transition) of conjugated polymer blends composed of the semicrystalline P(NDI2OD-T2) and the amorphous PCPDTBT polymers because it is relatively more clear than other 2nd order transition. As shown in Figure 4.11a, the 1st heating curve, the melting point is depressed from 323.35 °C at 100 % P(NDI2OD-T2) to 317.83 °C at 80 % to 312.79 °C at 50 %, which is a trend observed in the 1st cooling and 2nd heating curves, as well. Here note that in Figure 4.11b, at PCPDTBT:P(NDI2OD-T2) = 50:50, the melting peak looks very broad, indicating that, in blend system, a semicrystalline component should be required at least at 50 % for observing a clear and sharp T_m peak.

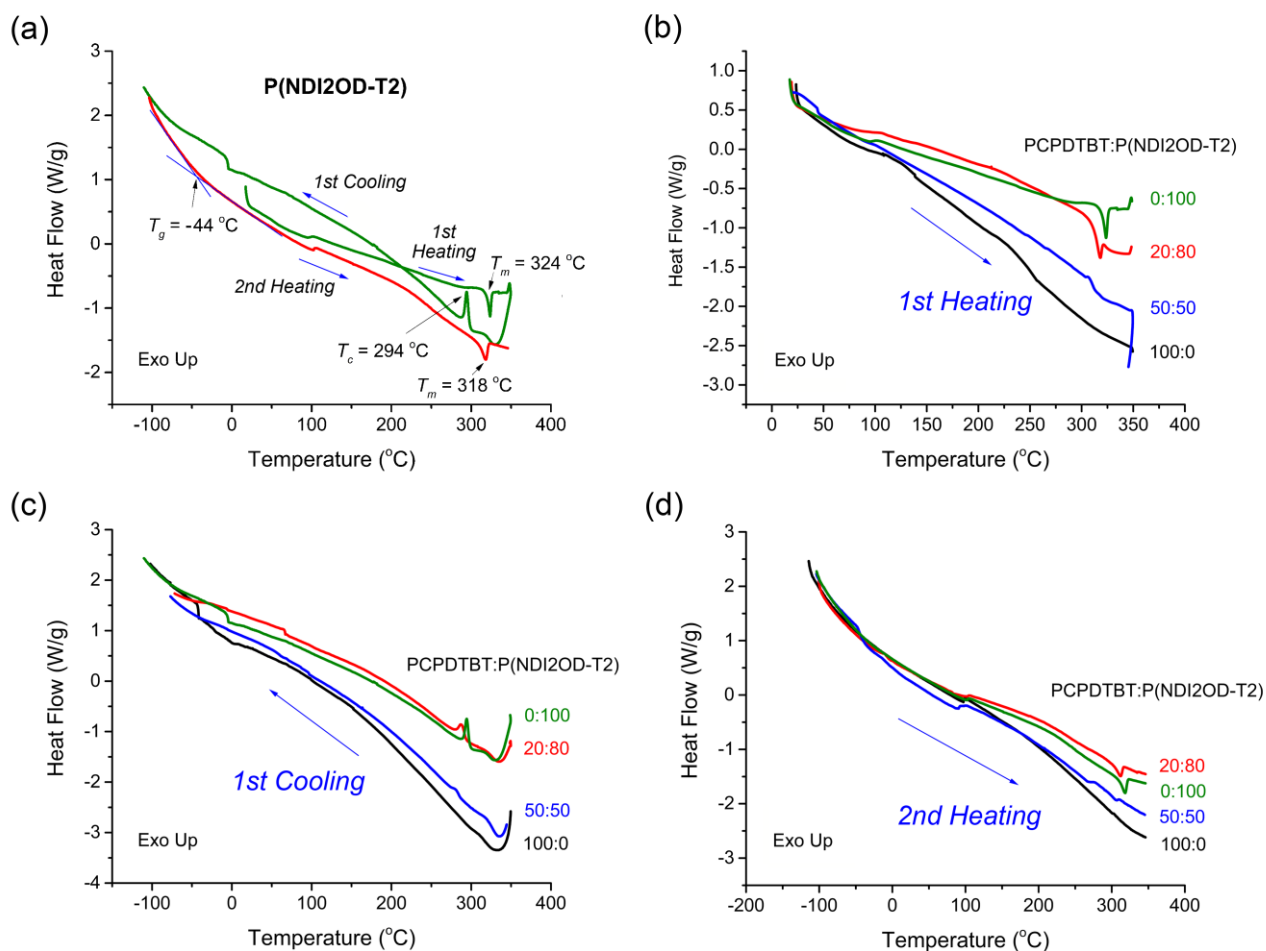


Figure 4.11 DSC curves. (a) Heating-cooling-heating curves for P(NDI2OD-T2). (b) 1st heating, (c) 1st cooling, and (d) 2nd heating curves for P(NDI2OD-T2):PCPDTBT = 100:0, 80:20, 50:50 and 0:100 (wt. ratio), respectively.

Then, the results were summarized in Figure 4.12, displaying both the T_m and T_c depression, in which the average difference ($\Delta T = T_m - T_c$) between T_m and T_c is 30.0 ± 1.6 °C in the first-cycling thermal curve. The origin of this depression comes from the new equilibrium between crystalline lamellar and amorphous (liquid) chains of P(NDI2OD-T2) when a diluent PCPDTBT was introduced into the semicrystalline P(NDI2OD-T2) system for forming polymer blends. Specifically, PCPDTBT has one order lower molecule weight, $M_n = 4.5$ kg/mol compared to P(NDI2OD-T2) with $M_n = 32.1$ kg/mol, indicating that many available end groups in PCPDTBT may serve as impurities in blend systems. However, a liquid state PCPDTBT chain molecule

itself may act as impurities in semicrystalline P(NDI2OD-T2) blends, depressing the melting point of the polymer blend systems.

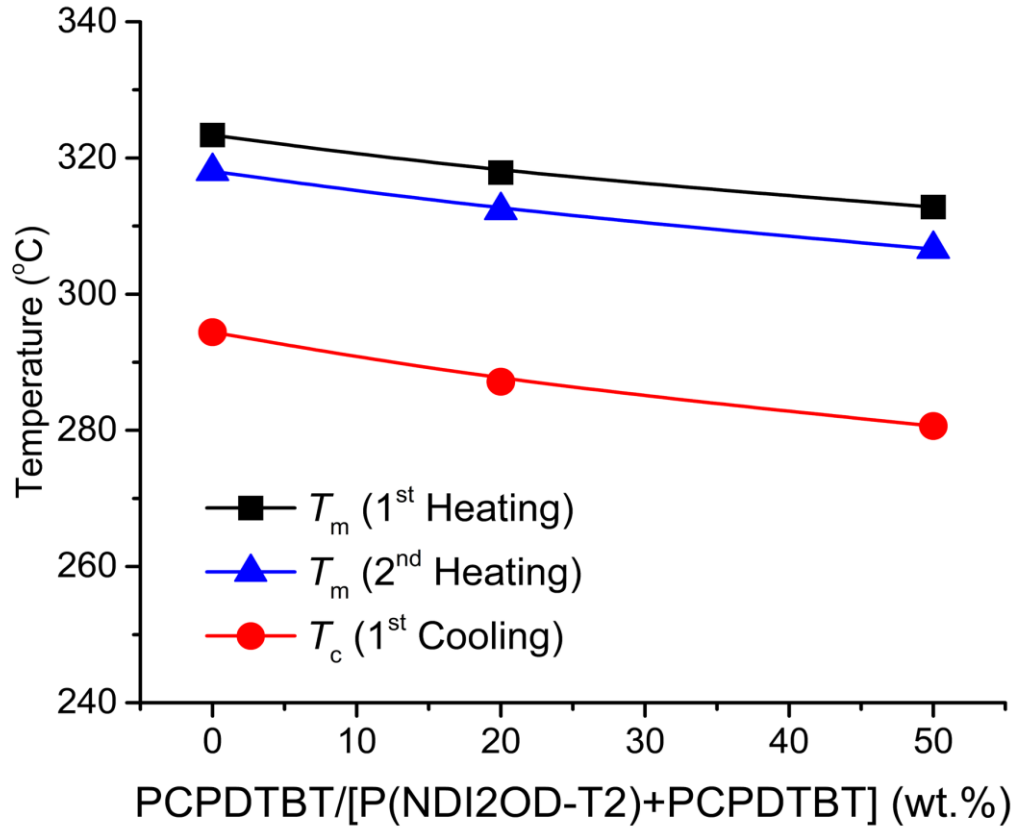


Figure 4.12 Melting and crystallization point depression of P(NDI2OD-T2)/PCPDTBT blends.

4.2.2 Morphology-X-ray Diffraction of Polymer Films Analysis

Figure 4.13 shows the XRD patterns of pure P(NDI2OD-T2), mixed P(NDI2OD-T2)/PCPDTBT blends, and pure PCPDTBT, respectively, in the range of $2\theta = 10^\circ$ – 100° . At $2\theta \sim 26^\circ$, some peaks related with π - π stacking are observed. Here, the crystallite size (t) could be estimated based on Scherrer's equation, $t = 0.9\lambda / (B \cos \theta)$ (Kim and Frisbie, 2008, Cullity and Stock, 2001), where λ is the X-ray wavelength ($= 0.154$ nm) and B is the full width at half maximum at the diffraction angle θ . The results are summarized in Table 4.4, indicating that the crystallite size decreases from 2.5 nm at 100 % P(NDI2OD-T2) to 2.0 nm at 50 %. In the case of PCPDTBT, its nominal crystallite size is very small ~ 1.4 nm, indicating that it is an amorphous material because the length scale is around the unit cell. Importantly, if we recall the DSC results

in Figure 4.11, when the crystallite size (related with π -stacking) is larger than 2 nm, we may observe melting transition in DSC.

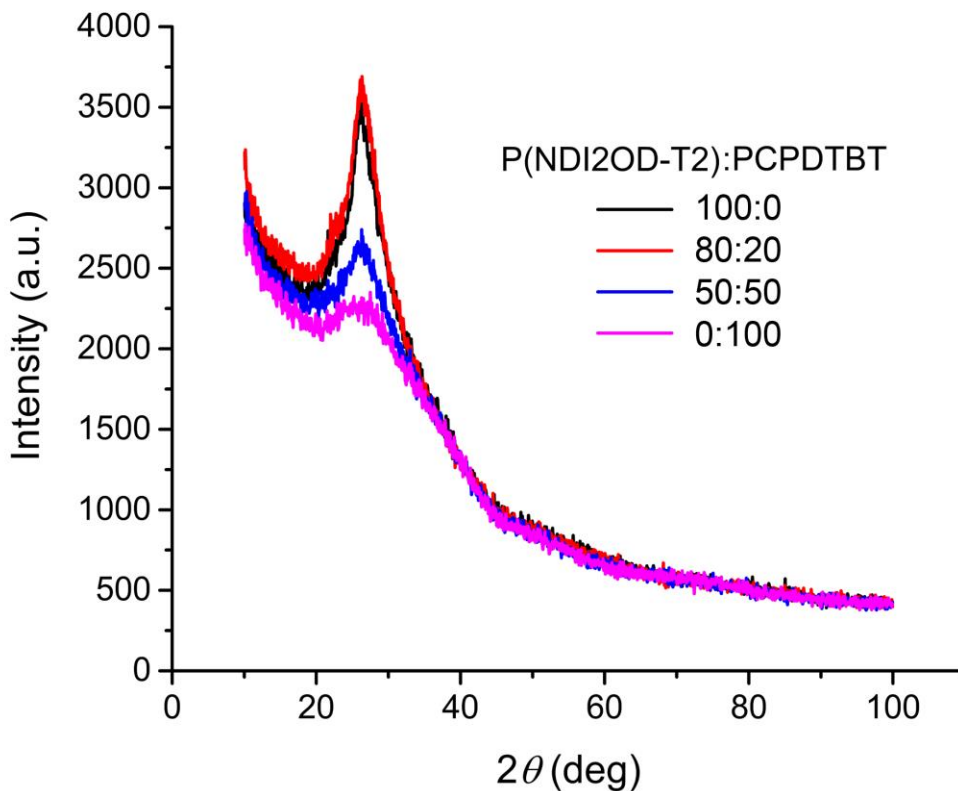


Figure 4.13 XRD patterns of P(NDI2OD-T2):PCPDTBT blends with 100:0, 80:20, 50:50 and 0:100 (wt. ratio).

It is notable also that, in polymer science, the typical unit cell, chain-folded lamella, and spherulite have dimensions of ~ 0.2 – 2 nm, ~ 10 – 50 nm thick and several microns wide, and ~ 100 – 1000 μm , respectively (Kim et al., 2012). In the case of conjugated polymer, thin-film samples for OPV, we usually observe up to a lamella scale because a film thickness is ~ 100 – 200 nm. However, there are some exception reporting a three-dimensional spherulite structure (Fischer et al., 2015, Dörfling et al., 2017, Ou et al., 2019, Armas et al., 2019). At this moment, for interesting readers, the detailed XRD data about P(NDI2OD-T2) films are available in the literatures (Rivnay et al., 2010, Brinkmann et al., 2012, Takacs et al., 2013, Zhou et al., 2014, Zhou et al., 2015, Zhang et al., 2016, Armas et al., 2019), in which edge-on and face-on morphologies were also reported.

Table 4.4 Crystallite size (t) and d -spacing of P(NDI2OD-T2):PCPDTBT blends with 100:0, 80:20, 50:50, and 0:100 (wt. ratio) at the diffraction angle θ , when X-ray has wavelength (λ) of 0.154 nm. Herein, d -spacing between lattice planes is calculated based on Bragg's law, $\lambda = 2d \sin \theta$.

P(NDI2OD-T2):PCPDTBT	$2\theta(^{\circ})$	$\theta(^{\circ})$	$B(\text{Radians})$	$t(\text{nm})$	$d\text{-Spacing}(\text{nm})$
100:0	26.16	13.08	0.05667	2.5	0.34
80:20	26.31	13.05	0.06319	2.3	0.34
50:50	26.26	13.13	0.06606	2.0	0.34
0:100	25.47	12.74	0.09980	1.4	0.35

Based on the crystallite size analysis in Table 4.4, as well as the melting point depression in Figure 4.12, we suggest the scheme displayed in Figure 4.14. When we add the amorphous chain molecule PCPDTBT into the semicrystalline P(NDI2OD-T2) sample, the crystalline region of P(NDI2OD-T2) may be destroyed, which could be confirmed through the decrease in XRD peaks' intensity at $2\theta = \sim 26^{\circ}$, i.e., π - π stacking, as well as the diminished melting peak in DSC thermograms in Figure 4.11. However, it is notable that the aforementioned phenomena do not necessarily mean the miscibility of the two polymers, i.e., they are still in phase-separate state. They are immiscible because of the thermodynamic reason, $\Delta G_m > 0$. However, the above observation may affect the nano- and micro-structure of blend films, which should be important in all-PSCs because of the limited diffusion length of Frenkel excitons in the organic/polymer semiconductors with low dielectric constants.

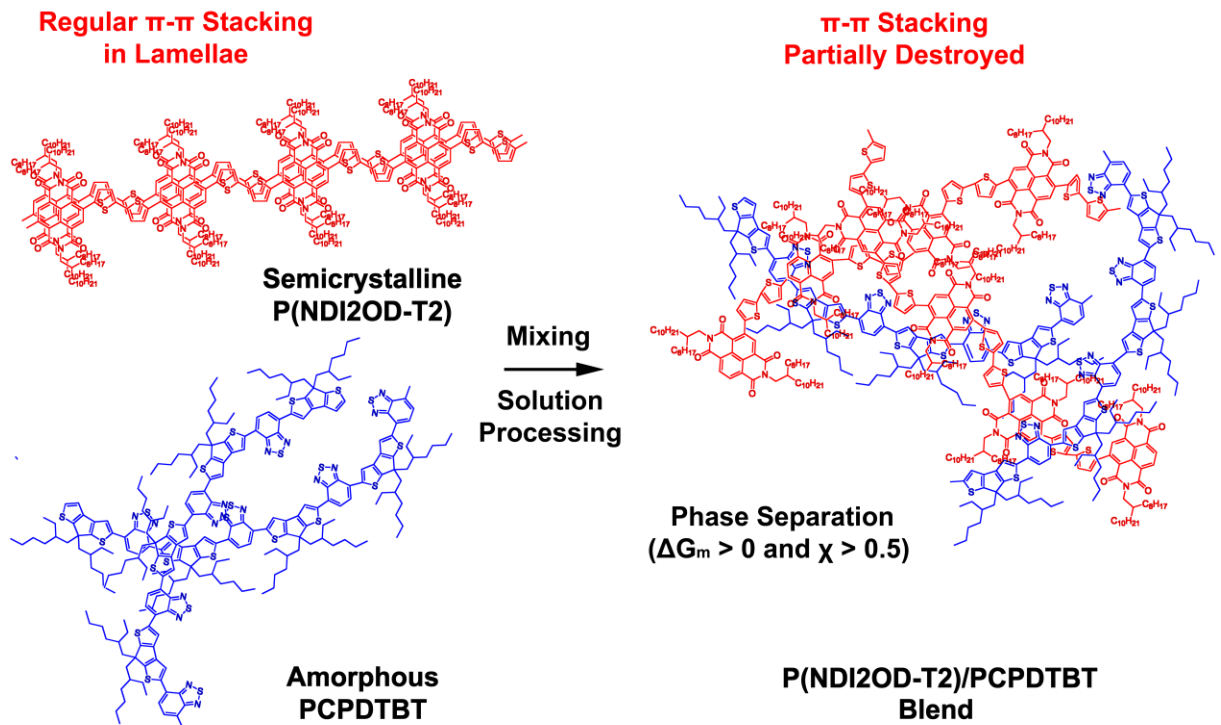


Figure 4.14 Schematic explanation of when semicrystalline P(NDI2OD-T2) and amorphous PCPDTBT polymers are mixed together through solution processing. Here, the regular π - π stacking could be destroyed by adding PCPDTBT into a crystalline P(NDI2OD-T2) lamellae.

4.2.3 Morphology-Tapping-Mode AFM of Polymer Films Analysis.

Figure 4.15. shows the AFM images of pure P(NDI2OD-T2), P(NDI2OD-T2)/PCPDTBT blend, and pure PCPDTBT. As shown in Figure 4.15a, P(NDI2OD-T2) film displays rod-shaped crystalline lamellae with a few μm . However, when P(NDI2OD-T2) was mixed with PCPDTBT with a 1:1 wt. ratio, the morphology changed dramatically. Here, elongated crystal domains were destroyed and diminished into a granular shape. Finally, PCPDTBT exhibits somewhat homogenous images when compared with P(NDI2OD-T2). This smoothness is expected because PCPDTBT is amorphous (disordered liquid or glass) based on both the DSC and XRD results.

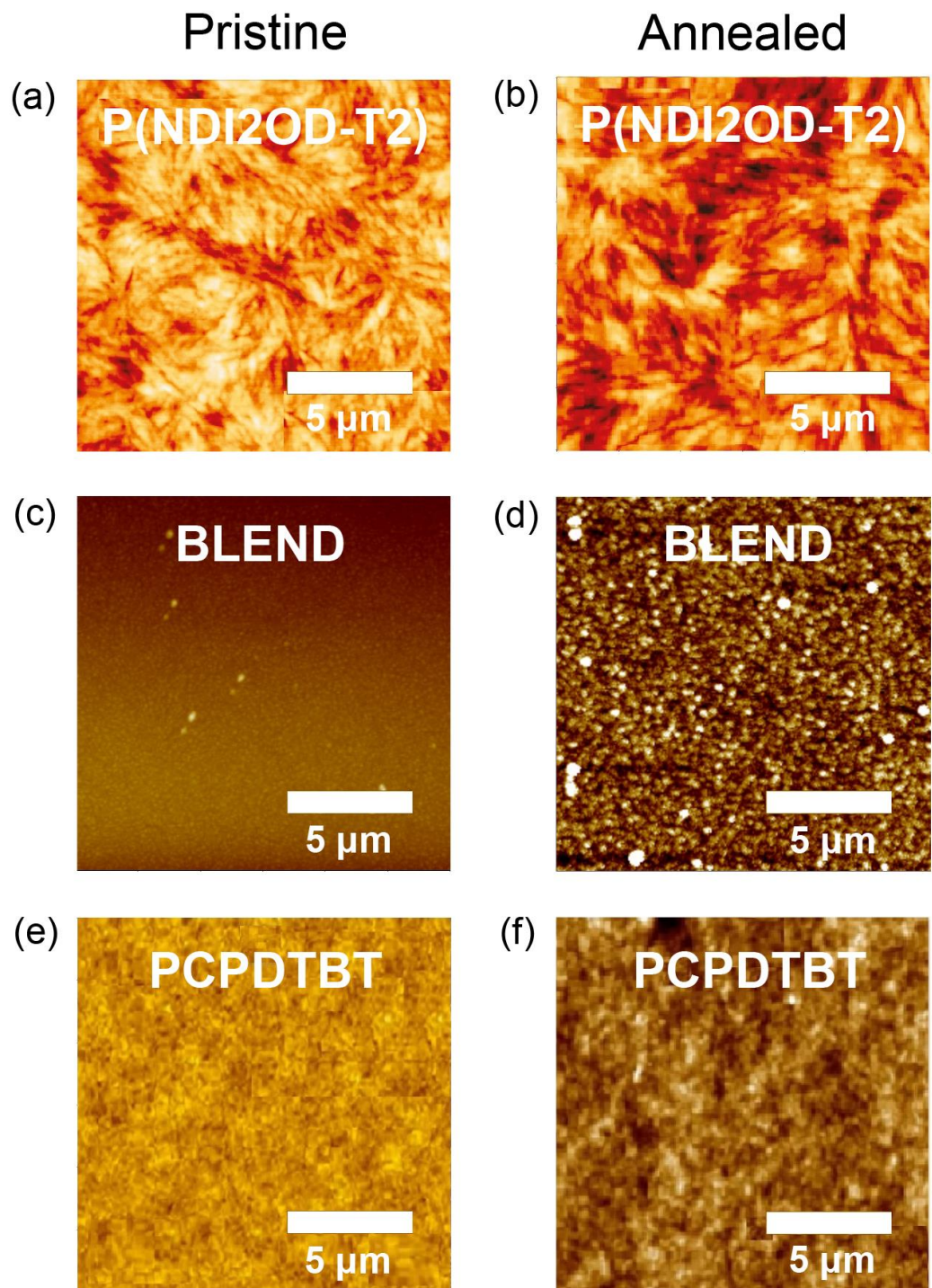


Figure 4.15 Tapping-mode AFM images of (a) pristine P(NDI2OD-T2), (b) annealed P(NDI2OD-T2), (c) pristine P(NDI2OD-T2):PCPDTBT = 1:1 blend, (d) annealed P(NDI2OD-T2):PCPDTBT = 1:1 blend, (e) pristine PCPDTBT, and (f) annealed PCPDTBT films, respectively.

5. GENERAL DISCUSSION

This part is the end part of this dissertation research and it has four parts. These includes, the overall dissertation research, strengths and limitation, conclusions; and also, useful method recommendations (i.e., which suggests future research direction) were developed based on the finding of the studies.

The work outlined in this dissertation was conducted with the goal of further understanding of all-polymer solar cell materials which includes the binary polymer-solvent and binary polymer-polymer blends, and then, the phase behavior of semicrystalline polymers, the r-reg P3HT/P(NDI2OD-T2) system, is studied based on both experimental and theoretical analyses. And also, an amorphous/semicrystalline conjugated polymer blend for which PCPDTBT and P(NDI2OD-T2) were chosen as a model system, and also the thermodynamic behavior of PCPDTBT/P(NDI2OD-T2) blends based on the thermal and structural analyses was studied.

The UV-VIS absorption spectra of n-type low bandgap P(NDI2OD-T2) was harvesting light near infrared regions about 855 nm. When P(NDI2OD-T2) is dissolved in a common solvent such as chlorobenzene, the solution color is almost black, but its film is bluish. For estimating the solubility parameter, we measured the contact angle and then both the solubility parameter and surface energy are calculated. As the result indicated that the P(NDI2OD-T2) is much more hydrophobic when compared to r-reg P3HT. Note that in some experimental observations, the Flory-Huggins interaction parameter is a function of not only a temperature-dependent interaction parameter, $D(T)$, but also a composition-dependent parameter $B(\phi_2)$. The theoretical phase diagrams of binary polymer solutions (i.e., P(NDI2OD-T2):CB blends), and the melting point depression curves are calculated for three hypothetical crystallinities of P(NDI2OD-T2), i.e., $x_c = 35\%$ (blue line), 45% (red), and 55% (green). The difference between $LLE > SLE$ and $SLE > LLE$ should make polymer solutions undergo different pathways for morphology formation, in which the former undergoes SD or NG, but the latter crystallization. For the purpose of clear comparison, when we calculated the phase diagrams of r-reg P3HT solution for the same solvent, CB, CF and XY, we can observe only Case 3 (i.e., SLE

> LLE). Hence, we can say that the r-reg P3HT solution may undergo phase separation primarily through crystallization, whereas P(NDI2OD-T2) solution may phase separate via SD or NG or crystallization or any combination of SD/NG and crystallization, depending on the solvent, CB or CF or XY. The pure polymers, P(NDI2OD-T2) and r-reg P3HT show T_m at 314.80 °C (with an enthalpy of 14.46 J/g) and at 211.37 °C (that of 17.80 J/g), respectively. These two polymers were mixed together and compositions of 20, 50, and 80 wt.% P(NDI2OD-T2) were made, resulting in the T_m and T_c , in which all the blend compositions showed each T_m and T_c , originating from pure P(NDI2OD-T2) and r-reg P3HT, indicating that these polymers were immiscible, as expected from two different polymer-polymer systems in the absence of any specific interaction. Note that P(NDI2OD-T2) and r-reg P3HT have a similar thermal stability, showing decomposition in the range of ~ 430–500 °C. As we constructed the temperature-composition phase diagram of the r-reg P3HT/P(NDI2OD-T2) system, in which the first observation was that T_m and T_c were very similar in blends compared to those of each pure polymer, indicating they were immiscible. The phase behavior of the r-reg P3HT/P(NDI2OD-T2) system was very simple, in which **L** and **S** stand for liquid and solid state, respectively. When the temperature was lower than T_m of r-reg P3HT, the resultant phase was two solid mixtures, $\mathbf{S}_{\text{P(NDI2OD-T2)}} + \mathbf{S}_{\text{r-reg P3HT}}$. However, when the temperature was increased above the T_m of r-reg P3HT but less than the T_m of P(NDI2OD-T2), the phase was $\mathbf{S}_{\text{P(NDI2OD-T2)}} + \mathbf{L}_{\text{r-reg P3HT}}$. Finally, when the temperature was increased above the T_m of P(NDI2OD-T2), the phase became a liquid state, **L**.

The two polymers, PCPDTBT and P(NDI2OD-T2) are theoretically immiscible. At this moment, keep in mind that the Flory-Huggins theory should be understood qualitatively, not quantitatively. Hence most polymer-polymer blends including PCPDTBT and P(NDI2OD-T2) are immiscible but phase-separated. Usually, the same structural units are more attractive each other than different ones, leading to aggregation and clusters, i.e., the phase separation of blends. Note that T_g is a second order transition, but in many conjugated polymer systems, it is hard to determine T_g due to a weak signal in DSC thermal curves. It may be from the rigid or semirigid

backbone structure of conjugated polymers, leading to relatively small free volume (and heat capacity) changes around the second-order transition when compared to flexible coil polymers. In this work, our research interest lies primarily in the S-L phase equilibria (the 1st order transition) of conjugated polymer blends composed of the semicrystalline P(NDI2OD-T2) and the amorphous PCPDTBT polymers because it is relatively more clear than other 2nd order transition. The 1st heating curve, the melting point is depressed from 323.35 °C at 100 % P(NDI2OD-T2) to 317.83 °C at 80 % to 312.79 °C at 50 %, which trend is observed in the 1st cooling and 2nd heating curves, as well. Here note that at PCPDTBT: P(NDI2OD-T2) = 50:50, the melting peak looks very broad, indicating that, in blend system, a semicrystalline component should be required at least 50 % for observing a clear and sharp T_m peak. Then, the results were displaying both the T_m and T_c depression, in which the average difference ($\Delta T = T_m - T_c$) between T_m and T_c is 30.0 ± 1.6 °C in the first-cycling thermal curve. The origin of this depression comes from the new equilibrium between crystalline lamellar and amorphous (liquid) chains of P(NDI2OD-T2) when a diluent PCPDTBT was introduced into the semicrystalline P(NDI2OD-T2) system for forming polymer blends. Specifically, PCPDTBT has one order lower molecule weight, $M_n = 4.5$ kg/mol compared to P(NDI2OD-T2) with $M_n = 32.1$ kg/mol, indicating that many available end groups in PCPDTBT may serve as impurities in blend systems. However, a liquid state PCPDTBT chain molecule itself may act as impurities in semicrystalline P(NDI2OD-T2) blends, depressing the melting point of the polymer blend systems. At $2\theta = \sim 26^\circ$, some peaks related with π - π stacking are observed. The results are indicating that the crystallite size decreases from 2.5 nm at 100 % P(NDI2OD-T2) to 2.0 nm at 50 %. In the case of PCPDTBT, its nominal crystallite size is very small ~ 1.4 nm, indicating that it is an amorphous material because the length scale is around the unit cell. Importantly, if we recall DSC results, when the crystallite size (related with π -stacking) is larger than 2 nm, we may observe melting transition in DSC. It is notable also that, in polymer science, the typical unit cell, chain-folded lamella, and spherulite have dimensions of ~ 0.2 –2 nm, ~ 10 –50 nm thick and several microns wide, and ~ 100 –1000 μm , respectively. In the case of conjugated polymer thin-film samples for OPV, we usually observe up to a lamella scale because a film thickness is ~ 100 –200 nm. However, there are some exception reporting a three-dimensional spherulite structure. At this moment, for interesting readers, the detailed XRD data about P(NDI2OD-T2)

films are available in the literatures, in which edge-on and face-on morphologies were reported. When we add the amorphous chain molecule PCPDTBT into the semicrystalline P(NDI2OD-T2) sample, the crystalline region of P(NDI2OD-T2) may be destroyed, which could be confirmed through the decrease of XRD peaks' intensity at $2\theta = \sim 26^\circ$, i.e., π - π stacking as well as the diminished melting peak in DSC thermograms. However, it is notable that the aforementioned phenomena do not necessarily mean the miscibility of the two polymers, i.e., they are still in phase-separate state. They are immiscible because of the thermodynamic reason, $\Delta G_m > 0$. The P(NDI2OD-T2) film displays rod-shaped crystalline lamellae with a few μm . However, when P(NDI2OD-T2) was mixed with PCPDTBT with a 1:1 wt. ratio, the morphology changed dramatically. Here, elongated crystal domains were destroyed and diminished into a granular shape. Finally, PCPDTBT exhibits somewhat homogenous images when compared with P(NDI2OD-T2). This smoothness is expected because PCPDTBT is amorphous (disordered liquid or glass) based on both the DSC and XRD results.

5.1 The Outputs of Dissertation Research

The dissertation research work focusses on the studies of the morphology and phase behavior of polymer/solvent solution and polymer/polymer blends. This research work contributes to the development of organic solar energy for devices that make use of polymer/solvent and polymer/polymer blend systems. Understanding the phase behavior of the polymer solutions and blends affecting morphologies plays an integral role towards developing polymer optoelectronic devices. Considering P(NDI2OD-T2) is a commonly used polymer acceptor material for all polymer solar cells, we believe our findings will be of great help for understanding the morphology-generation mechanism for active layers composed of polymer donor and polymer acceptor in all-polymer solar cells. Our dissertation research suggests an alternative to achieve well-defined morphology in polymer/solvent solution and polymer/polymer blends; and also provides a better understanding of the background knowledge of the thermodynamics and phase separation mechanism in polymer blends. To the best of our knowledge, in our dissertation research, we constructed for the first-time phase diagrams of binary n-type low bandgap P(NDI2OD-T2) solutions as a function of three different solvents, chlorobenzene, chloroform, and p-xylene, for which the Flory-Huggins lattice model was employed with a χ interaction parameter estimated from the solubility parameter. The other point of our research finding was, we have published internationally recognized research article on journals of web of science with high impact factor and highly indexed (i. e., in our case the area of research was Biopolymers and Polymer Physics on Polymers, Multidisciplinary Digital Publishing Institute (MDPI)).

5.2 Strengths and Limitation

Jimma University is primarily devoted to launch and run educational programs highly relevant for the nation with particular emphasis on those which are rarely or not at all offered by other national Universities. Materials Science and Engineering is among those programs that the University dared to launch a PhD program. In addition to this, Science and Technology Development is one of the factors, which should be pursued for both the effective import of foreign technologies and their application to the universities, research institutes and industries through technology transfer. In line with these objectives, Jimma University opened a PhD program in the Faculty of Materials Science and Engineering for building up human resources and providing them to the community, both local and global. However, the University is struggling with the program for its research demands intensive resources and high-tech laboratory that the University could not fulfill for a moment. As a result, I in Materials Science and Engineering could not complete my dissertation in time due to lack of laboratory facilities, lack of manpower in my research fields, lack of both office and internet facilities for students at JIT, purchasing polymeric materials, chemical reagents, financial limitations and problems in Jimma University; and also at country level in case of advanced researches for testing, solution preparation, film processing, characterizing of all polymer solar cell materials I have produced through my research in Ethiopia. The strength of my research methods was sample preparations of polymeric materials for different equipment's to test or characterize accordingly to the set up of the apparatus. The other strength of our research dissertation was, we were published internationally recognized research article papers in high impact journals (in our case on Polymers MDPI). One of the limitations of this research was unable to cover to solve the problems that were observed on polymer solar cell generally and specifically, all polymer solar cell materials. The other challenge was familiarized with the laboratory equipment's, because of the research area of all polymer solar cell materials is very competitive technology issue today in polymer solar cells research. It only focuses on problems related to film processing, polymeric materials characterizations as well as surface morphologies related problems. In these situations, and challenges, I have completed my PhD dissertation work supported by both the Ministry of Science and Higher Education-Ethiopia six months for lab. work and Erasmus plus scholarship five months for study, stayed at Silesian University of Technology, Gliwice, Poland.

5.3 Conclusions

In this study, we constructed for the first-time phase diagrams of binary n-type low bandgap P(NDI2OD-T2) solutions as a function of three different solvents, chlorobenzene, chloroform, and p-xylene, for which the Flory-Huggins lattice model was employed with an interaction parameter (χ) estimated from the solubility parameter. The P(NDI2OD-T2) solutions showed the three different types of phase behavior depending on the solvent, Case 1: liquid-liquid equilibria $>$ solid-liquid equilibria, Case 2: liquid-liquid equilibria \approx solid-liquid equilibria, and Case 3: solid-liquid equilibria $>$ liquid-liquid equilibria, corresponding to P(NDI2OD-T2)/chlorobenzene, P(NDI2OD-T2)/chloroform, and P(NDI2OD-T2)/p-xylene, respectively. Specifically, when we compared the phase behavior of the P(NDI2OD-T2) solutions and that of the r-reg P3HT ones, the latter showed only Case 3: solid-liquid equilibria $>$ liquid-liquid equilibria, indicating r-reg P3HT undergoes phase separation from solutions over crystallization, i.e., liquid-solid phase transition. It is unlikely that r-reg P3HT is phase separated out from solution through spinodal decomposition or nucleation/growth, because the liquid-liquid equilibria are far below the solid-liquid equilibria and room temperature. Finally, we constructed the phase diagram of a binary polymer-polymer, the r-reg P3HT/P(NDI2OD-T2) system for the first time. These two semicrystalline polymers showed spontaneous phase separation, i.e., immiscibility, due to both the absence of specific interaction and the entropic penalty coming from the mixing of polymeric chains. Importantly, based on melting point depression theory combined with the Flory-Huggins model, we successfully described the experimental melting points of the r-reg P3HT/P(NDI2OD-T2) system, for which the entropic contribution χ_s to χ was adjusted to be -0.185, indicating an increase of entropy by forming a new contact between two polymer segments. Considering P(NDI2OD-T2) is a commonly used polymer acceptor material for all polymer solar cells, we believe our findings will be of great help for understanding the morphology-generation mechanism for active layers composed of polymer donor and polymer acceptor in all polymer solar cells. Two low bandgap conjugated polymers, semicrystalline P(NDI2OD-T2) and amorphous PCPDTBT, were mixed together for a study on phase behavior. Here, P(NDI2OD-T2) is a high-performance n-type semiconductor, whereas PCPDTBT is a p-type one when applied to optoelectronic devices. And although two polymers

were immiscible with $\chi_{12} = 1.26$ at $T = 298.15$ K, the blend exhibited the melting and crystallization temperature depression phenomena because PCPDTBT acts as a diluent or impurity for the P(NDI2OD-T2) lamellae. In this process, PCPDTBT molecules make it difficult for the P(NDI2OD-T2) chains to form lamellae, leading them to destroy the regular π - π stacking in the polymer lamellae, which was confirmed through XRD and AFM data. Specifically, when the size of crystallite-related π -stacking was larger than 2 nm, we observed the melting points in DSC. Finally, when we apply conjugated polymer blends to electronic and optoelectronic devices, it is very important to understand a phase-separation mechanism leading to a specific morphology.

5.4 Recommendations

From the result of this dissertation research study I would like to recommend as a future work it will be very important: -

- To further elucidate the phase-separation mechanism (i.e., spinodal decomposition or nucleation/growth or crystallization) experimentally for π -conjugated polymer solutions and blends.
- To further study will be designed for understanding other photovoltaic polymer blends with amorphous/amorphous, semicrystalline/amorphous, and semicrystalline/semicrystalline structures.
- To further study the device processing, performance and reliability of various P3HT/P(NDI2OD-T2) and PCPDTBT/P(NDI2OD-T2) systems for characterizing all-polymer solar cells in terms of short circuit current density, open circuit voltage, fill factor, and power conversion efficiency.

6. REFERENCES

- AGOSTINELLI, T., FERENCZI, T. A. M., PIRES, E., FOSTER, S., MAURANO, A., LLER, C. M., BALLANTYNE, A., HAMPTON, M., LILLIU, S., CAMPOY-QUILES, M., AZIMI, H., MORANA, M., BRADLEY, D. D. C., DURRANT, J., MACDONALD, J. E., STINGELIN, N. & NELSON, J. **2011**. The Role of Alkane Dithiols in Controlling Polymer Crystallization in Small Band Gap Polymer: Fullerene Solar Cells. *J. Polym. Sci. Part B: Polym. Phys.*, *49*, 717-724.
- ALBRECHT, S., JANIETZ, S., SCHINDLER, W., FRISCH, J., KURPIERS, J., KNIEPERT, J., INAL, S., PINGEL, P., FOSTIROPOULOS, K., KOCH, N. & NEHER, D. **2012**. Fluorinated Copolymer PCPDTBT with Enhanced Open-Circuit Voltage and Reduced Recombination for Highly Efficient Polymer Solar Cells. *J. Am. Chem. Soc.*, *134*, 14932-14944.
- ALI, R., MANSUR, T. M. N. T., BAHARUDIN, N. H. & HASSAN, S. I. S. **2016**. Environmental Impacts of Renewable Energy. *Electric Renewable Energy Systems, Elsevier Inc.*, 520-546.
- AMERI, T., MIN, J., LI, N., MACHUI, F., BARAN, D., FORSTER, M., SCHOTTLER, K. J., DOLFEN, D., SCHERF, U. & BRABEC, C. J. **2012**. Performance Enhancement of the P3HT/PCBM Solar Cells Through NIR Sensitization Using a Small-Bandgap Polymer. *Adv. Eng. Mater.*, *2*, 1-5.
- ANTHONY, J. E. **2011**. Small-Molecule, Nonfullerene Acceptors for Polymer Bulk Heterojunction Organic Photovoltaics. *Chem. Mater.*, *23*, 583-590.
- ARIAS, A. C., MACKENZIE, J. D., STEVENSON, R., HALLS, J. J. M., INBASEKARAN, M., WOO, E. P., RICHARDS, D. & FRIEND, R. H. **2001**. Photovoltaic Performance and Morphology of Polyfluorene Blends: A Combined Microscopic and Photovoltaic Investigation. *Macromol.*, *34*, 6005-6013.
- ARMAS, J. A., REYNOLDS, K. J., MARSH, Z. M., FERNÁNDEZ-BLÁZQUEZ, J. P., AYALA, D., CRONIN, A. D., DELAGUILA, J., FIDELDY, R., ABDU, J. P. & BILGER, D. W. **2019**. Supramolecular Assembly of Oriented Spherulitic Crystals of Conjugated Polymers Surrounding Carbon Nanotube Fibers. *Macromol. Rapid Commun.*, *40*, 1-5.
- ASIF, M. & MUNEER, T. **2007**. Energy Supply, Its Demand and Security Issues for Developed and Emerging Economies. *J. Renewable Sustainable Energy Reviews*, *11*, 1388-1413.
- AVTAR, R., SAHU, N., AGGARWAL, A. K., CHAKRABORTY, S., KHARRAZI, A., YUNUS, A. P., DOU, J. & KURNIAWAN, T. A. **2019**. Exploring Renewable Energy Resources Using Remote Sensing and GIS-A review. *J. Resources*, *8*, 149.
- AYGÜL, U., BATCHELOR, D., DETTINGER, U., YILMAZ, S., ALLARD, S., SCHERF, U., PEISER, T. H. & CHASSÉ, T. **2012**. Molecular Orientation in Polymer Films for Organic Solar Cells Studied by NEXAFS. *J. Phys. Chem. C*, *116*, 4870-4874.

- BANAL, J.L., SUBBIAH, J., GRAHAM, H., LEE, J.-K., GHIGGINO, K.P. & WONG, W.W.H. **2012**. Electron Deficient Conjugated Polymers Based on Benzotriazole. *Polym. Chem.*, 1-7.
- BATTERSBY, S. **2019**. News Feature: The Solar Cell of the Future. *J. Proceedings of the National Academy of Sci.*, 116, 7-10.
- BATES, F.S. **1991**. Polymer-Polymer Phase Behavior. *J. Sci.*, 251, 898-905.
- BATES, F.S. & FREDRICKSON, G.H. **1990**. Block Copolymer Thermodynamics: Theory and Experiment. *J. Annu. Rev. Phys. Chem.*, 41, 525-557.
- BAVEL, S.V., VEENSTRA, S. & LOOS, J. **2010**. On the Importance of Morphology Control in Polymer Solar Cells. *Macromol. Rapid Commun.*, 31, 1835-1845.
- BEAUJUGE, P.M. & FRECHET, J.M.J. **2011**. Molecular Design and Ordering Effects in π -Functional Materials for Transistor and Solar Cell Applications. *J. Am. Chem. Soc.*, 133, 20009-20029.
- BELMARES, M., BLANCO, M., GODDARD, W.A., III, ROSS, R.B., CALDWELL, G., CHOU, S.-H., PHAM, J., OLOFSON, P.M. & THOMAS, C. **2004**. Hildebrand and Hansen Solubility Parameters from Molecular Dynamics with Applications to Electronic Nose Polymer Sensors. *J. Comput. Chem.*, 25, 1814-1826.
- BENTEN, H., MORI, D., OHKITA, H. & ITO, S. **2016**. Recent Research Progress of Polymer Donor/Polymer Acceptor Blend Solar Cells. *J. Mater. Chem. A*, 4, 5340-5365.
- BINDER, K. **1983**. Collective Diffusion, Nucleation, and Spinodal Decomposition in Polymer Mixtures. *J. Chem. Phys.*, 79, 6387-6409.
- BOTIZ, I. & DARLING, S.B. **2010**. Optoelectronics Using Block Copolymers. *Mater. Today* 13, 42-51.
- BOUDREAULT, P.L.T., NAJARI, A. & LECLERC, M. **2011**. Processable Low-Bandgap Polymers for Photovoltaic Applications. *Chem. of Mater.*, 23, 456-469.
- BRINKMANN, M., GONTHIER, E., BOGEN, S.F., TREMEL, K., LUDWIGS, S., HUFNAGEL, M. & SOMMER, M. **2012**. Segregated Versus Mixed Interchain Stacking in Highly Oriented Films of Naphthalene Diimide Bithiophene Copolymers. *J. ACS Nano.*, 6, 10319-10326.
- CAHN, J.W. **1965**. Phase Separation by Spinodal Decomposition in Isotropic Systems. *J. Chem. Phys.*, 42, 93-99.
- CHAMBON, S., R., KOENVANDEWAL, E.C., MARKUSSCHARBER, L.G., J., JEANMANCA, D. & PETERAD, R. **2012**. Influence of Octanedithiol on The nano morphology of PCPD T B

- :PCBM Blends Studied By solid-State NMR. *Solar Energy Mater. & Solar Cells*, 96, 210-217.
- CHEN, H., HSIAO, Y.-C., HU, B. & DADMUN, M. **2014**. Tuning the Morphology and Performance of Low Bandgap Polymer: Fullerene Heterojunctions via Solvent Annealing in Selective Solvents. *Adv. Funct. Mater.*, 24, 1-8.
- CHEN, J.W. & CAO, Y. **2009**. Development of Novel Conjugated Donor Polymers for High-Efficiency Bulk-Heterojunction Photovoltaic Devices *Account. Chem. Research*, 42, 1709-1718.
- CHENG, Y.J., YANG, S.H. & HSU, C.S. **2009**. Synthesis of Conjugated Polymers for Organic Solar Cell Applications. *Chemical Reviews*, 109, 5868-5923.
- CLARK, J., CHANG, J.-F., SPANO, F.C., FRIEND, R.H. & SILVA, C. **2009**. Determining Exciton Bandwidth and Film Microstructure in Polythiophene Films Using Linear Absorption Spectroscopy. *Appl. Phys. Lett.*, 94, 163306.
- CLARKE, T.M. & DURRANT, J.R. **2010**. Charge Photogeneration in Organic Solar Cells. *Chem. Rev.*, 110, 6736-6767.
- CULLITY, B. & STOCK, S. **2001**. Elements of X-Ray Diffraction, Prentice Hall. *Upper Saddle River, New Jersey*, 388.
- DEREJE, M.M., JI, D., KANG, S.-H., YANG, C.D. & NOH, Y.-Y. **2017**. Effect of Pre-aggregation in Conjugated Polymer Solution on Performance of Diketopyrrolopyrrole-Based Organic Field-effect Transistors. *Dyes Pigments*, 145, 270-276.
- DING, G., YUAN, J., HUANG, X., LIU, Z., SHI, G., SHI, S., DING, J., WANG, H.-Q. & MA, W. **2015**. Efficient All Polymer Solar Cells Employing Donor Polymer Based on Benzo[1,2-b:4,5-b'] dithiophene Unit. *AIP Adv.*, 5, 117126.
- DOLAN, J.A., WILTS, B.D., VIGNOLINI, S., BAUMBERG, J.J., STEINER, U. & WILKINSON, T.D. **2015**. Optical Properties of Gyroid Structured Materials: From Photonic Crystals to Metamaterials. *J. Adv. Optical Mater.*, 3, 12-32.
- DÖRLING, B., SÁNCHEZ-DÍAZ, A., ARTEAGA, O., VECIANA, A., ALONSO, M.I. & CAMPOY-QUILES, M. **2017**. Controlled Pinning of Conjugated Polymer Spherulites and Its Application in Detectors. *Adv. Optical Mater.*, 5, 1700276.
- ETZOLD, F., HOWARD, I.A., FORLER, N., CHO, D.M., MEISTER, M., MANGOLD, H., SHU, J., HANSEN, M.R., MÜLLEN, K. & LAQUAI, F.D.R. **2012**. The Effect of Solvent Additives on Morphology and Excited-State Dynamics in PCPDTBT:PCBM Photovoltaic Blends. *J. Am. Chem. Soc.*, 134, 10569-10583.

- EARMME, T., HWANG, Y.-J., MURARI, N.M., SUBRAMANIYAN, S. & JENEKHE, S.A. **2013**. All-Polymer Solar Cells with 3.3% Efficiency Based on Naphthalene Diimide-Selenophene Copolymer Acceptor. *J. Am. Chem. Soc.*, 135, 14960-14963.
- EARMME, T., HWANG, Y.-J., SUBRAMANIYAN, S. & JENEKHE, S.A. **2014**. All-Polymer Bulk Heterojunction Solar Cells with 4.8% Efficiency Achieved by Solution Processing from a Co-Solvent. *Adv. Mater.*, 6080.
- FABIANO, S., CHEN, Z., VAHEDI, S., FACCHETTI, A., PIGNATAROC, B. & LOI, M.A. **2011**. Role of Photoactive Layer Morphology in High Fill Factor All-Polymer Bulk Heterojunction Solar Cells. *J. Mater. Chem.*, 21, 5891-5896.
- FACCHETTI, A. **2011**. Pi-Conjugated Polymers for Organic Electronics and Photovoltaic Cell Applications. *Chem. of Mater.*, 23, 733-758.
- FACCHETTI, A. **2013**. Polymer Donor-Polymer Acceptor (all-Polymer) Solar Cells. *Mater. Today*, 16, 123-132.
- FAN, B., YING, L., ZHU, P., PAN, F., LIU, F., CHEN, J., HUANG, F. & CAO, Y. **2017**. All-Polymer Solar Cells Based on a Conjugated Polymer Containing Siloxane-Functionalized Side Chains With Efficiency Over 10%. *Adv. Mater.*, 29, 1703906.
- FAN, B., ZHANG, D., LI, M., ZHONG, W., ZENG, Z., YING, L., HUANG, F. & CAO, Y. **2019**. Achieving Over 16% Efficiency for Single-Junction Organic Solar Cells. *Sci. China Chem.*, 62, 405.
- FANTA, G.M., JARKA, P., SZELUGA, U., TAŃSKI, T. & KIM, J.Y. **2019**. Phase Diagrams of n-type Low Bandgap Naphthalenediimide-Bithiophene Copolymer Solutions and Blends. *J. Polymers*, 11, 1474.
- FAVVAS, E.P. & MITROPOULOS, A.C. **2008**. What is Spinodal Decomposition? *J. Eng. Sci. Technol. Rev.*, 1, 25-37.
- FENG, K., HUANG, J., ZHANG, X., WU, Z., SHI, S., THOMSEN, L., TIAN, Y., WOO, H.Y., MCNEIL L, C.R. & GUO, X. **2020**. High-Performance All-Polymer Solar Cells Enabled by n-Type Polymers with an Ultranarrow Bandgap Down to 1.28 eV. *J. Adv. Mater.*, 2001476.
- FISCHER, F.S., TREFZ, D., BACK, J., KAYUNKID, N., TORNOW, B., ALBRECHT, S., YAGER, G., SINGH, G., KARIM, A. & NEHER, D. **2015**. Highly Crystalline Films of PCPDTBT with Branched Side Chains by Solvent Vapor Crystallization: Influence on Opto-Electronic Properties. *J. Adv. Mater.*, 27, 1223-1228.
- FLORY, P.J. **1942**. Thermodynamics of High Polymer Solutions. *J. Chem. Phys.*, 10, 51-61.

- FLORY, P.J. **1953**. Principles of Polymer Chemistry. Cornell University Press, Ithaca New York, USA, 3-354.
- FLORY, P.J., MANDELKERN, L. & HALL, H.K. **1951**. Crystallization in High Polymers VII Heat of Fusion of Poly-(N,N'-sebacoylpiperazine) and its Interaction With Diluents. *J. Am. Chem. Soc.*, 73, 2532-2538.
- FRONK, S.L., WANG, M., FORD, M., COUGHLIN, J., MAI, C.-K. & BAZAN, G.C. **2016**. Effect of Chiral 2-Ethylhexyl Side Chains on Chiroptical Properties of the Narrow Bandgap Conjugated Polymers PCPDTBT and PCDTPT. *Chem. Sci.*, 1-3.
- FUKUTOMI, Y., NAKANO, M., HU, J.-Y., OSAKA, I. & TAKIMIYA, K. **2013**. Naphthodithiophene diimide (NDTI): Synthesis, Structure, and Applications. *J. Am. Chem. Soc.*, 135, 11445-11448.
- GANESAMOORTHY, R., VIJAYARAGHAVAN, R. & SAKTHIVEL, P. **2017**. Perylene Diimide-Thiophene Based Polymer Acceptors for Solution-Processed All-Polymer Bulk Heterojunction Solar Cells. *Inter. J. of Chem Tech Research*, 10, 264-269.
- GAO, L., ZHANG, Z.-G., XUE, L., MIN, J., ZHANG, J., WEI, Z. & LI, Y. **2016**. All-Polymer Solar Cells Based on Absorption-Complementary Polymer Donor and Acceptor with High Power Conversion Efficiency of 8.27%. *Adv. Mater.*, 28, 1884-1890.
- GENG, Y., HUANG, J., TAJIMA, K., ZENG, Q. & ZHOU, E. **2015**. A Low Band Gap n-Type Polymer Based on Dithienosilole and Naphthalene Diimide for All-Polymer Solar Cells Application. *Polymer*, 03, 010.
- GENENE, Z., MAMMO, W., WANG, E. & ANDERSSON, M.R. **2019**. Recent Advances in n-Type Polymers for All-Polymer Solar Cells. *J. Adv. Mater.*, 31, 1807275.
- GUILBERT, A.A., FROST, J.M., AGOSTINELLI, T., PIRES, E., LILLIU, S., MACDONALD, J.E. & NELSON, J. **2014**. Influence of bridging atom and side chains on the structure and crystallinity of cyclopentadithiophene-benzothiadiazole polymers. *Chem. Mater.*, 26, 1226-1233.
- GUO, X., TU, D. & LIU, X. **2015**. Recent Advances in Rylene Diimide Polymer Acceptors for All-Polymer Solar Cells. *J. Energy Chem.*, 24, 675-685.
- GU, Y., WANG, C. & RUSSELL, T.P. **2012**. Multi-length-Scale Morphologies in PCPDTBT/PCBM Bulk-Heterojunction Solar Cells. *J. Adv. Funct. Mater.*, 2, 683-690.
- GREGG, B.A. **2003**. Excitonic Solar Cells. *J. Phys. Chem. B* 107, 4688-4698.
- GREGG, B.A. & HANNA, M.C. **2003**. Comparing Organic to Inorganic Photovoltaic Cells: Theory, Experiment, and Simulation. *J. Appl. Phys.*, 93, 3605-3614.

- GU,X.,YAN,H.,KUROSAWA,T.,SCHROEDER,B.C.,GU,K.L.,ZHOU,Y.,TO,J.W.,OOSTERHOUT,S.D.,SAVIKHIN,V.&MOLINA-LOPEZ,F.**2016**. Comparison of the Morphology Development of Polymer-Fullerene and Polymer-Polymer Solar Cells During Solution- Shearing Blade Coating. *J. Adv.Energy Mater.*,6,1601225.
- GU,Y.,WANG,C.,LIU,F.,CHEN,J.,DYCK,O.E.,DUSCHERD,G.&RUSSELL,T.P.**2014**. Guided Crystallization of P3HT in Ternary Blend Solar Cell Based on P3HT:PCPDTBT:PCBM. *Eng. Environ. Sci.*,7,3782-3790.
- GÜNES,S.,NEUGEBAUER,H.&SARICIFTCI,N.S.**2007**. Conjugated Polymer-Based Organic Solar Cells. *Chem. Rev.*,107, 1324-1338.
- GUO,X.,FACCHETTI,A.&MARKS,T.J.**2014**. Imide- and Amide-Functionalized Polymer Semiconductors. *Chem. Rev.*,114, 8943-9021.
- GUO,Y.,LI,Y.,AWARTANI,O.,ZHAO,J.,HAN,H.,ADE,H.,ZHAO,D.&YAN,H.**2016**. A Vinylene-Bridged Perylene diimide-Based Polymeric Acceptor Enabling Efficient All-Polymer Solar Cells Processed Under Ambient Conditions. *Adv. Mater.*, 02387.
- HAITZ,R.&TSAO,J.Y.**2011**. Solid-State Lighting: 'The Case' 10 Years After and Future Prospects. *Phys.Status Solidi A*, 208, 17-29.
- HANSEN,C.M.**2007**. *Hansen Solubility Parameters: A User's Handbook*, 2nd Ed. Boca Rato, FL; CRC press LLC, New York.
- HE,Z.,ZHONG,C.,SU,S.,XU,M.,WU,H.&CAO,Y.**2012**. Enhanced Power-Conversion Efficiency in Polymer Solar Cells Using an Inverted Device Structure. *Nat. Photonics*,6, 1-5.
- HE,Y.B.**1989**. *Contact Angle Measurements on Fine Coal Particles*. Thesis, University of British Columbia, Canada.
- HELGESEN,M.,GEVORGYAN,S.A.,KREBS,F.C.&JANSSEN,R.A.J.**2009**. Substituted 2,1,3-Benzothiadiazole- and Thiophene-Based Polymers for Solar Cells-Introducing a New Thermocleavable Precursor. *Chem. Mater.*,21, 4669-4675.
- HIEMENZ,P.C.and LODGE,T.P.**2007**. *Polymer Chemistry*,2nd ed.;CRC Press, New York, USA, 247-556.
- HOLCOMBE,T.W.,NORTON,J.E.,RIVNAY,J.,WOO,C.H.,GORIS,L.,PILIEGO,C.,GRIFFINI,G.,SELLINGER,O.A.,BREDAS,J.-L.,SALLEO,A.&FRECHET,J.M.J.**2011**. Steric Control of the Donor/Acceptor Interface: Implications in Organic Photovoltaic Charge Generation. *J. Am. Chem. Soc.*, 133, 12106-12114.
- HORIE,M.,MAJEWSKI,L.A.,FEARN,M.J.,YU,C.-Y.,LUO,Y.,SONG,A.,SAUNDERS,B.R.&TURNER,M.L.**2010**. Cyclopentadithiophene Based Polymers-a Comparison of Optical,

- Electrochemical and Organic Field-Effect Transistor Characteristics. *J. Mater. Chem.*,20, 4347-4355.
- HUGGINS,M.L.**1942**.Some Properties of Solutions of Long-Chain Compounds. *J. Phys. Chem.*, 46, 151-158.
- HWANG,I.-W.,SOCI,C.,MOSES,D.,ZHU,Z.,WALLER,D.,GAUDIANA,R.,BRABEC,C.J.& HEGER,A.J.**2007**.Ultrafast Electron Transfer and Decay Dynamics in a Small Band Gap Bulk Heterojunction Material. *Adv.Mater.*,19, 2307-2312.
- HWANG,Y.-J.,COURTRIGHT,B.A.E.,FERREIRA,A.S.,TOLBERT,S.H.&JENEKHE,S.A. **2015**. 7.7% Efficient All-Polymer Solar Cells. *Adv.Mater.*,27, 4578-4584.
- HWANG,H.,LEE,H.,SHAFIAN,S.,LEE,W.,SEOK,J.,RYU,K.Y.,DU RYU,Y.&KIM,K.**2017**. Thermally Stable Bulk Heterojunction Prepared by Sequential Deposition of Nanostructured Polymer and Fullerene. *Polymers*, 9, 456.
- J.LIPOM,D.,HALBERTCHONG,V.M.J.,& ZHENANBAO **2012**.Toward Mechanically Robust and Intrinsically Stretchable Organic Solar Cells: Evolution of Photovoltaic Properties With Tensile Strain. *Solar Energy Mater. & Solar Cells*,107, 355-365.
- JIA,T.,ZHANG,J.,ZHONG,W.,LIANG,Y.,ZHANG,K.,DONG,S.,YING,L.,LIU,F.,WANG,X.& HUANG,F.**2020**.14.4% Efficiency All-Polymer Solar Cell With Broad Absorption and Low Energy Loss Enabled by a Novel Polymer Acceptor. *J.Nano Energy*,72, 104718.
- JOHN WILEY & SONS, I. **2015**. *Physical, Thermal, and Mechanical Properties of Polymers, Biosurfaces: A Materials Science and Engineering Perspective*, The American Ceramic Society, 329-344.
- JUNG,I.H.,LO,W.-Y.,JANG,J.,CHEN,W.,ZHAO,D.,LANDRY,E.,S.;LU,L.,TALAPIN,D.V.& YU,L.**2014**.Synthesis and Search for Design Principles of New Electron Accepting Polymers for All-Polymer Solar Cells. *Chem.Mater.*,26,3450-3459.
- KADEM,B.Y.,AL-HASHIMI,M.K.&HASSAN,A.**2014**.The Effect of Solution Processing on the Power Conversion Efficiency of P3HT-Based Organic Solar Cells. *J.Energy Procedia.*, 50, 237-245.
- KALOGERAS, I. M. **2016**. Glass-Transition Phenomena in Polymer Blends. *In: ISAYEV, A. I. (ed.) Encyclopedia of Polymer Blends*. Wiley-VCH Verlag GmbH & Co. KGaA.
- KAMANZI,J.&KAHN,M.T.**2017**.Development of a Model for Highly Efficient Solar Power Panels. *Inter. J.Appl.Engineering Research*, 12, 2171-2181.

- KANG,H.,KIM,K.-H.,CHOI,J.,LEE,C.&KIM,B.J.**2014**. High-Performance All-Polymer Solar Cells Based on Face-On Stacked Polymer Blends with Low Interfacial Tension. *ACS Macro Lett.*,3,1009-1014.
- KANG,H.,UDDIN,M.A.,LEE,C.,KIM,K.-H.,NGUYEN,T.L.,LEE,W.,LI,Y.,WANG,C.,WOO,H.Y.&KIM,B.J.**2015**.Determining the Role of Polymer Molecular Weight for High-Performance All-Polymer Solar Cells: Its Effect on Polymer Aggregation and Phase Separation. *J.Am.Chem.Soc.*,137, 2359-2365.
- KIETZKE,T.,HO`RHOLD,H.-H.&NEHER,D.**2005**. Efficient Polymer Solar Cells Based on M3EH-PPV. *Chem.Mater.*,17, 6532-6537.
- KIM,J.Y.,LEE,K.,COATES,N.E.,MOSES,D.,NGUYEN,T.Q.,DANTE,M.&HEEGER,A.J.**2007**. Efficient Tandem Polymer Solar Cells Fabricated by All-Solution Processing.*Sci.*,317, 222-225.
- KIM,T.,KIM,J.-H.,KANG,T.E.,LEE,C.,KANG,H.,SHIN,M.,WANG,C.,MA,B.,JEONG,U.,KIM,T.-S.&KIM,B.J.**2015**.Flexible, Highly Efficient All-Polymer Solar Cells. *Nat. Commun.*, 6, 8547.
- KIM,M.-S.**2009**.Understanding Organic Photovoltaic Cells:Electrode, Nanostructure, Reliability, and Performance. *University of Michigan*, 1-115.
- KIM,J.Y.**2018**.Order-Disorder Phase Equilibria of Regioregular Poly(3-hexylthiophene-2,5,diyl) Solution. *Macromol.*,51, 9026-9034.
- KIM,J.Y.**2019**. Phase Diagrams of Binary Low Bandgap Conjugated Polymer Solutions and Blends. *Macromol.*,52, 4317.
- KIM,J.Y.&FRISBIE,C.D.**2008**.Correlation of Phase Behavior and Charge Transport in Conjugated Polymer/Fullerene Blends. *J. Phys.Chem. C*,112, 17726-17736.
- KIM,J.Y.,CHO,H.,NOH,S.,LEE,Y.,NAM,Y.M.,LEE,C.&JO,W.H.**2012**.Charge Transport in Amorphous Low Bandgap Conjugated Polymer/Fullerene Films. *J.Appl.Phys.*,111, 043710.
- KOLHE,N.B.,LEE,H.,KUZUHARA,D.,YOSHIMOTO,N.,KOGANEZAWA,T.&JENEKHE,S.A. **2018**. All-Polymer Solar Cells with 9.4% Efficiency from Naphthalene Diimide-Biselenophene Copolymer Acceptor. *Chem. Mater.*,30, 6540-6548.
- KONINGSVELD, R. & STAVERMAN, A. J. **1968**. Liquid-liquid Phase Separation in Multicomponent Polymer Solutions. II. The Critical State. *J. Polym. Sci. Part A-2: Polym. Phys.*, 6, 325.

- KOUIJZER,S.,MICHELS,J.J.,BERG,M.V.D.,GEVAERTS,V.S.,TURBIEZ,M.,WIENK,M.M.& JANSSEN,R.A.J.**2013**.Predicting Morphologies of Solution Processed Polymer:Fullerene Blends. *J. Am.Chem. Soc.*,135, 12057-12067.
- KUMAR,M.**2020**. Social, Economic, and Environmental Impacts of Renewable Energy Resources. *Wind Solar Hybrid Renewable Energy System*. Intech Open, 1-11.
- LATE,D.J.,ROUT,C.S.,CHAKRAVARTY,D.&RATHA,S.**2015**. Emerging Energy Applications of Two-Dimensional Layered Materials. *Canadian Chemical Transactions*, 3,118-157.
- LEI,Y.,SUN,J.,YUAN,J.,GU,J.,DING,G.&MA,W.**2016**. Controlling Molecular Weight of Naphthalenediimide-Based Polymer Acceptor P(NDI2OD-T2) for High Performance All-Polymer Solar Cells. *J. Mater. Sci. & Techno.*,33, 411-417.
- LEIBLER,L.**1980**.Theory of Microphase Separation in Block Copolymers. *J.Macromol.*,13, 1602-1617.
- LI,Z.,YING,L.,ZHU,P.,ZHONG,W.,LI,N.,LIU,F.,HUANG,F.&CAO,Y.**2019**. A Generic Green Solvent Concept Boosting the Power Conversion Efficiency of All-Polymer Solar Cells to 11%. *Energy Environ.Sci.*,12, 157-163.
- LIPATOV,Y.S.&NESTEROV,A.E.**1997**.Thermodynamics of Polymer Blends;Technomic Publishing Co. Inc., Lancaster, 1-443.
- LI,C.,LIU,M.,PSCHIRER,N.G.,BAUMGARTEN,M.&MULLEN,K.**2010**.Polyphenylene-Based Materials for Organic Photovoltaics. *Chem. Rev.*,110, 6817-6855.
- LI,H.,HWANG,Y.J.,EARMME,T.,HUBER,R.C.,COURTRIGHT,B.,E.,A.,O'BRIEN,C.TOLBERT& S.H.JENEKHE,S.A.**2015**. Polymer/Polymer Blend Solar Cells UsingTetraazabenzodifluoranthene Diimide Conjugated Polymers as Electron Acceptors. *Macromol.*,48, 1759-1766.
- LI,N.,MACHUI,F.,WALLER,D.,KOPPE,M.&J.BRABEC,C.**2011**.Determination of Phase Diagrams of Binary and Ternary Organic Semiconductor Blends for Organic Photovoltaic Devices. *Solar Energy Mater. & Solar Cells*, 95, 3465-3471.
- LI,P.,CHEN,C.,ZHANG,J.,LI,S.,SUN,B.&BAO,Q.**2014**.Graphene-Based Transparent Electrodes for Hybrid Solar Cells. *Frontiers in Materials/Optics and Photonics*,1, 1-7.
- LI,D.&NEUMANN,A.W.**1990**. Reformulation of the Equation of State for Interfacial Tensions. *J. Colloid Interface. Sci.*,137, 304-307.
- LI,D.&NEUMANN,A.W.**1992**.ContactAngles on Hydrophobic Solid Surfaces and Their Interpretation. *J. Colloid Interface. Sci.*,148, 190-200.

- LI,Z.,XU,X.,ZHANG,W.,MENG,X.,GENENE,Z.,MA,W.,MAMMO,W.,YARTSEV,A.,ANDERSSON,M.R.&JANSSEN,R.A.J.E.A. **2017**. 9.0 % Power Conversion Efficiency from Ternary All-Polymer Solar Cells. *Energy Environ. Sci.*,10, 2212-2221.
- LI,Z.,YING,L.,XIE,R.,ZHU,P.,LI,N.,ZHONG,W.,HUANG,F.&CAO,Y.**2018**.Designing Ternary Blend All-Polymer Solar Cells With an Efficiency of Over 10% and a Fill Factor of 78%. *Nano Eng.*,51, 434-441.
- LIN,Y.Z.,LI,Y.F.&ZHAN,X.W.**2012**.Small Molecule Semiconductors for High-Efficiency Organic Photovoltaics. *Chem. Soc. Reviews*, 41, 4245-4272.
- LIU,J.,XUE,Y.,ZHANG,M.&DAI, L.**2012**.Graphene-Based Materials for Energy Applications. *MRS Bulletin*,37, 1265-1272.
- LIU,Z.,GAO,Y., DONG,J.,YANG,M.,LIU,M.,ZHANG,Y.,WEN,J.,MA,H.,GAO,X.&CHEN,W. E.A.**2018**. Chlorinated Wide-Bandgap Donor Polymer Enabling Annealing Free Non-Fullerene Solar Cells With the Efficiency of 11.5%. *J. Phys. Chem. Lett.*, 9, 6955-6962.
- LIU,Z.,WU,Y.,ZHANG,Q.&GAO,X. **2016**. Non-Fullerene Small Molecule Acceptors Based on Perylene Diimides. *J.Mater. Chem. A*, 4, 17604-17622.
- LIU,Z.,ZENG,D.,GAO,X.,LI,P.,ZHANG,Q.&PENG,X.**2019**. Non-Fullerene Polymer Acceptors Based on Perylene Diimides in All-Polymer Solar Cells. *Solar Eng.Mat.Sol.C*,189,103-117.
- LIU,Z.,ZHANG,L.,SHAO,M.,WU,Y.,ZENG,D.,CAI,X.,DUAN,J.,ZHANG,X.&GAO,X.**2018**. Fine-Tuning the Quasi-3D Geometry: Enabling Efficient Non-Fullerene Organic Solar Cells Based on Perylene Diimides. *ACS Appl.Mater.Interfaces*,10,762-768.
- LIU,Q.,JIANG,Y.,JIN,K.,QIN,J.,XU,J.,LI,W.,XIONG,J.,LIU,J.,XIAO,Z.&SUN,K.**2020**.18% Efficiency Organic Solar Cells. *Sci. Bulletin*, 65, 272-275.
- LIU,X.,LI,X.,ZHENG,N.,GU,C.,WANG,L.,FANG,J.&YANG,C.**2019**.Insight into the Efficiency and Stability of All-Polymer Solar Cells Based on Two 2D-Conjugated Polymer Donors: Achieving High Fill Factor of 78%. *J.ACS Appl. Mater. Interfaces* 11, 43433-43440.
- LIU,F.,GU,Y.,WANG,C.,ZHAO,W.,CHEN,D.,BRISENO,A.L.&RUSSELL,T.P. **2012**. Efficient Polymer Solar Cells Based on a Low Bandgap Semi-crystalline DPP Polymer-PCBM Blends. *Adv. Mater.*,24, 3947-3951.
- LU,L.,ZHENG,T.,WU,Q.,SCHNEIDER,A.M.,ZHAO,D.&YU,L.**2015**.Recent Advances in Bulk Heterojunction Polymer Solar Cells. *Chem. Rev.*,115, 12666-12731.

- MA, L., XU, Y., ZU, Y., LIAO, Q., XU, B., AN, C., ZHANG, S. & HOU, J. **2020**. A Ternary Organic Solar Cell With 300nm Thick Active Layer Shows Over 14% Efficiency. *Sci.China Chem.*, *63*, 21-27.
- MACHUI, F. **2014**. Formulation of Semiconductor Solutions for Organic Photovoltaic Devices. Doctor of philosophy, der Friedrich-Alexander-Universität Erlangen-Nürnberg, Germany.
- MARTINS, F., FELGUEIRAS, C., SMITKOVA, M. & CAETANO, N. **2019**. Analysis of Fossil Fuel Energy Consumption and Environmental Impacts in European Countries. *J.Energies*, *12*, 964.
- MATYSIAK, W., TAŃSKI, T. & ZABOROWSKA, M. **2017**. Analysis of the Optical Properties of PVP/ZnO Composite Nanofibers. In *Properties and Characterization of Modern Materials; Advanced Structured Materials*, Springer, Singapore, 33. 43-49.
- MCNEILL, C.R., ABRUSCI, A., HWANG, I., RUDERER, M.A., MÜLLER-BUSCHBAUM, P. & GREENHAM, N.C. **2009**. Photophysics and Photocurrent Generation in Polythiophene /Polyfluorene Copolymer Blends. *Adv. Funct. Mater.*, *19*, 3103-3111.
- MCNEILL, C.R., WATTS, B., THOMSEN, L., BELCHER, W.J., GREENHAM, N.C., DASTOOR, P. C. & ADE, H. **2009**. Evolution of Laterally Phase-Separated Polyfluorene Blend Morphology Studied by X-ray Spectromicroscopy. *Macromol.*, *42*, 3347-3352.
- MCNEILL, C.R. **2012**. Morphology of All-Polymer Solar Cells. *Energy Environ. Sci.*, *5*, 5653-5667.
- MCNEILL, C.R., ABRUSCI, A., ZAUMSEIL, J., WILSON, R. & MCKIERNAN, M.J. **2007**. Dual Electron Donor/Electron Acceptor Character of a Conjugated Polymer in Efficient Photovoltaic Diodes. *Appl. Phys. Lett.*, *90*, 193506.
- MCNEILL, R.C. & GREENHAM, C.N. **2009**. Conjugated-Polymer Blends for Optoelectronics. *Adv.Mater.*, *21*, 3840-3850.
- MIKHENENKO, O.V., BLOM, P.W. & NGUYEN, T.-Q. **2015**. Exciton Diffusion in Organic Semiconductors. *J. Energy Environ. Sci.*, *8*, 1867-1888.
- MORANA, M., WEGSCHEIDER, M., BONANNI, A., KOPIDAKIS, N., SHAHEEN, S., SCHARBER, M., ZHU, Z., WALLER, D., GAUDIANA, R. & BRABEC, C. **2008**. Bipolar Charge Transport in PCPDTBT-PCBM Bulk-Heterojunctions for Photovoltaic Applications. *J. Adv. Funct. Mater.*, *18*, 1757-1766.
- MÜHLBACHER, D., SCHARBER, M., MORANA, M., ZHU, Z., WALLER, D., GAUDIANA, R. & BRABEC, C. **2006**. High Photovoltaic Performance of a Low-Bandgap Polymer. *Adv. Mater.*, *18*, 2884-2889.

- MIKHENKO,O.V.,AZIMI,H.,SCHARBER,M.,MORANA,M.,BLOMAD,P.W.M.&LOI,M.A.
2012. Exciton Diffusion Length in Narrow Bandgap Polymers. *Energy Environ. Sci.*,**5**,
6960-6965.
- MIKHENKO,O.V.,BLOM,P.W.M.&NGUYEN,T.-Q.**2015.**Exciton Diffusion in Organic
Semiconductors. *Energy Environ. Sci.*,**8**, 1867-1888.
- MILLER,N.C.,GYSEL,R.,MILLER,C.E.,VERPLOEGEN,E.,BEILEY,Z.,HEENEY,M.,MCCUL
LOCH,I.,BAO,Z.,TONEY,M.F.& MCGEHEE,M.D.**2011.**The Phase Behavior of a Poly
mer-Fullerene Bulk Heterojunction System that Contains Bimolecular Crystals. *J.Polym
.Sci.,Part B:Polym. Phys.*,**49**, 499-503.
- MOONS,E.**2002.**Conjugated Polymer Blends:Linking Film Morphology to Performance of Light
Emitting Diodes and Photodiodes. *J. Phys. Condens. Matter*,**14**, 12235-12260.
- MOORE,J.R.,ALBERT-SEIFRIED,A.,RAO,A.,MASSIP,S.,WATTS,B.,MORGAN,D.J., FRIEN
D,R.H.,MCNEILL,C.R.&SIRRINGHAUS,H.**2011.**Polymer Blend Solar Cells Based on a
High-Mobility Naphthalenediimide-Based Polymer Acceptor:Device Physics, Photo physics
ics and Morphology. *Adv.Eng.Mater.*,**1**, 230-240.
- MORANA,M.,AZIMI,H.,DENNLER,G.,EGELHAAF,H.-J.,SCHARBER,M.,FORBERICH,K.,
HAUCH,J.,GAUDIANA,R.,WALLER,D.,ZHU,Z.,HINGERL,K.,BAVEL,S.S.V.,LOOS,
J.&BRABEC,C.J.**2010.**Nanomorphology and Charge Generation in Bulk Heterojunctions
Based on Low-Bandgap Dithiophene Polymers With Different Bridging Atoms. *Adv.
Funct. Mater.*,**20**,1180-1188.
- MORI,D.,BENTEN,H.,OKADA,I.,OHKITA,H.&ITO,S.**2013.** Low-Bandgap Donor/Acceptor
Polymer Blend Solar Cells with Efficiency Exceeding 4%. *Adv. Energy Mater.*, 01006.
- MORI,D.,BENTEN,H.,OKADA,I.,OHKITA,H.&ITO,S.**2014.**Highly Efficient Charge-Carrier
Generation and Collection in Polymer/Polymer Blend Solar Cells with a Power Conv ers
ion Efficiency of 5.7%. *Eng. Environ. Sci.*,**7**, 2939-2943.
- MÜHLBACHER,D.,SCHARBER,M.,MORANA,M.,ZHU,Z.,WALLER,D.,GAUDIANA,R.&B
RABEC,C.**2006.**High Photovoltaic Performance of a Low-Bandgap Polymer. *Adv. Mater*
.,**18**, 2884-2889.
- NAKAMURA,S.,MUKAI,T.&SENOH,M.**1994.** Candela-Class High-Brightness In GaN/AlGaN
Double-Heterostructure Blue-Lightemitting Diodes. *Appl. Phys. Lett.*,**64**, 1687-1689.
- NAKANO,K.,NAKANO,M.,XIAO,B.,ZHOU,E.,SUZUKI,K.,OSAKA,I.,TAKIMIYA,K.&TAJI
MA,K. **2016.** Naphthodithiophene Diimide-Based Copolymers: Ambipolar Semiconduct
ors in Field-Effect Transistors and Electron Acceptors with Near-Infrared Response in
Polymer Blend Solar Cells. *Macromol.*, **49**,1752-1760.

- NILSSON,S.,BERNASIK,A.,BUDKOWSKI,A.&MOONS,E.**2007**.Morphology and Phase Segregation of Spin-Casted Films of Polyfluorene/PCBM Blends. *Macromol.*,40, 8291-8301.
- NOEL,N.K.,STRANKS,S.D.,ABATE,A.,WEHRENFENNIG,C.,GUARNERA,S.,AGHIGHIRAD,A.A.,SADHANALA,A.,EPERON,G.E.,JOHNSTON,M.B.,PETROZZA,A.M.,HERZ,L.M.&SNAITH,H.J.**2013**.Lead-Free Organic-Inorganic Tin Halide Perovskites for Photovoltaic Applications. *Energy Environ. Sci.*, 1-3.
- OHKITA,H.&ITO,S.**2011**.Transient Absorption Spectroscopy of Polymer-Based Thin-Film Solar Cells. *Polymer*, 52, 4397-4417.
- OHKITA,H.&ITO, S. **2013**. Organic Solar Cells-Materials and Device Physics. *Springer-Verlag, London*, 103-137.
- OHKITA,H.,TAMAI,Y.,BENTEN,H.&ITO,S.**2016**.Transient Absorption Spectroscopy for Polymer Solar Cells. *IEEE J. Selected Topics in Quantum Electronics*, 22, 4100112.
- OLABISI,O.R.,L.M.;SHAW,M.T.**1979**.Polymer-Polymer Miscibility,Academic Press;New York, USA, 19-316.
- OU,C.,CHEETHAM,N.J.,WENG,J.,YU,M.,LIN,J.,WANG,X.,SUN,C.,CABANILLAS-ONZALEZ,J.,XIE,L.&BAI,L. **2019**. Hierarchical Uniform Supramolecular Conjugated Spherulites with Suppression of Defect Emission. *J. science*, 16, 399-409.
- PARK,S.H.,ROY,A.,BEAUPRE,S.,CHO,S.,COATES,N.,MOON,J.S.,MOSES,D.,LECLERC,M.,LEE,K.&HEEGER,A.J.**2009**. Bulk Heterojunction Solar Cells With Internal Quantum Efficiency Approaching 100%. *Nat. Photonics*, 3, 297-303.
- PATTERSON,D.**1969**. Free Volume and Polymer Solubility. A Qualitative View. *Macromol.*,2, 672-677.
- PAUL,D.R.&BARLOW,J.W.**1980**. Polymer Blends (or Alloys). *J. Macromol. Sci.-Rev. Macromol. Chem.*,C18, 109-168.
- PAUL,D.R.&NEWMAN,S.**1978**. Polymer Blends. Academic Press: New York, 1, 1-14.
- PEET,J.,KIM,J.Y.,COATES,N.E.,MA,W.L.,MOSES,D.,HEEGER,A.J.&BAZAN,G.C.**2007**.Efficiency Enhancement in Low-Bandgap Polymer Solar Cells by Processing With Alkane Dithiols. *Nature Mater.*,6, 497-500.
- POPE,M.&SWENBERG,C.E.**1999**. Electronic Processes in Organic Crystals and Polymers. 2nd Edition, New York, Oxford University Press, USA, 646-671.

- RIVNAY, J., TONEY, M.F., ZHENG, Y., KAUVAR, I.V., CHEN, Z., WAGNER, V., FACCHETTI, A. & SALLEO, A. **2010**. Unconventional Face-on Texture and Exceptional In-Plane Order of a High Mobility N-Type Polymer. *J. Adv. Mater.*, 22, 4359-4363.
- PRICE, S.C., STUART, A.C., YANG, L.Q., ZHOU, H.X. & YOU, W. **2011**. Fluorine Substituted Conjugated Polymer of Medium Band Gap Yields 7% Efficiency in Polymer-Fullerene Solar Cells. *J. Ame. Chem. Soc.*, 133, 4625-4631.
- QIAN, C., MUMBY, S.J. & EICHINGER, B.E. **1991**. Phase Diagrams of Binary Polymer Solutions and Blends. *Macromol.*, 24, 1655-1661.
- QIN, J., AN, C., ZHANG, J., MA, K., YANG, Y., ZHANG, T., LI, S., XIAN, K., CUI, Y. & TANG, Y. **2020**. 15.3% Efficiency All-Small-Molecule Organic Solar Cells Enabled by Symmetric Phenyl Substitution. *Sci. China Mater.*, 1-9.
- REINEKE, S. **2013**. White Organic Light-Emitting Diodes: Status and Perspective. *Rev. Mod. Phys.*, 85, 1245-1293.
- RICHARDS, R.B. **1946**. The Phase Equilibria Between a Crystalline Polymer and Solvents. *Trans. Faraday Soc.*, 42, 10-28.
- RIEDL, B. & PRUD'HOMME, R.E. **1988**. Thermodynamics of Miscible Polymer Blends Using a Concentration-Dependent χ Parameter. *J. Polym. Sci. B Polym. Phys.*, 26, 1769-1780.
- RIVNAY, J., STEYRLEUTHNER, R., JIMISON, L.H., CASADEI, A., CHEN, Z., TONEY, M.F., FACCHETTI, A., NEHER, D. & SALLEO, A. **2011**. Drastic Control of Texture in a High Performance n-Type Polymeric Semiconductor and Implications for Charge Transport. *Macromol.*, 44, 5246-5255.
- ROGERS, J.T., SCHMIDT, K., TONEY, M.F., KRAMER, E.J. & BAZAN, G.C. **2011**. Structural Order in Bulk Heterojunction Films Prepared With Solvent Additives. *Adv. Mater.*, 23, 2284-2288.
- SAVAGATRUP, S., PRINTZ, A.D., O'CONNOR, T.F., ZARETSKI, A.V., RODRIQUEZ, D., SAWYER, E.J., RAJAN, K.M., ACOSTA, R.I., ROOT, S.E. & LIPOMI, D.J. **2015**. Mechanical Degradation and Stability of Organic Solar Cells: Molecular and Microstructural Determinants. *Energy Environ. Sci.*, 8, 55-80.
- SCHUBERT, M., COLLINS, B.A., MANGOLD, H., HOWARD, I.A., SCHINDLER, W., VANDEWAL, K., ROLAND, S., BEHREND, J., KRAFFERT, F., STEYRLEUTHNER, R., CHEN, Z., FOSTIROPOULOS, K., BITTL, R., SALLEO, A., FACCHETTI, A., LAQUAI, F., ADE, H.W. & NEHER, D. **2014**. Correlated Donor/Acceptor Crystal Orientation Controls Photocurrent Generation in All-Polymer Solar Cells. *Adv. Func Mater.*, 24, 4068-4081.

- SCHUBERT, M., DOLFEN, D., FRISCH, J., ROLAND, S., STEYRLEUTHNER, R., STILLER, B., CHEN, Z., SCHERF, U., KOCH, N. & FACCHETTI, A. **2012**. Influence of Aggregation on the Performance of All-Polymer Solar Cells Containing Low-Bandgap Naphthalene diimide Copolymers. *Adv. Eng. Mater.*, **2**, 369-380.
- SCHUETTFORT, T., HUETTNER, S., LILLIU, S., MACDONALD, J.E., THOMSEN, L. & MCNEILL, C.R. **2011**. Surface and Bulk Structural Characterization of a High-Mobility Electron-Transporting Polymer. *Macromol.*, **44**, 1530-1539.
- SCHUETTFORT, T., THOMSEN, L. & MCNEILL, C.R. **2013**. Observation of a Distinct Surface Molecular Orientation in Films of a High Mobility Conjugated Polymer. *American Chemical Society*, **135**, 1092-1101.
- SCHULZ, G.L., FISCHER, F.S.U., TREFZ, MELNYK, A., HAMIDI-SAKR, A., BRINKMANN, M., ANDRIENKO, D. & LUDWIGS, S. **2017**. The PCPDTBT Family: Correlations Between Chemical Structure, Polymorphism, and Device Performance. *Macromol.*, 1-13.
- SHARMA, S., KOLHE, N.B., GUPTA, V., BHARTI, V., SHARMA, A., DATT, R., CHAND, S. & ASH A, S. **2016**. Improved All-Polymer Solar Cell Performance of n-Type Naphthalene Diimide-Bithiophene P(NDI2OD-T2) Copolymer by Incorporation of Perylene Diimide as Coacceptor. *Macromolecules*, **49**, 8113-8125.
- SHROTRIYA, V. **2009**. Organic Photovoltaics: Polymer Power. *Nat. Photon.*, **3**, 447-449.
- STEYRLEUTHNER, R., SCHUBERT, M., HOWARD, I., KLAUMUNZER, B., SCHILLING, K., CHEN, Z., SAALFRANK, P., LAQUALI, F., FACCHETTI, A. & NEHER, D. **2012**. Aggregation in a High-Mobility n-Type Low-Bandgap Copolymer With Implications on Semicrystalline Morphology. *J. Am. Chem. Soc.*, **134**, 18303-18317.
- STHEL, M.S., TOSTES, J.G. & TAVARES, J.R. **2013**. Current Energy Crisis and Its Economic and Environmental Consequences: Intense Human Cooperation. *Natural Sci.*, **5**, 244-252.
- STROBL, G. **2007**. The Physics of Polymers-Concepts for Understanding Their Structures and Behavior. 3rd Edition, Berlin Heidelberg, Springer, 69-157.
- SUN, H., LIU, B., WANG, Z., LING, S., ZHANG, Y., ZHANG, G., WANG, Y., ZHANG, M., LI, B. & YANG, W. **2020**. Side Chain Engineering of Polymer Acceptors for All-Polymer Solar Cells With Enhanced Efficiency. *J. Mater. Chem. C*, **8**, 4012-4020.
- SWARAJ, S., WANG, C., YAN, H., WATTS, B., NING, J.L., MCNEILL, C.R. & ADE, H. **2010**. Nanomorphology of Bulk Heterojunction Photovoltaic Thin Films Probed With Resonant Soft X-ray Scattering. *Nano Lett.*, **10**, 2863-2869.

- TAKACS,C.J.,TREAT,N.D.,KRAMER,S.,CHEN,Z.,FACCHETTI,A.,CHABINYC,M.L.&HEEGER,A.J.**2013**.Remarkable Order of a High-Performance Polymer. *Nano Lett.*,13, 2522-2527.
- TAMAI,Y.,OHKITA,H.,BENTEN,H.&ITO,S.**2015**. Exciton Diffusion in Conjugated Polymers: From Fundamental Understanding to Improvement in Photovoltaic Conversion Efficiency *J. Phys.Chem. Lett.*,6, 3417-3428.
- TAMAI,Y.,MATSUURA,Y.,OHKITA,H.,BENTEN,H.&ITO,S.**2014**.One-Dimensional Singlet Exciton Diffusion in Poly(3-hexylthiophene) Crystalline Domains. *J.Phys.Chem. Lett.*,5, 399-403.
- TANAKA,H.&NISHI,T.**1985**. New Types of Phase Separation Behavior During the Crystallization Process in Polymer Blends with Phase Diagram. *Phys.Rev.Lett.*,55, 1102-1105.
- TAŃSKI,T.,JARKA,P.,SZINDLER,M.,DRYGAŁA,A.,MATYSIAK,W.&LIBERA,M.**2019**.Study of Dye Sensitized Solar Cells Photoelectrodes Consisting of Nanostructures. *Appl. Surf. Sci.*, 491, 807.
- TAŃSKI,T.,MATYSIAK,W.&HAJDUK,B.**2016**. Manufacturing and Investigation of Physical Properties of Polyacrylonitrile Nanofibre Composites With SiO₂, TiO₂ and Bi₂O₃ Nanoparticles. *Beilstein J. Nanotechnol*, 7, 1141-1155.
- TULLER,H.L.**2017**.Solar to Fuels Conversion Technologies: A Perspective. *J.Mater. for Renewable Sustainable Energy*, 6, 3.
- THOMPSON,B.C.&FRECHET,J.M.J.**2008**. Polymer-Fullerene Composite Solar Cells. *Angew. Chem. Int. Ed.*,47, 58-77.
- USHASREE,P.M. and BORA,B.**2019**. Chapter 1: Silicon Solar Cells, in *Solar Energy Capture Mater.*, 1-55.
- VANDEWAL,K.,ALBRECHT,S.,HOKE,E.T.,GRAHAM,K.R.,WIDMER,J.,DOUGLAS,J.D.,SCHUBERT,M.,MATEKER,W.R.,BLOKING,J.T.,BURKHARD,G.F.,SELLINGER, A.,FRÉCHET,J.M.J.,AMASSIAN,A.,RIEDE,M.K.,MCGEHEE,M.D.,NEHER,D.&SALLO,A. **2013**. Efficient Charge Generation by Relaxed Charge-Transfer States at Organic Interfaces. *Nat.Mater.*,13, 1-6.
- VANFRANEKER,J.J.,TURBIEZ,M.,LI,W.,WIENK,M.M.&JANSSEN,R.A.**2015**.AReal-Time Study of the Benefits of Co-Solvents in Polymer Solar Cell Processing. *Nat.Comm.*,6, 6229.
- VAYNZOF,Y.,KABRA,D.,ZHAO,L.,CHUA,L.L.,STEINER,U.&FRIEND,R.H.**2011**.Surface-irected Spinodal Decomposition in Poly[3-hexylthiophene] and C₆₁-Butyric Acid Methyl Ester Blends. *ACS Nano*,5, 329-336.

- VENKATARAMAN,D.,YURT,S.,VENKATRAMAN,B.H.&GAVVALAPALLI,N.**2010**.Role of Molecular Architecture in Organic Photovoltaic Cells.*J.Phys. Chem. Lett.*,1, 947-958.
- VENKATRAM,S.,KIM,C.,CHANDRASEKARAN,A.&RAMPRASAD,R.**2019**.Critical Assessment of the Hildebrand and Hansen Solubility Parameters for Polymers. *Chemical Information and Modeling*, 59, 4188-4194.
- WANG,J.&HIGASHIHARA,T.**2013**.Synthesis of All-Conjugated Donor-Acceptor Block Copolymers and Their Application in All-Polymer Solar Cells. *Polym. Chem.*, 1- 9.
- WANG,X.,HUANG,J.,TAJIMA,K.,XIAO,B.&ZHOU,E. **2015**. An Amorphous n-type Polymer Based on Perylenediimide and Selenophene for All-Polymer Solar Cells Application. *Mater.Today Commun.*,4, 16-21.
- WANG,Y.,BENTEN,H.,OHARA,S.,KAWAMURA,D.,OHKITA,H.&ITO,S.**2014**.Measurement of Exciton Diffusion in a Well-Defined Donor/Acceptor Heterojunction Based on a Conjugated Polymer and Cross-Linked Fullerene Derivative.*ACS Appl. Mater. Interfaces*, 6,14108-14115.
- WANG,G.,MELKONYAN,F.S.,FACCHETTI,A.&MARKS,T.J.**2019**. All-Polymer Solar Cells: Recent Progress, Challenges, and Prospects. *Angew. Chem.*,58, 4129-4142.
- WATERS,H.,KETTLE,J.,CHANG,S.-W.,SU,C.-J.,WU,W.-R.,JENG,U.-S.,TSAIB,Y.-C.& HORIE,M.**2013**.Organic Photovoltaics Based on a Crosslinkable PCPDTBT Analogue; Synthesis, Morphological Studies, Solar Cell Performance and Enhanced Lifetime. *J. Mater. Chem. A*, 1- 9.
- WEN,S.,YU,Y.,WANG,Y.,LI,Y.,LIU,L.,JIANG,H.,LIU,Z.&YANG,R.**2018**.Pyran-Bridged Indacenodithiophene as a Building Block for Constructing Efficient A-D-A-Type Non-Fullerene Acceptors for Polymer Solar Cells. *Chem. Sus. Chem.*,11, 360-366.
- WHITESIDES,G.M.&BONCHEVA,M.**2002**. Beyond Molecules: Self-Assembly of Mesoscopic and Macroscopic Compounds. *PNAS*, 99, 4769-4774.
- WHITESIDES,G.M.&GRZYBOWSKI,B.**2002**.Self-Assembly at All Scales. *Science*,295, 2418-2421.
- Wikipedia, the free encyclopedia (https://en.wikipedia.org/wiki/Materials_science).
- WU,J.-S.,CHENG,S.-W.,CHENG,Y.-J.&HSU,C.-S.**2015**. Donor-Acceptor Conjugated Polymers Based on Multifused Ladder-Type Arenes for Organic Solar Cells. *Chem. Soc.Rev.*,44, 1113.

- WU,J.,MENG,Y.,GUO,X.,ZHU,L.,LIU,F.&ZHANG,M.**2019**. All-Polymer Solar Cells Based on a Novel Narrow-Bandgap Polymer Acceptor With Power Conversion Efficiency Over 10%. *J. Mater. Chem. A* 7, 16190-16196.
- WÜRTHNER,F.&STOLTE,M.**2011**.Naphthalene and Perylene Diimides for Organic Transistors. *Chem. Commun.*,47, 5109.
- XIAO,B.,DING,G.,TAN,Z.A.&ZHOU,E.**2015**.The Comparison of n-type Copolymers Based on Cyclopentadithiophene and Naphthalene Diimide/Perylene Diimides for All-Polymer Solar Cells Application. *Polym. Chem.*,1-3.
- YAN,H.,COLLINS,B.A.,GANN,E.,WANG,C.,ADE,H.&MCNEILL,C.R.**2012**. Correlating the Efficiency and Nanomorphology of Polymer Blend Solar Cells Utilizing Resonant Soft X-ray Scattering. *ACS Nano*, 6, 677- 688.
- YAN,H.,CHEN,Z.,ZHENG,Y.,NEWMAN,C.,QUINN,J.R.,DO'TZ,F.,KASTLER,M.&FACCHE TTI,A.**2009**.A High-Mobility Electron-Transporting Polymer for Printed Transistors. *Nature*, 457, 679-686.
- YANG,J.,XIAO,B.,TAJIMA,K.,NAKANO,M.,TAKIMIYA,K.,TANG,A.&ZHOU,E.**2017**.Comparison Among Perylene Diimide(PDI), Naphthalene Diimide(NDI), and Naphthodithiophene Diimide (NDTI) Based n-type Polymers for All-Polymer Solar Cells Application. *Macromol.*,50, 3179-3185.
- YANG,Q.,WANG,J.,ZHANG,X.,ZHANG,J.,FU,Y.&XIE,Z.**2015**.Constructing Vertical Phase Separation of Polymer Blends Via Mixed Solvents to Enhance Their Photovoltaic Performance. *J. Sci.China Chem.*,58, 309-316.
- YAO,H.,BAI,F.,HU,H.,ARUNAGIRI,L.,ZHANG,J.,CHEN,Y.,YU,H.,CHEN,S.,LIU,T.&LAI,J.Y.L.E.A.**2019**. Efficient All-Polymer Solar Cells Based on a New Polymer Acceptor Achieving 10.3% Power Conversion Efficiency. *ACS Eng. Lett.*,4, 417- 422.
- YE,L.,JIAO,X.,ZHOU,M.,ZHANG,S.,YAO,H.,ZHAO,W.,XIA,A.,ADE,H.&HOU,J.**2015**.Manipulating Aggregation and Molecular Orientation in All-Polymer Photovoltaic Cells. *Adv. Mater.*,27, 6046-6054.
- YE,L.,HU,H.,GHASEMI,M.,WANG,T.,COLLINS,B.A.,KIM,J.H.,JIANG,K.,CARPENTER,J.H.,LI,H.&LI,Z.E.A.**2018**. Quantitative Relations Between Interaction Parameter,Miscibility and Function in Organic Solar Cells. *Nat. Mater.*,17, 253.
- YU,J.,ZHENG,Y.&HUANG,J **2014**.Towards High Performance Organic Photovoltaic Cells: A Review of Recent Development in Organic Photovoltaics. *Polym.*,6, 2473-2509.
- ZAPPIA,S.,MENDICHI,R.,BATTIATO,S.,SCAVIA,G.,MASTRIA,R.,SAMPERI,F.&DESTRI,S.**2015**.Characterization of Amphiphilic Block-Copolymers Constituted of a Low Band

gap Rigid Segment (PCPDTBT) and P4VP Based Coil Block Synthesized By Two Different Strategies. *Polym.*, 80, 245-258.

ZERSON,M.,NEUMANN,M.,STEYRLEUTHNER,R.,NEHER,D.&MAGERLE,R.**2016**.Surface Structure of Semicrystalline Naphthalene Diimide-Bithiophene Copolymer Films Studied With Atomic Force Microscopy. *Macromol.*,49, 6549-6557.

ZHAN,X.,FACCHETTI,A.,BARLOW,S.,MARKS,T.J.,RATNER,M.A.,WASIELEWSKI,M.R.&MARDER,S.R.**2011**.Rylene and Related Diimides for Organic Electronics. *Adv.Mater.*, 23, 268-284.

ZHAN,X.W.&ZHU,D.B.**2010**.Conjugated Polymers for High-Efficiency Organic Photovoltaics. *Polym.Chem.*,1, 409-419.

ZHANG,Z.-G.&LI,Y.**2014**.Side-Chain Engineering of High-Efficiency Conjugated Polymer Photovoltaic. *Mater. Sci.China Chem.*,1-19.

ZHANG,R.,YANG,H.,ZHOU,K.,ZHANG,J.,YU,X.,LIU,J.&HAN,Y.**2016**.Molecular Orientation and Phase Separation by Controlling Chain Segment and Molecule Movement in P3HT/N2200 Blends. *Macromol.*, 49, 6987-6996.

ZHAO,R.,WANG,N.,YU,Y.&LIU,J.**2020**. Organoboron Polymer for 10% Efficiency All-Polymer Solar Cells. *J. Chem. Mater.*,32, 1308-1314.

ZHOU,K.,ZHANG,R.,LIU,J.,LI,M.,YU,X.,XING,R.&HAN,Y.**2015**. Donor/Acceptor Molecular Orientation-Dependent Photovoltaic Performance in All-Polymer Solar Cells. *ACS Appl. Mater. Interfaces*,7, 25352-25361.

ZHOU,N.,LIN,H.,LOU,S.J.,YU,X.,GUO,P.,MANLEY,E.F.,LOSER,S.,HARTNETT,P.,HUANG,H.&WASIELEWSKI,M.R.**2014**. Morphology-Performance Relationships in High-Efficiency All-Polymer Solar Cells. *J. Adv. Energy Mater.*,4, 1300785.

ZHU,L.,ZHONG,W.,QIU,C.,LYU,B.,ZHOU,Z.,ZHANG,M.,SONG,J.,XU,J.,WANG,J.&ALI,J.**2019**. Aggregation-Induced Multilength Scaled Morphology Enabling 11.76% Efficiency in All-Polymer Solar Cells Using Printing Fabrication. *J.Adv. Mater.*,31, 1902899.

ZHAO,X.G.&ZHAN,X.W.**2011**. Electron Transporting Semiconducting Polymers in Organic Electronics. *Chem. Soc. Reviews*, 40, 3728-3743.

ZHAO,J.,SWINNEN,A.,ASSCHE,G.V.,MANCA,J.,VANDERZANDE,D.&MELE,B.V.**2009**.PhaseDiagram of P3HT/PCBM Blends and Its Implication for the Stability of Morphology. *J.Phys.Chem. B*, 113, 1587-1591.

- ZHOU,E.,CONG,J.,WEI,Q.,TAJIMA,K.,YANG,C.&HASHIMOTO,K.**2011**. All-Polymer Solar Cells from Perylene Diimide Based Copolymers: Material Design and Phase Separation Control. *Angew. Chem. Int. Ed.*, 50, 2799-2803.
- ZHOU,H.X.,YANG,L.Q.,STUART,A.C.,PRICE,S.C.,LIU,S.B.&YOU,W.**2011**.Development of Fluorinated Benzothiadiazole as a Structural Unit for a Polymer Solar Cell of 7% Efficiency. *Angew. Chemie-Inter. Edition*. 50, 2995-2998.
- ZHOU,E.,CONG,J.,HASHIMOTO,K.&TAJIMA,K.**2013**.Control of Miscibility and Aggregation Via the Material Design and Coating Process for High-Performance Polymer Blend Solar Cells. *Adv.Mater.*, 25, 6991- 6996.
- ZHOU, E.,NAKANO, M.,IZAWA,S.,CONG,J.,OSAKA,I.,TAKIMIYA,K.&TAJIMA,K. **2014**. All-Polymer Solar Cell with High Near-Infrared Response Based on a Naphthodithiophene Diimide (NDTI) Copolymer. *ACS Macro Lett.*,3, 872-875.
- ZHOU,K.,LIU,J.,LI,M.,YU,X.,XING,R.&HAN,Y.**2015**.Phase Diagram of Conjugated Polymer Blend P3HT/PF12TBT and the Morphology-Dependent Photovoltaic Performance. *J. Phys. Chem.C*,119,1729-1736.
- ZHOU,R.,ZHENG,Y.,QIAN,L.,YANG,Y.,HOLLOWAY,P.H.&XUE,J.**2012**.Solution-Processed,Nanostructured Hybrid Solar Cells With Broad Spectral Sensitivity and Stability. *Nano scale*, 4, 3507-3514.
- ZHOU,Y.,KUROSAWA,T.,MA,W.,GUO,Y.,FANG,L.,VANDEWAL,K.,DIAO,Y.,WANG,C.,YAN,Q.,REINSPACH,J.,MEI,J.,APPLETON,A.L.,KOLEILAT,G.I.,GAO,Y.,MANNSELD, S. C. B., SALLEO, A., ADE, H., ZHAO, D. & BAO, Z. **2014**. High Performance All-Polymer Solar Cell Via Polymer Side-Chain Engineering. *Adv. Mater.*, 26, 3767.
- ZHU,Z.,WALLER,D.,GAUDIANA,R.,MORANA,M.,MUEHLBACHER,D.,SCHARBER,M.&BRABEC,C.**2007**.Panchromatic Conjugated Polymers Containing Alternating Donor/Acceptor Units for Photovoltaic Applications, *Macromol.*,40, 1981-1986.

7. ANNEXES

7.1 Annex I - Curriculum Vitae of PhD Candidate



1. Personal Identification:

1.1 Full name: Gada Muleta Fanta

1.2 Birth date: September, 12/09/1983

1.3 Birth place: Oromia Region State, Wollega, Ethiopia

1.4 Sex: Male

1.5 Blood type: O⁻ (Negative)

1.6 Nationality: Ethiopian

2. Educational Backgrounds:

2.1 Primary Education

2.1.1 Name of School: Homi and Shambu primary school, Shambu, Oromia, Ethiopia

2.1.2 Dates attended: September 1992–June 1999

2.2 Secondary Education

2.2.1 Shambu Sen. Sec. School, Shambu, Oromia, Ethiopia

2.2.2 Dates attended: September 2000–June 2003

2.3 Tertiary Education

A. Bachelor of Science in Chemistry

2.3.1 Name of institution: Haramaya University, Haramaya, Ethiopia

2.3.2 Dates attended: September 2003/04–July 8, 2006

2.3.3 Credential obtained: Bachelor of Science in Chemistry

B. Masters of Science in Chemistry

2.3.4 Name of institution: Haramaya University, Haramaya, Ethiopia

2.3.5 Dates attended: January 2007/08–July 10, 2010

2.3.3 Credential obtained: Masters of Science in Organic Chemistry

3. Work Experience:

3.1 Instructor: 08/07/2006 to 09/03/2008 Fincha Preparatory School, Fincha, Oromia, Ethiopia

3.2 Lecturer: 28/04/2010 to present Arba Minch University, Arba Minch, Gamo Gofa, Ethiopia

3.3 Researcher: 08/06/2011 to 2013 in Arba Minch University

3.4 Founder of BSc Curriculum: October 20/09/2014 Bachelor of Science in Forensic Chemistry and Toxicology, Arba Minch University, new in Ethiopia.

3.5 Working on a PhD Degree Project: Since October 2014

4. Current Responsibilities:

4.1 Conducting a Research: All Polymer Solar Cell Materials: Structure-Property Relationship for Low Bandgap P(NDI2OD-T2) Solution and Blends.

4.2 Scientific Seminar: Participation in national and international seminars, trainings, conferences, symposiums.

4.3 Submitting and Publishing: Research papers on journals with high impact factor and highly indexed in Web of Science.

4.4 Collaboration: National and international on (grant fund, study, laboratory, teaching and supervising).

4.5 Credential Getting: Doctor of Philosophy in Materials Science and Engineering (Polymer Engineering), Jimma Institute of Technology, Faculty of Materials Science and Engineering, Jimma University, Jimma, Ethiopia.

4.6 Searching: Post-doctoral Research Associate.

5. Publications:

5.5. Fanta, G.M., et al., **2020.** Phase Behavior of Amorphous/Semicrystalline Conjugated Polymer Blends. *Polymers*, 12, 1726. <https://doi.org/10.3390/polym12081726> [**IF: 3.43**].

5.4. Fanta, G.M., et al., **2019.** Phase Diagrams of n-Type Low Bandgap Naphthalenediimide-Bithiophene Copolymer Solutions and Blends. *Polymers*, 11, 1474. <https://doi.org/10.3390/polym11091474> [**IF: 3.43**].

5.3. Fanta,G.M., **2016.** Electropolymerization for Dopamine Detection. *Inter. J. Innovative and Appl. Res.*, 4, 1-17. www.journalijiar.com [**IF: 2.90**].

5.2. Fanta,G.M. and A.G. Ede, **2014.** Analyzing Selected Heavy Metals Content of Compost used in Ethiopia. *Inter. J. Innovative and Appl. Res.*, 2, 5-11.www.journalijiar.com [**IF: 2.90**].

5.1. Fanta,G.M., et al., **2013.** Biocide Value Characterization of Essential Oil from *Boswellia neglecta* S.against Pathogenic Termite, Cockroach, Ticks, E.coli and Staphylococcus aureus. Inter.J. Modern Chem., 5, 145-158.

6. Contributions to International, National Conferences and Mobility

6.1 International Mobility (training, study, laboratory and research)

6.1.1 The Second Materials Research School of the JUAMI: The Joint Undertaking for an African Material, Institute on Materials for Sustainable Energy, Conducted in Arusha, Tanzania, 29th May 2016 – 10th June 2016.

6.1.2 Erasmus plus scholarship KA107 (ICM) exchange student's intake for study a period of five months, spring semester 2016/2017 at Silesian University of Technology, Gliwice, Poland.

6.1.3 Laboratory and research works for a period of six months in 2017/2018 at the Institute of Materials and Biomaterials Engineering, Silesian University of Technology, Gliwice, Poland.

6.2 International Conference or Educational Support (oral presentation)

6.2.1 The Academic Staff Week, Silesian University of Technology, Gliwice, Poland, 21-25 May 2018, "Seminar on Active Layer Materials for Organic Photovoltaic Cells".

6.3 National Conference (oral presentation)

6.3.1 "Phase Diagrams of n-Type Low Bandgap Naphthalenediimide-Bithiophene Copolymer Solutions and Blends" at the 10th Annual Research Conference of Jimma University and the 9th Global Knowledge Exchange Network (GKEN) Annual Event which was jointly organized from April 18-19, 2019 in Jimma, Ethiopia.

References: Professor Jung Yong Kim (PhD)

School of Chemical Engineering, Jimma Institute of Technology, Jimma University, P. O. Box 378, Jimma, Ethiopia.

E-mail: kim.jungyong@gmail.com

Professor Tomasz Tanski (Dr.-Ing.)

Institute of Engineering Materials and Biomaterials, Faculty of Mechanical Engineering, Silesian University of Technology, 44-100 Gliwice, Poland.

E-mail: tomasz.tanski@polsl.pl

Professor Aman Dekebo (PhD)

College of Natural Sciences, Department of Chemistry, Adama Science and Technology University, Adama, Ethiopia,

E-mail: aman_d00@yahoo.com

7.2 Annex II - Declaration Form (PhD Dissertation Work)

I, the undersigned, declared that no portion of the work referred to the dissertation has been submitted in support of an application for another degree or qualification of this or any other University or other Institute of learning.

Name of **PhD candidate's**: Gada Muleta Fanta.

Signature: _____

Date: _____

Place of submission: _____

Date of submission: _____

This dissertation has been submitted for examination with my approval as **candidate's first Promoter (Supervisor)**.

Name: Professor Jung Yong Kim (PhD)

Signature: _____

Date: _____

Candidate's Second Promoter (Supervisor).

Name: Professor Tomasz Tanski (Dr.-Ing.)

Signature: _____  _____

Date: _____